Model Free Operational Space Control of Mechanical Manipulators

by

Muhammad Saad Saleem

Thesis

Submitted by Muhammad Saad Saleem

in total fulfillment of the Requirements for the Degree of

Doctor of Philosophy

School of Science and Engineering
University of Ballarat

PO Box 663, University Drive, Mount Helen, Ballarat, Victoria 3353, Australia

March, 2009

Model Free Operational Space Control of Mechanical Manipulators

Abstract

For successful model-based control of mechanical manipulators, accurate values for model parameters have to be defined and used in the system mathematical model. Tasks are generally specified in operational space and control actions are defined in joint space. However, a small error in joint space can translate to a large error in operational space, which may negatively influence the effectiveness of the control scheme. To overcome this problem, this thesis presents a set of novel *direct adaptive* controllers for the dynamic learning operational space control of mechanical manipulators. These controllers determine the dynamics of the manipulator online and synthesize an operational space controller in real-time. It has been shown that the proposed framework can be extended to a variety of control schemes. Using subspace identification with post-modern controllers, such as $\mathscr{H}_2$ and $\mathscr{H}_\infty$ optimal controllers, provides a strong mathematical foundation. The proposed approach sheds a new light on the application of generalized predictive controllers (GPC) in the area of manipulator control. Moreover, the reference trajectory is still given in the operational space, which has numerous benefits.

The thesis treats the mechanical manipulator as a black box, and no priori knowledge of the dynamics of the manipulator is required. Subspace identification has been used to evaluate a predictor for the manipulator. An introduction to the problem and a story-line literature survey is presented in Chapter 1 of the thesis. Chapter 2 reviews the initial steps used in numerical algorithms for subspace state space identification (N4SID) to calculate the subspace predictor. To cater for the inconsistent excitations of the plant, an efficient method of calculating the subspace predictor is

proposed for rank deficient matrices. A simplified and computationally efficient way for updating the subspace predictor is also developed in Chapter 2.

Chapter 3 formulates the model free subspace based operational space $\mathscr{H}_\infty$ optimal controller for a serial manipulator. The controller uses the linear subspace predictor and synthesizes a control law using $\mathscr{H}_\infty$ optimization criterion in real-time. The controller minimizes the torque (control effort) and the trajectory error. The controller has been extended to $\mathscr{H}_2$ based control. A robust version of the controller has been proposed to incorporate additive uncertainties. Additive uncertainties compensate for the nonlinearities in the system, which were initially ignored at the time of the controller design.

Chapter 4 extends the concepts discussed in Chapter 3 to derive a controller that enables the end-effector to interact with the environment using the concept of hybrid force/position interaction control. In the hybrid force/position control, the controller minimizes the force acting on the manipulator along with the torque and the trajectory error. Another controller is formulated based on the fundamental concept of impedance control. In impedance control, the controller tries to follow a given trajectory in operational space as much as possible with the least possible control effort. As a consequence, the manipulator looses its joint stiffness and maintains a dynamic relation between the end-effector and the acting force. The choice between the hybrid force/position controller and the impedance controller depends on the application. Both of these controllers treat the interacting forces as disturbances. Scaling properties of the force signal are also explored and extended to the scaling of the reference signal and the force signal in impedance control.

Chapter 5 applies the hybrid controller formulated in Chapter 4 to remove bias from the dynamic behaviour of the manipulator. The controller minimizes the difference between the torque generated by the actuators and the torque sensed by the strain gauges. Similar approaches have been used in the literature to remove the effects of the gravitational force and coupling. Another application of the hybrid

control is found in the control of a parallel manipulator. First the kinematic framework is formulated and then the hybrid controller is designed to exploit the dynamic behaviour of the manipulator.

Chapter 6 presents the implementation details of the controller described in Chapter 3. Other controllers can be implemented in the same manner. A mathematical relation is presented to simplify the controller implementation process. The system is then simulated on MATLAB, and a controller is derived to optimize the value of the damping factor in real-time. Chapter 7 presents the summary of the thesis and offers recommendations for future work.

Model Free Operational Space Control of Mechanical Manipulators

Declaration

Except where explicit reference is made in the text of the thesis, this thesis contains no material published elsewhere or extracted in whole or in part from a thesis by which I have qualified for or been awarded another degree or diploma. No other person's work has been relied upon or used without due acknowledgment in the main text and bibliography of the thesis.

Muhammad Saad Saleem
March 1, 2009

Acknowledgments

I would first like to extend my sincere thanks to my supervisor Dr. Ibrahim A. Sultan, for his excellent guidance and support that made it possible to conclude this journey. I greatly appreciate his patience while watching me wander down all the "blind alleys". His valuable comments have always helped in improving my work.

I would like to acknowledge the Government of Australia, the Research Committee, and the School of Science and Engineering for providing me the funds to undertake such an endeavoring and fruitful task. I would like to appreciate the role of the staff at the School of Science and Engineering for providing all the logistic support during the candidature. I am also grateful to Dr. Rana Abdul Jabbar who inspired me to pursue a research career.

I want to thank a number of my friends who provided quality company and I got a chance to learn from them. In particular, I want to thank Dante, Asim, Hassan, Amin, Riko, Hany, Junaid, and Basel for keeping me cheerful. I would also like to thank Olive Gunnel who took care of me during my stay at her place and George Gardoz for his intellectual conversations.

Being a member of the vast network of Wikipedians, I would like to thank all those members who corrected me and taught me valuable lessons. The struggle for the *multiple points of views* instead of the *neutral point of view* has greatly helped me in understanding conflict resolution.

Furthermore, I would like to mention a few people whose work helped me become a better person and inspired me during my candidature; Rhonda Byrne, the author of "The Secret" from whom I learned the *not so mechanical* nature of the Universe; Anthony Robbins, from whom I learned the *power of negative thinking*; and Javed Ghamidi, for his excellent work on rationality in religion.

I sincerely thank my younger sister who always kept me happy and laughing. And most importantly, I want to thank my parents for their love, wisdom, guidance, and understanding through these years. They prayed for me and brought me great comfort during times of extreme stress.

Muhammad Saad Saleem

University of Ballarat

March 2009

To Abbu and Ammi

for their love and care

Contents

List of Figures

Notation

Symbols, Operators and Functions

$\rightarrow$	Approaches to
γ	A scalar quantity that represents performance objective of an optimization criterion
$\in$	Belongs to
A^i	i^{th} column of the matrix A
A^*	Conjugate transpose of A
$C(q, \dot{q})$	Coriolis matrix
$\dot{q}(t)$	Derivative of $q(t)$ with respect to time
$\otimes$	Element-wise matrix multiplication
$\equiv$	Equal by definition that has been defined
$\triangleq$	Equal by definition under certain assumptions taken in context
$\{A\}_{1:m}$	First m rows of A
$\forall$	For all
$f_i(q)$	Forward kinematics function, which relates joint space variables, q, to i^{th} degree of freedom in operational space
$\|\|A\|\|_F$	Frobenius norm, $\sqrt{\text{trace}(A^*A)}$

max	Global maxima
min	Global minima
$G(q)$	Gravitational matrix
$\mathscr{H}$	Hardy space
$H_{hess}(\bullet)$	Hessian of matrix $\bullet$
$M(q)$	Inertial matrix
$q_i(t)$	i^{th} joint variable, in radians if joint i is revolute or in meters if joint i is prismatic
$J(q)$	Jacobian
$\bar{\lambda}$	Largest eigenvalue
$\bar{\sigma}$	Largest singular value
λ	Levenberg-Marquardt operator used in kinematic damping
$\mapsto$	Maps to
$\Re^{n \times m}$	Matrix of $n \times m$ real numbers
$A^{\dagger}$	Pseudo-inverse of matrix A
r	Reference trajectory in operational space, $\left[x_r^T, \dot{x}_r^T, \ddot{x}_r^T\right]^T$
Φ	Regressor matrix
sup	Supremum
$\|\|g\|\|_{\infty}$	$\sup_{\omega} \bar{\sigma}(g(\omega))$
t	Time variable
A^T	Transpose of A

z^{-1}	Unit delay, used in difference equation
$\mathscr{L}^p$ space	Vector space, named after Lebesgue
$\Re^n$	Vector of n real numbers
τ	Vector of motor torques
Θ	Vector of (unknown) parameters
x	Vector of end-effector position in operational space
y	Vector of joint positions, velocities, and accelerations, $\left[q^T, \dot{q}^T, \ddot{q}^T\right]^T$

Abbreviations and Acronyms

3-RPR	A parallel manipulator with 3 serial links, each link consists of two rotatory and a prismatic joint. The underlined joint is the actuated joint
ARMAX	Auto Regression Moving Average with eXogenous input
ARX	Auto Regression with eXogenous input
BJ	Box Jenkins
BLUE	Best Linear Unbiased Estimate
DLS	Damped Least-Squares
DOF	Degrees Of Freedom
GPC	Generalized Predictive Controllers
IRB	Industrial RoBot, used in the name of robots built by ABB
JTF	Joint-Torque sensory Feedback
LQG	Linear Quadratic Gaussian
LSE	Least-Squares Estimate

LTI	Linear Time Invariant
MATLAB	MATrix LABoratory, a computer software used for simulations
MIMO	Multiple Input Multiple Output
MOESP	MIMO Output-Error State sPace model
MRAC	Model Reference Adaptive Control
N4SID	Numerical algorithms for SubSpace State Space IDentification
OE	Output Error
PD	Proportional-Derivative
PE	Prediction Error
PID	Proportional-Integral-Derivate
PRBS	Pseudo-Random Binary Sequence
SIM	Subspace Identification Method
SimMechanics	A toolbox of MATLAB to simulate mechanical systems
SISO	Single Input Single Output
STC	Self-Tuning Control
SVD	Singular Value Decomposition
WLSE	Weighted Least-Squares Estimate

Chapter 1

Introduction

1.1 Background

Since the advent of 1970's, control of mechanical manipulators has been an active area of research. A number of approaches have been proposed in the literature. The most common approach adopted in industrial robots features decentralized "proportional, integral, derivate" (PID) control used for each degree of freedom [52]. In *decentralized control* schemes, i.e., when a single manipulator joint is controlled independently of others, linear control schemes can be used to control the manipulator especially if electric motors are coupled with reduction gears of high ratios [89]. Most industrial robots are designed with such actuation mechanisms and utilize the linear controllers [52].

More advanced non-linear control schemes have been developed, such as *computer torque control*, which linearizes and decouples the equations of motion. Adaptive control techniques were developed to cater for the uncertainties and identify on-line the dynamic parameters of the robot. Apart from model-based controllers, there are Lyapunov based and passivity-based controllers. Both of these controllers neither linearize nor decouple the system nonlinear dynamics. Lyapunov based controllers

search for asymptotic stability – exponentially, if possible; and passivity-based controllers exploit the passivity properties of the robot manipulator dynamics [27].

When using a model-based approach to control a robot, it is essential to have a good understanding of its dynamic behaviour. This understanding can be represented explicitly by a mathematical model or implicitly by its input-output data. Normally, the mathematical model can be derived in form of equations of motion, but as the manipulator parameters are constantly changing during operation, it becomes imperative to adopt a direct adaptive control strategy. Direct adaptive controllers are those controllers that require no priori knowledge about the plant and there is no explicit formation of the plant model. The experimental data is used directly in the synthesis of a controller. The plant is treated as a black box and the controller "learns" the dynamics of the plant and synthesizes a controller in realtime. These controllers belong to the category of generalized predictive controllers (GPC) and they have been referred to as model free or data-driven controllers [45]. Many implementations of model free control can be found in the literature [32, 96, 48].

The work presented in this dissertation builds on the results obtained by Woodley [117] for model free control strategy. However, the work presented here is distinguished from Woodley's contribution by three main aspects. Whilst Woodley uses only linear blocks in the proposed control system, kinematic nonlinearities are accounted for in the system proposed here. Also, Woodley optimizes the cost function to reduce the output error and control effort. In this thesis, the cost function is optimized for different parameters for different cases of manipulator control. Moreover, Woodley limits implementation discussions to linear systems, whilst in this thesis, implementation issues are discussed for nonlinear systems, such as, serial and parallel manipulators.

It should be noted that the task specification (end-effector motion and forces) is usually carried out in operational space while the control actions (joint actuator generalized forces) are performed in joint space [89]. This leads to two different kinds of control schemes:

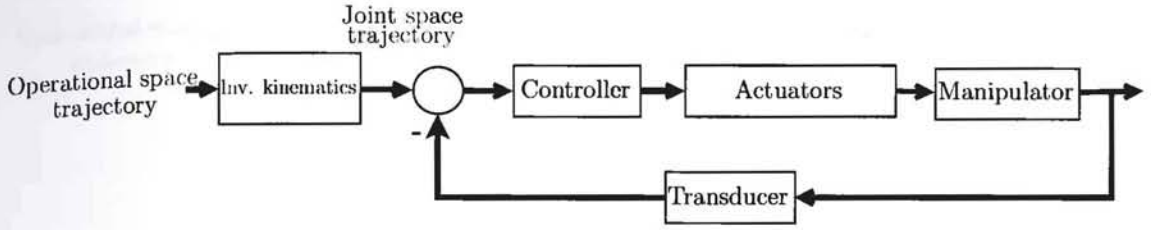

Figure 1.1: Joint space control

- Joint space control
- Operational space control

As suggested in Figure 1.1, joint space control consists of two subproblems. First, manipulator inverse kinematics is performed and then joint space control scheme is devised. The inverse kinematics analysis is typically undertaken to calculate the joint motor displacements required to locate the end-effector at a specific position and orientation in space. The main computational burden of the joint space control scheme is incurred by the inverse kinematics procedure, which is normally performed by using optimization techniques; particularly in redundant systems where there can be infinite solutions for a given task [56]. Many implementations of joint space control can be found in the literature [61, 51, 6, 50, 111, 105, 103, 121].

Operational space control, on the other hand, implies that the inverse kinematics is embedded in the closed-loop control law and not explicitly performed. This is shown in Figure 1.2. The operational space control scheme follows a global approach that requires greater algorithmic complexity because the inverse kinematics is now embedded in the controller. However, It has been suggested that operational space control and task space control allude to the same concept [119].

If joint space control is employed, a small error in joint space can project a larger error in operational space. On the other hand, if operational space control is used, the stability of the control depends heavily on the accuracy of the dynamic parameters of the manipulator. It has been shown in [75] that a small error in the inertia matrix can make the system unstable. This makes it imperative to design a

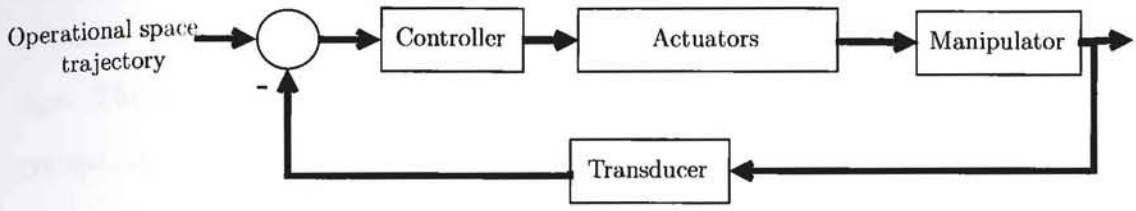

Figure 1.2: Operational space control

direct adaptive operational space controller that can update the dynamic parameters of the robot in realtime.

1.2 Control of an Articulated Manipulator

Dynamics of an articulated manipulator are nonlinear and highly coupled. Consider an articulated manipulator of n links. The vector of joint variables and its derivatives can be denoted by $q, \dot{q}, \ddot{q} \in \Re^n$. In case of a revolute joint, q signifies an angle while in the case of a prismatic joint, q represents a linear distance. The torque generated by rotatory actuators, or force generated by prismatic actuators, is represented by $\tau \in \Re^n$. The rigid body model can be given by

$$M(q)\ddot{q} + C(q,\dot{q})\dot{q} + v(q) + \xi(q,\dot{q}) = \tau \tag{1.1}$$

where $M(q) \in \Re^{n\times n}$ is the mass or inertia matrix, $C(q,\dot{q}) \in \Re^{n\times n}$ is the Coriolis and centrifugal torque coefficient matrix, $v(q) \in \Re^n$ is the gravitational vector, and $\xi(q,\dot{q})$ is a vector of unmodeled non-linearities. It is assumed that the mechanical manipulator is fully actuated and the forward kinematics model, which relates the joint variables to the end-effector position, is known. The presence of the Coriolis and gravity components renders the system non-linear, even though the system is linear in dynamic parameters [52, 67].

Model-based robot control schemes proposed in the literature for articulated manipulators can be broadly divided into two categories. In the first type of control

schemes, the non-linearities and the coupling effect is considered in the control design. The second type of controllers treat each link of the manipulator as a linear system. Related non-linearities and coupling effects are taken as disturbance signals.

1.2.1 Computer Torque Control

A mechanical manipulator, whose dynamics are described in (1.1), can be controlled using the resolved acceleration control [64] or the computed torque method [24, 4, 8]. The computed torque method has also been referred to as the *inverse dynamics control* [27]. The basic idea of inverse dynamics is to find a nonlinear feedback control law such that

$$\tau = g(q, \dot{q}, t) \tag{1.2}$$

which, when substituted in (1.1) results in a linear closed-loop system [94]. If $\hat{M}(q)$, $\hat{C}(q, \dot{q})$, and $\hat{v}(q)$ are the estimated values of the mass matrix, Coriolis matrix, and the gravity vector, respectively, for given joint position and velocity vectors, then the torque produced by the actuators can be expressed by

$$\hat{M}(q)a_q + \hat{C}(q, \dot{q})\dot{q} + \hat{v}(q) = \tau \tag{1.3}$$

The term a_q denotes a new input vector. From the comparison of (1.1) and (1.3), it is obvious that

$$\ddot{q} = a_q$$

It has been shown in the literature that the control described in (1.3) has achieved remarkable results, and does describe the system as linear and decoupled [94]. Since a_q is used to control a linear second order system, it can be calculated using proportional-derivative (PD) control as

$$a_q = \ddot{q}_d(t) - K_0\tilde{q} - K_1\dot{\tilde{q}} \tag{1.4}$$

where $\widetilde{q} = q - q_d, \dot{\widetilde{q}} = \dot{q} - \dot{q}_d, K_0, K_1$ are digonal matrices with diagonal elements consisting of position and velocity gain, respectively, and the reference trajectory

$$t \mapsto (q_d(t), \dot{q}_d(t), \ddot{q}_d(t))$$

defines the desired joint positions, velocities, and accelerations [94].

The performance of the various approaches developed on the basis of the above premises depends on the precise knowledge of the robot parameters and loads. The performance may degrade significantly if the model parameters are not accurately known [4, 114]. Adaptive control was suggested to deal with the parametric uncertainties [30, 68]. Craig et al. [25] and Slotine and Li [93] developed adaptive control techniques that utilize the linearity of the manipulator dynamic parameters. However, these techniques come under the category of indirect adaptive control schemes since a priori knowledge of the dynamic parameters of the manipulator is required. In the literature, this technique is also referred to as the model reference adaptive control (MRAC) [26].

1.2.2 Linear Control of Mechanical Manipulators

A linearized representation of a nonlinear dynamic system is often sought in control design. Each link of the manipulator can be considered a separate single input single output SISO control problem. Nonlinearities and coupling effect are treated as disturbance signals in these controllers [89]. Many of these controllers come under the category of self-tuning control (STC) [26]. The most straightforward approach is to generate analytical, closed-form, nonlinear equations of motion; and then linearize them by first-order Taylor expansion [62]. If the plant is linearized on the node point, i.e., q_0, then the robot dynamic equations can be written in the form of a difference equation [26]. This is usually expressed as follows;

$$A(z^{-1})q_i(k) = B(z^{-1})\tau_i(k-2) + C(z^{-1})\xi(k) + h(k) \tag{1.5}$$

where h is biasing or the gravitational force, z^{-1} is a unit delay, and A, B, and C are the linear blocks in z-domain that can be identified by employing linear prediction algorithms. The above model is only valid in the vicinity of q_0. If the manipulator moves far from q_0, the model needs to be updated.

Remarkable efforts have been made to model the manipulator as a linear system and to apply existing adaptive control methods [58, 57, 30, 18]. For example, Chung and Leininger [18] employed pole-placement STC method on the linearized model of a JPL-Stanform Arm. Dubowsky and Deforges [30] proposed an MRAC that uses a linear second-order time invariant differential equation as a reference model for each degree of freedom of the robot arm. Koivo and Guo [58] presented a self-tuning auto-regression method to fit the input-output data from the manipulator assuming that there is no coupling forces between joints. Koivo [57] chose to ignore the dynamic complexity and fit the measured data to a second-order linear time-varying model using a recursive least-squares approach [93]. Cui and Shin [26] employed linear model predictive control on a serial manipulator. Swarup and Gopal [98] used Linear Quadratic Gaussian (LQG) cost function on each link of the manipulator assuming linear behaviour in the neighborhood of an operating point.

Linearized time-varying models of mechanical manipulators assume that during the adaptation process the parameters are not changing quickly. However, for fast motion applications, this assumption is not valid [92]. Stability has always been an issue in this approach and no mathematical proof of the stability has ever been provided [107].

1.3 Problem Statement and Methodology

The operational space control scheme offers an elegant approach to task control. Not only does it provide dynamically consistent control, but it also incorporates constrained manipulator motions [88], compliant control, force control, and many other favourable features [54, 76]. Operational space control has also been studied as

an optimal control problem originally introduced by Khatib [54]. Many of the suggested controllers, which fall under this category, can be described as a constrained optimization problem [77]. This can be expressed as follows;

$$\min_{\tau} L(\tau) = \tau^T N \tau \text{ subject to } J\ddot{q} = \ddot{x}_{ref} - \dot{J}\dot{q} \tag{1.6}$$

where N denotes a positive definite matrix that weighs the contribution of the motor commands to a cost function, $L(\tau)$, and $\ddot{x}_{ref} = \ddot{x}_d(t) + K_d(\dot{x}_d(t) - \dot{x}(t)) + K_p(x_d(t) - x(t))$ denotes a reference attractor in operational space with gain matrices K_d and K_p. Peters and Schaal [76] employed the framework of optimal operational space control in conjunction with reinforcement learning to form a *learning operational space* controller that also learns the kinematics model of the manipulator.

In this thesis, a *supervisory* learning operational space control is proposed. The proposed control scheme is equipped with the ability to learn the dynamics of the mechanical manipulator and synthesize a controller in realtime. This problem is equivalent to obtaining the following mapping;

$$(q, \dot{q}, \ddot{q}, x_r, \dot{x}_r, \ddot{x}_r) \mapsto \tau \tag{1.7}$$

where $x_r, \dot{x}_r$, and $\ddot{x}_r$ denote the reference trajectory in the operational space. Unlike the learning operational space proposed by Peters and Schaal [76], it is assumed in this thesis that the forward kinematics model of the manipulator is known. Moreover, a direct adaptive controller is developed that learns the linear model of the manipulator similar to the one mentioned in (1.5) and then synthesizes $\mathscr{H}_\infty$ optimal controller using several cost functions for different situations. A feature common to the controllers proposed is that they try to minimize both the control effort (torque generated by the actuators) and the error between the reference and the end-effector trajectory. The proposed controllers are similar in their structure to model free controllers designed by Favoreel et al. [33], Kadali et al. [48], and Woodley et al. [118].

All of these controllers use subspace predictors in the cost function, which is then optimized for different parameters.

There are several benefits of using model free architecture. Model-based controllers reduce the plant order to form the plant model for infinite horizon. In contrast, model free controllers use a finite prediction horizon. The predictor is then used to synthesize a controller without losing any valuable information of the plant. There is no explicit formation of the plant model. The seamless integration between the identification of the plant and the controller synthesis makes it favourable for direct adaptive control. In $\mathscr{H}_\infty$ optimization criterion, the controller is designed for the worst case value of the disturbance signal. This ensures the stability of the system.

1.4 Scope of Work

The aim of this thesis is to develop tracking operational space direct adaptive controllers for mechanical manipulators using GPC theory. Assuming that the gravity compensators are installed on the mechanical manipulator, a computationally fast method will be presented to calculate the linear subspace predictor of the manipulator for rank deficient matrices of input data.

Using the linear subspace predictor, model free subspace based operational space $\mathscr{H}_\infty$ control will be developed for a serial rigid body robot. A framework will also be formulated to cater for the forward and inverse kinematics operations. The controller will be synthesized directly from the experimental data. Details of the controller implementation will be presented with the simulation results.

Exploiting the properties of $\mathscr{H}_\infty$ control, $\mathscr{H}_2$ control will be formulated. A robust version of the model free subspace based operational space $\mathscr{H}_\infty$ control will also be developed to cater for the additive uncertainties. Additive uncertainties compensate for the nonlinearities in the system, which were initially ignored at the time of the design of the controller.

One of the benefits of using operational space control is that it can incorporate interaction control. A hybrid force/position and impedance controller will be developed that will enable the manipulator end-effector to interact with the environment. In the hybrid force/position control, the controller tries to minimize the effect of the interacting force vector. As a result, the manipulator moves into its force and position subspaces to counter the effect of the acting force. Another controller will be formulated based on the fundamental concept of impedance control. In the impedance control, the manipulator looses its joint stiffness and only maintains a dynamic relation between the end-effector and the acting force.

Joint-torque sensory feedback will be used in conjunction with the hybrid force/position controller to remove the bias from the dynamic behavior of the system. The controller will minimize the difference between the torque generated by the actuators and the torque sensed by the strain gauges. Similar approaches have been used in the literature to remove the effect of the gravitational force and coupling.

Hybrid force/position controller will be extended to control of parallel manipulators. An expression for the forward kinematics function of a parallel manipulator will be evaluated analytically to form the kinematic framework that will cater for the forward and inverse kinematics operation in parallel manipulators. Contribution of the torque from the passive joints onto the active joints will be used as an exogenous force signal in the hybrid control.

1.5 Thesis Outline

Chapter 2 reviews the initial steps used in numerical algorithms for subspace state space identification (N4SID) to calculate the subspace predictor as described in [73, 117]. A simplified and computationally efficient method of calculating and updating the subspace predictor is also developed be in Chapter 2. Chapter 3 formulates the model free subspace based operational space $\mathscr{H}_\infty$ optimal controller for a serial manipulator. The concept is also extended to $\mathscr{H}_2$ optimal control. A robust version of the controller is also derived to cater for the additive uncertainties.

Chapter 4 extends the concepts discussed in Chapter 3 to derive a controller that enables the end-effector to interact with the environment using the concept of hybrid force/position interaction control. Another controller is formulated on the fundamental concept of impedance control. Scaling properties of the force signal are also explored and extended to the scaling of the reference signal and the force signal in impedance control. Chapter 5 applies the hybrid controller formulated in Chapter 4 for removing bias from the dynamic behaviour of a manipulator. Another application of the hybrid control is found in the control of a parallel manipulator. First the kinematic framework is formulated, and the hybrid controller is used by exploiting the dynamic behaviour of a parallel manipulator.

Chapter 6 presents the implementation details of the controller described in Chapter 3. Other controllers can be implemented on the same lines. A mathematical relation is presented to simplify the controller implementation process. Using these guidelines, the system is simulated using MATLAB, and a controller is developed to optimize the value of the damping factor, used in the inverse kinematics block. Chapter 7 presents the summary of the thesis and offers recommendations for future work.

Chapter 2

Subspace Identification

System identification is used to build dynamic models from measured input-output data of a plant. There are many system identification methods. The list starts with the classical prediction error (PE) and its variants; the auto regression with exogenous input (ARX), output error (OE), auto regression moving average with exogenous input (ARMAX), and Box Jenkins (BJ) [71, 63]. Subspace identification methods (SIM) have got a lot of fame in the last ten years since they were introduced in 1996 by Overschee and Moor [74] and made their way into a variety of applications, including the identification of the dynamic parameters of mechanical manipulators.

In this chapter, Sections 2.1 and 2.2 discuss issues related to the identification of dynamic models for rigid robot manipulators. A review of the methods and techniques employed to get reliable estimates of model parameters is presented. Sections 2.3 and 2.4 discuss subspace prediction and review the methods to calculate subspace predictor. Section 2.5 proposes a new algorithm for faster online calculation of subspace predictor. Section 2.6 discusses results obtained from simulations of different mechanical systems.

The subspace predictor used in this thesis resembles N4SID [73], in which the future outputs project onto the past inputs, outputs, and future outputs. A similar predictor has been used in the model free subspace based control by Favoreel et al. [33] and Woodley et al. [118].

2.1 Rigid Body Dynamics

There are two rigid body dynamic models usually used for the identification of robot dynamics.[1] The *differential model* and the *energy model*. For the differential model, the barycentric parameters [34] are employed with the modified Newton-Euler parameters [9] to express the system in the form of

$$\tau = W(q, \dot{q}, \ddot{q})\Theta \tag{2.1}$$

where $W \in \Re^{n \times b}$ is an observation matrix, $\Theta \in \Re^b$ is a vector of dynamic parameters, n is the number of joints, and b is the number of base parameters. The energy (difference) model, which is also called the *integral model*, is expressed as follows [60];

$$\Delta w(q, \dot{q})\Theta = \Delta W = W(t_b) - W(t_a) = \int_{t_a}^{t_b} \tau^T \dot{q} dt \tag{2.2}$$

Both models are linear in dynamic parameters. The integral model consists of only one equation and is not dependant on the acceleration of joint variables, while the differential model consists of n equations and its dependance on the joint acceleration makes it richer in information than the integral model [113]. The differential model is also easier to implement.

There are three kinds of parameters. The first class of parameters are called base parameters or independent parameters. These are absolutely identifiable and correspond to different columns of Θ. Khalil and Kleinfinger [53] showed that different columns of Θ show linear dependance. These parameters that are linear combination of base parameters comprise the second class of parameters. The last class of parameters are those which are unidentifiable through normal methods of parameter identification. These unidentifiable parameters do not directly contribute to the resulting torque, hence they can be neglected. Therefore, the order of the plant can be considered less than $10n$ since the objective is to calculate a predictor for an articulated manipulator to be controlled and not the individual identification of

[1] This classification is according to Kozlowski [60]

parameters. However, even in the most reduced set of base parameters, there are at most $7n$ parameters that are nonzero [37] even if all the parameters are nonzero.

Using the differential model described in (2.1), N samples of data of $\{q(t_i), \dot{q}(t_i), \ddot{q}(t_i), \tau(t_i)\}$ such that $i = 1, 2, \ldots, N$, can be expressed as

$$\underbrace{\begin{bmatrix} W(q(t_1), \dot{q}(t_1), \ddot{q}(t_1)) \\ W(q(t_2), \dot{q}(t_2), \ddot{q}(t_2)) \\ \vdots \\ W(q(t_N), \dot{q}(t_N), \ddot{q}(t_N)) \end{bmatrix}}_{\Phi} \Theta = \underbrace{\begin{bmatrix} \tau_{t_1} \\ \tau_{t_2} \\ \vdots \\ \tau_{t_N} \end{bmatrix}}_{Y} + \rho \tag{2.3}$$

where Φ is a regressor and ρ is a residual error vector. It is usually the case that $N \gg c$, where c is the number of dynamic parameters to be found. If exciting trajectories are not orthogonal to each other, a singularity would occur in the solution. Hence, it is important that at all times, exciting trajectories are orthogonal. If regressor matrix is based on a large number of trajectories to increase the fidelity of the solution, then the condition of orthogonality is sometimes hard to meet. In such cases, the system depicted in (2.3) is overdetermined, i.e., there are more number of equations than the parameters to be found. For overdetermined systems, techniques like singular value decomposition (SVD) or QR factorization are useful in producing numerically stable results [41]. The estimated value $\hat{\Theta}$ can be given by

$$\hat{\Theta} = \min_{\Theta} ||\rho||^2 \tag{2.4}$$

which is a standard least-squares estimate (LSE) problem. If Φ is of full rank, the explicit solution of this problem can be given by [52]

$$\hat{\Theta} = (\Phi^T \Phi)^{-1} \Phi^T Y = \Phi^{\dagger} Y \tag{2.5}$$

where $\dagger$ denotes Moore-Penrose inverse, also called pseudoinverse or generalized inverse. It should be noted that the LSE is biased because the regressor Φ and ρ

are realizations of random and correlated variables [36]. Nonlinear friction in link joints also increases the bias of the system, this is why it is recommended to model friction. To overcome this shortcoming and to find the best linear unbiased estimate (BLUE), weighted least-squares estimate (WLSE) [101] is used, i.e.,

$$\hat{\Theta} = \min_{\Theta} \frac{1}{2}(Y - \Phi\Theta)^T Z(Y - \Phi\Theta) = (\Phi^T Z \Phi)^{-1}\Phi^T ZY \tag{2.6}$$

where Z is the weighting matrix or the covariance matrix of the actuator torque data, which is a dense matrix if noise is correlated. The only difference between WLSE and LSE is that the data is weighted with the inverse of covariance of the actuator torque measurement noise, and therefore discriminates between accurate and inaccurate data [101]. One of the important property of WLSE is its maximum likelihood estimation. There are numerous ways suggested in the literature to choose the weight. Examples can be found in the works of Swevers et al. [99] and Poignet and Gautier [81].

2.1.1 Gravity Compensators and Dynamic Coupling

The inertia of geared actuator rotors and gravity compensating devices contribute significantly to the dynamic behaviour of the robotic manipulator. Gravity compensating devices are preloaded springs mounted between the first and second link, approximated to compensate for the static torque caused by the mass of the payload [52]. Dynamic coupling and gravity-compensating springs behave linearly, hence their effect can be conveniently fit within the linear-in-parameters model structure described in (2.1) [101].

2.2 Excitation

In the identification of any system, the choice of excitation signal is made so that the maximum information can be deduced from a given experiment. For mechanical manipulators, the excitation signal is selected in two steps. The first step involves

trajectory parameterization and the second one involves the calculation of trajectory parameters, usually by means of optimization.

2.2.1 Trajectory Parameterization and Optimization

The most general technique has been proposed by Armstrong [7], and it involves finite sequences of joint accelerations. Gautier and Khalil [38] proposed a technique in which fifth-order polynomials were used, interpolating between sets of joint positions and velocities separated in time, assuming initial and final acceleration values. Swevers et al. [99] parameterized the trajectory as a finite Fourier series, where the optimization variables are the coefficients in this series. Pfeiffer and Holzl [79] optimized the trajectory such that the trajectory always follow the steepest descent of the optimization criterion. Even though, these trajectories provide adequate excitation of the robot dynamics, the resulting data is neither periodic nor band-limited. It has been seen that processing periodic and band-limited data is more accurate for the parameter estimation [101].

Periodic and band-limited trajectories can be generated using the following simple finite Fourier series for $q_i(t), i = \{1, \ldots, n\}$ joints;

$$q_i(t) = q_{i,0} + \sum_{k=1}^{N} (a_{i,k} \sin(k\omega_f t) + b_{i,k} \cos(k\omega_f t)) \tag{2.7}$$

where $q_i(t)$ corresponds to the ith joint position, t represents time, and ω_f is the sampling frequency which is same for all joints. Fourier series contains $2N + 1$ parameters in the frequency range of $[\omega_f, N_{\omega_f}]$, which are degrees of freedom (DOF) for trajectory optimization [101]. By selecting a lower fundamental frequency, ω_f, a large work space can be covered at the cost of time. Increasing the coverage improves the accuracy of the parameter estimates [80]. On the other hand, high fundamental frequency increases the joint acceleration, which is a requirement for accurate estimation of moments and products of inertia. The highest frequency that should be generated in the robot should fall below the lowest resonance frequency.

So there is a trade-off between the accuracy of parameter estimates and the accuracy of the estimates of moments and products of inertia [101]. Chirped sinusoidal, sum of sinusoids, pseudo-random binary sequence (PRBS), and pulse-impact testing are suggested in literature for better trade-off [80].

Trajectory parameters can be calculated by either trial and error method or solving a nonlinear optimization problem. One of the popular criteria for the optimization is the logarithm of the determinant of the covariance matrix of the model parameter estimates, known as *d-optimality* criterion [63]. The criterion calculates the size of the uncertainty region of the model parameter estimates, and it is insensitive to model parameters if the joint position, velocity, and acceleration data are free of noise. In this case, the criterion depends only on the robot trajectory through the identification matrix, Φ, as well as on the covariance of the noise in the actuator torque measurements [36]. This property of the criterion is very useful when there is no prior knowledge of the model parameters available.

In the direct adaptive control methodology proposed in this thesis, the subspace predictor is calculated online, hence it is most important that the reference trajectory for the manipulator is optimized to form a good-conditioned case for system identification algorithm. However, a detailed overview and a deep insight into the trajectory parameterization and optimization are outside the scope of this dissertation.

2.3 Subspace Identification

As the dynamic parameters have a linear relationship, other identification techniques developed for linear plants like subspace identification can also be used [5]. SIMs are based on the solution of sequence of least-squares problems [74]. SIMs have many advantages over other classical system identification techniques [74]. Notables are:

- From plant's input and output data, a predictor is found. This bears similarity to the Kalman filter states, and transforms the analysis into a simple least

squares problem. As such, the whole architecture could be streamlined in a user-friendly fashion.

- When implemented in direct adaptive control, the plant model does not require simplification. Simplification or model reduction can omit useful information. Instead, in SIMs, all the plant information is stored in a compact form of a subspace predictor.

- The output of SIMs can be in the state space form which makes it easy to implement on a computer. However, its architecture has been exploited in different model free implementations as well [118, 33].

- Galvao et al. [35] compared N4SID with ARX identification and found that the state-space models identified by the N4SID algorithm consistently outperformed the ARX models at identifying the underlying dynamics in the structure. A marked improvement was observed to the identification of the eighth-order system by exciting the structure using a chirped signal. Interestingly, the improvements in the ARX residuals were not so visible, which suggests that in this example, the ARX model did not take full advantage of the richness in the excitation [35].

- For a six DOF of robot, the number of base dynamic parameters are 42. SIMs can handle the large dimensional problems commonly found in system identification for process control, producing fast and robust results. However, it must be pointed out that SIMs estimates are generally less accurate than those obtained from PE methods and standard SIMs are biased under closed-loop conditions [106].

In literature, there are many examples where SIMs have been used in the identification of the dynamic parameters of mechanical manipulators. Wernholt [113] used SIM to solve system identification problem for an ABB IRB-6600 robot. Hsu et al. [44] used N4SID in style translation for human motion. Johansson et al. [47] used

multiple input multiple output (MIMO) output-error state space model (MOESP) and N4SID subspace identification algorithms on an ABB IRB-2000 to derive a state space model for a mechanical manipulator. In this experiment, identification results were satisfactory but an innovation model could not be derived. Saleem and Sultan [84] proposed the use of subspace predictors in a predictive control of mechanical manipulators. Cescon [15] examined in detail the use of subspace algorithms in the identification of dynamic parameters of mechanical manipulators. These are some example applications of SIMs in the identification of mechanical manipulators.

2.4 Calculation of Subspace Predictor

In the first step, a predictor is calculated for the system described in (2.1). In order to formulate it, take T_p and T_f as the past and the future inputs of the system, respectively. Similarly, Y_p and Y_f are the past and the future outputs of the system. In model free control, the predictor predicts only a number of steps ahead, called the *prediction horizon.* Suppose that the prediction horizon is i and there are j different observations of prediction horizons, each of i length. For an n-link articulated manipulator, T_p and T_f can be written in the form of Hankel matrices as

$$T_p \triangleq \begin{bmatrix} \tau_0 & \tau_1 & \cdots & \tau_{j-1} \\ \tau_1 & \tau_2 & \cdots & \tau_j \\ \vdots & \vdots & \cdots & \vdots \\ \tau_{i-1} & \tau_i & \cdots & \tau_{i+j-2} \end{bmatrix} \in \Re^{in \times j} \tag{2.8}$$

$$T_f \triangleq \begin{bmatrix} \tau_i & \tau_{i+1} & \cdots & \tau_{i+j-1} \\ \tau_{i+1} & \tau_{i+2} & \cdots & \tau_{i+j} \\ \vdots & \vdots & \cdots & \vdots \\ \tau_{2i-1} & \tau_{2i} & \cdots & \tau_{2i+j-2} \end{bmatrix} \in \Re^{in \times j} \tag{2.9}$$

where each entry in the matrix corresponds to an n input-vector of torque generated by the joint actuators. Similarly, Y_p and Y_f can be written as

$$Y_p \triangleq \begin{bmatrix} y_0 & y_1 & \cdots & y_{j-1} \\ y_1 & y_2 & \cdots & y_j \\ \vdots & \vdots & \cdots & \vdots \\ y_{i-1} & y_i & \cdots & y_{i+j-2} \end{bmatrix} \in \Re^{3in \times j}$$

$$Y_f \triangleq \begin{bmatrix} y_i & y_{i+1} & \cdots & y_{i+j-1} \\ y_{i+1} & y_{i+2} & \cdots & y_{i+j} \\ \vdots & \vdots & \cdots & \vdots \\ y_{2i-1} & y_{2i} & \cdots & y_{2i+j-2} \end{bmatrix} \in \Re^{3in \times j}$$

where $y_k = \begin{bmatrix} q^T, \dot{q}^T, \ddot{q}^T \end{bmatrix}_k^T$. The Hankel matrix for the past outputs and inputs is defined as

$$W_p \triangleq \begin{bmatrix} T_p \\ Y_p \end{bmatrix} \tag{2.10}$$

The linear least squares predictor of Y_f with given W_p and T_f can be written as a minimization norm, i.e.,

$$\min_{L_w, L_\tau} \left\| Y_f - \begin{bmatrix} L_w & L_\tau \end{bmatrix} \begin{bmatrix} W_p \\ T_f \end{bmatrix} \right\|_F^2 \tag{2.11}$$

where $||\bullet||_F$ is the Frobenius norm or the Hilbert-Schmidt norm and L_w and L_τ are the subspace orthogonal projections. Frobenius norm of an $m \times n$ matrix is defined as the square root of the sum of the absolute squares of its elements. L_w and L_τ are calculated here using orthogonal projection of Y_f onto $\begin{bmatrix} W_p^T, T_F^T \end{bmatrix}^T$ similar to N4SID [90] as follows;

$$\hat{Y}_f = Y_f \begin{bmatrix} W_p \\ T_f \end{bmatrix}^T \left(\begin{bmatrix} W_p \\ T_f \end{bmatrix} \begin{bmatrix} W_p \\ T_f \end{bmatrix}^T \right)^\dagger \begin{bmatrix} W_p \\ T_f \end{bmatrix} \tag{2.12}$$

Substituting (2.12) in (2.11) yields

$$\begin{bmatrix} L_w & L_\tau \end{bmatrix} = Y_f \begin{bmatrix} W_p \\ T_f \end{bmatrix}^T \left(\begin{bmatrix} W_p \\ T_f \end{bmatrix} \begin{bmatrix} W_p \\ T_f \end{bmatrix}^T \right)^\dagger \tag{2.13}$$

where $L_w \in \Re^{3in \times 4in}$ and $L_\tau \in \Re^{3in \times in}$. This solution assumes that the problem is over-constrained; i.e., there are more independent equations than unknowns. If the problem is under-constrained, the pseudo-inverse cannot be computed. Future outputs can be predicted from the past inputs, past outputs, and the future inputs as follows;

$$\begin{bmatrix} \hat{y}_k \\ \vdots \\ \hat{y}_{k+i-1} \end{bmatrix} = L_w \begin{bmatrix} \tau_{k-i} \\ \vdots \\ \tau_{k-1} \\ y_{k-i} \\ \vdots \\ y_{k-1} \end{bmatrix} + L_\tau \begin{bmatrix} \tau_k \\ \vdots \\ \tau_{k+i-1} \end{bmatrix} \tag{2.14}$$

or

$$\hat{y}_f = L_{w1}(w_p)_k + L_\tau \tau_f \tag{2.15}$$

where $\hat{y}_f$ is a strictly causal estimate of future values for the joint variables; i.e., joint positions, joint velocities, and joint accelerations over a period of i steps. Figure 2.1 is a block diagram representation of subspace predictor indicated in (2.14). This predictor will be used in Chapter 3 to derive the model free control law.

2.4.1 Calculation of L_w, L_τ Using QR Decomposition

QR decomposition is considered to be the most widely used solution for least squares solution. It is renowned for providing a numerically stable solution. If

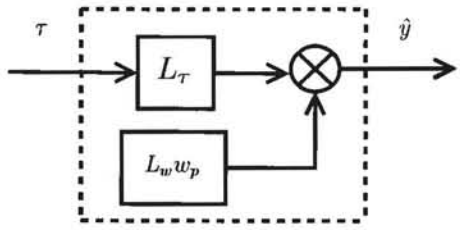

Figure 2.1: Subspace predictor

$$\begin{bmatrix} W_p \\ T_f \\ Y_f \end{bmatrix} = R^T Q^T = \begin{bmatrix} R_{11} & 0 & 0 \\ R_{21} & R_{22} & 0 \\ R_{31} & R_{32} & R_{33} \end{bmatrix} Q^T \tag{2.16}$$

then

$$\begin{bmatrix} L_w & L_\tau \end{bmatrix} = \begin{bmatrix} R_{31} & R_{32} \end{bmatrix} \begin{bmatrix} R_{11} & 0 \\ R_{21} & R_{22} \end{bmatrix}^\dagger \tag{2.17}$$

The pseudoinverse is normally calculated through SVD such that

$$\begin{bmatrix} R_{11} & 0 \\ R_{21} & R_{22} \end{bmatrix}^\dagger = U_{svd} \Sigma^{-1} V_{svd}^T \tag{2.18}$$

where U_{svd} and V_{svd}^T are orthogonal matrices and Σ is a diagonal matrix such that

$$\Sigma^{-1} = \begin{bmatrix} \sigma_1^{-1} & 0 & \dots & 0 \\ 0 & \sigma_2^{-1} & \dots & 0 \\ \vdots & \vdots & \ddots & \vdots \\ 0 & 0 & \dots & \sigma_{4in}^{-1} \end{bmatrix} \tag{2.19}$$

The computational complexity of QR decomposition is $O(i^2 j)$ and the computational complexity of SVD algorithm is $O(i^3)$. Hence, the overall complexity of QR factorization is $O(i^2 j + i^3)$ with storage requirement of $O(ij)$ [41].

2.4.2 Calculation of L_w, L_τ Using Cholesky Factorization

Cholesky factorization is a special type of LU factorization in which the matrix under consideration is Hermitian and positive definite. To solve (2.13), let

$$A \triangleq \begin{bmatrix} U_p \\ Y_p \\ U_f \\ Y_f \end{bmatrix} \in \Re^{8in \times j} \tag{2.20}$$

then using (2.16), the following expression can be written;

$$AA^T = R^T Q^T Q R \tag{2.21}$$

where Q is an orthogonal matrix; i.e., $Q^T Q = I$, hence

$$AA^T = R^T R \in \Re^{8in \times 8in} \tag{2.22}$$

where R is an upper triangular matrix, also called *Cholesky factor* [12]. It can be calculated using Cholesky factorization, i.e.,

$$R = \text{chol}(A^T A) \tag{2.23}$$

where chol($\bullet$) is a routine in MATLAB to calculate the Cholesky factor of $\bullet$ and $R \in \Re^{8in \times 8in}$. The computational complexity of calculating Cholesky factorization is $O(i^3)$ [41].

Multiplication of Hankel Matrices

$A^T A$ can be directly computed using a "brute force" technique that has the computational complexity of $O(i^2 j)$. So when combined with the Cholesky factorization, it results in overall complexity of $O(i^2 j + i^3)$, which is similar to QR/SVD algorithm.

Woodley et al. [118] exploited the structure of Hankel matrix in a way that dramatically reduces the number of steps required to perform the multiplication of these matrices. Using the definition in (2.20), AA^T can be expanded as

$$AA^T = \begin{bmatrix} T_pT_p^T & T_pY_p^T & T_pT_f^T & T_pY_f^T \\ Y_pT_p^T & Y_pY_p^T & Y_pT_f^T & Y_pY_f^T \\ T_fT_p^T & T_fY_p^T & T_fT_f^T & T_fY_f^T \\ Y_fT_p^T & Y_fY_p^T & Y_fT_f^T & Y_fY_f^T \end{bmatrix} \in \Re^{8in \times 8in} \tag{2.24}$$

Using the definitions in (2.8) and (2.9), $T_pT_f^T$ can be written as

$$T_pT_f^T = \left[\begin{array}{c|ccc} [T_pT_f^T]_{1,1} & [T_pT_f^T]_{1,2} & \cdots & [T_pT_f^T]_{1,i} \\ \hline [T_pT_f^T]_{2,1} & [T_pT_f^T]_{2,2} & \vdots & \vdots \\ \vdots & \vdots & \ddots & \vdots \\ [T_pT_f^T]_{i,1} & \cdots & \cdots & [T_pT_f^T]_{i,i} \end{array}\right] \in \Re^{in \times in} \tag{2.25}$$

where the grayed $(i-1)i$ entries are calculated directly in $2ij - j$ steps. The rest of the $(i-1)^2$ entries can be calculated using the following recursion;

$$\begin{aligned} [T_pT_f^T]_{r+1,s+1} &= [T_pT_f^T]_{r,s} + [T_p]_{r+1,j}[T_f^T]_{j,s+1} - [T_p]_{r,1}[T_f^T]_{1,s} \\ &\forall \quad 1 \le r \le i-1, \quad \forall \quad 1 \le s \le i-1 \end{aligned} \tag{2.26}$$

The above recursion reduces the computational complexity of $T_pT_f^T$ from $O(i^2j)$ to $O(ij + i^2)$. This is a significant improvement, especially when $j \gg i$. The same technique can be used to calculate other entries of AA^T. It can be seen in (2.24) that AA^T is symmetric. Hence, 10 entries of the upper triangular block of AA^T are sufficient to calculate AA^T.This further reduces the steps required to calculate AA^T.

Updating and Downdating of L_w, L_τ

If Cholesky/SVD method is used for calculation, the Cholesky factor can be updated in $O(i^2)$. New data available (τ_n, y_n) can be incorporated by appending a new column

at the end of A such that $A_{new} = \begin{bmatrix} A & a_{new} \end{bmatrix}$. The Cholesky factor R can be update using the following rank-1 update of Cholesky factorization;

$$\begin{aligned} R_{new} &= \text{chol}(AA^T + a_{new}a_{new}^T) \\ &= \text{cholupdate}(R, a_{new}, '+') \end{aligned}$$

where cholupdate is a Cholesky factor-update routine in MATLAB. Similarly, Cholesky factor can be downdated using

$$\begin{aligned} R_{new} &= \text{chol}(AA^T - a_{old}a_{old}^T) \\ &= \text{cholupdate}(R, a_{old}, '-') \end{aligned}$$

MATLAB employs a library to update Cholesky factor and that takes $O(i^2)$ operations to update Cholesky factor [28]. The actual details of updating Cholesky factorization are complex and are not presented here.

2.5 Faster Calculation of L_w, L_τ using Cholesky Factorization for Rank Deficient Matrices

The method proposed here is computationally faster. The memory requirement for this algorithm is $O(ij)$ and the complexity of this algorithm is $O(ij+i^3)$. It is shown in Table 2.1 that the proposed technique is faster than the one mentioned in 2.4.2. It should be noted that, for a fair comparison, the faster Hankel matrix multiplication as described in Section 2.4.2, was used for all the methods. These calculations were carried out in MATLAB on a workstation with a serial processor. This technique is specifically recommended when the data in Hankel matrices is rank deficient. The rank deficiency can occur when the plant is not properly excited, or if i and j are set too high.

Table 2.1: Computation time (in seconds) of different techniques to calculate subspace predictor

i	j	QR/SVD	Cholesky/SVD	Cholesky for rank deficient matrices
10	100	0.0055	0.0047	0.00090403
10	1000	0.0143	0.0062	0.0024
100	1000	1.2569	0.9353	0.1983

Theorem 2.1. *If measurements from the actuator torque (τ) is available for times $\{k-2i-j,\ldots,k-2,k-1\}$ and the measurements from the joint position, joint velocity, and joint acceleration is available for times $\{k-2i-j,\ldots,k-2,k-1\}$, then the subspace predictor can be calculated using following the relation;*

$$\begin{bmatrix} L_w & L_\tau \end{bmatrix} = \begin{bmatrix} Y_f T_p & Y_f Y_p & Y_f T_f \end{bmatrix} L^T (LL^T)^{-1} (LL^T)^{-1} L \tag{2.27}$$

where L is the Cholesky factor of $\begin{bmatrix} W_p^T, T_f^T \end{bmatrix}^T \begin{bmatrix} W_p^T, T_f^T \end{bmatrix}$ after removing zero rows.

L can be calculated on MATLAB using `cholinc(•,'inf')` command, where • is $\begin{bmatrix} W_p^T, T_f^T \end{bmatrix}^T \begin{bmatrix} W_p^T, T_f^T \end{bmatrix}$. Although, Cholesky/SVD and the proposed technique have the same complexity. However, the proposed method outperforms because the `inv` routine in MATLAB is optimized for positive-definite Hermitian matrices; while in Cholesky/SVD method, the `svd` command consumes more computational cycles to calculate the pseudoinverse.

Provided there are sufficient number of processors available, the computational complexity of Cholesky factorization, which is of order $O(i^3)$, can be reduced to $O(i)$ on a parallel architecture. Similarly, $(LL^T)^{-1}$ can be calculated on a parallel architecture in $O(\log i)$ [22].

The method presented by Courrieu [23] to calculate the pseudoinverse of rank deficient matrices and the following mathematical result [83] will be used in the proof of Theorem 2.1.

Lemma 2.1. *If A and B exist, then*

$$(AB)^\dagger = B^T (A^T ABB^T)^\dagger A^T \tag{2.28}$$

Proof of Theorem 2.1. Suppose $\left[W_p^T, T_f^T\right]^T = G$. Suppose $GG^T \in \Re^{i\times i}$ and the rank of of this matrix is r such that $r < i$. If Cholesky factorization is applied on this matrix, a unique upper triangular matrix is produced, let it be called S, with $i-r$ zero rows, such that $SS^T = GG^T$. If $i-r$ rows are removed from the matrix S, we get another matrix called L such that

$$GG^T = SS^T = L^T L \tag{2.29}$$

where $L \in \Re^{r\times i}$. If $B = G$ and $A = G^T$ in (2.28) and using it in (2.29), then it can be written that

$$(GG^T)^T = (L^T L)^T = L^T(LL^T)^{-1}(LL^T)^{-1}L \tag{2.30}$$

As

$$G = \begin{bmatrix} W_p \\ T_f \end{bmatrix} = \begin{bmatrix} T_p \\ Y_p \\ T_f \end{bmatrix}$$

then

$$GG^T = \begin{bmatrix} T_pT_p^T & T_pY_p^T & T_pT_f \\ Y_pT_p^T & Y_pY_p^T & Y_pT_f \\ T_fT_p^T & T_fT_p^T & T_fT_f^T \end{bmatrix}$$

The above matrix is symmetric, hence calculating the upper triangular part is sufficient to calculate the whole matrix. T_pT_f can be calculated intuitively using the recursive relationship in (2.26). Similarly, all the other terms can be calculated the same way. Subspace predictor can be calculated by substituting (2.30) in (2.13):

$$\begin{bmatrix} L_w & L_\tau \end{bmatrix} = \begin{bmatrix} Y_fT_p & Y_fY_p & Y_fT_f \end{bmatrix} L^T(LL^T)^{-1}(LL^T)^{-1}L \tag{2.31}$$

where Y_fT_p, Y_fY_p, and Y_fT_f can also be calculated using (2.26). □

2.5.1 Updating and Downdating of L_w, L_τ

The matrices T_p, T_f, Y_p, and Y_f can be downdated and updated in two steps. In the first step, the matrix is circular-shifted and in the second step, the last column is replaced with the new data. The complexity of first step is $O(ij)$ and the second step is $O(i)$. In MATLAB, `circshift` command is used to perform this operation. It has been found experimentally that this technique is significantly faster than first downdating by removing the first column, and then updating by concatenating a vector of new data at the end of the matrix. The performance is degraded in this process because a new memory location is allocated for the matrix when a column is removed or when a column is concatenated.

Let's suppose a mechanical manipulator with 6 DOF where $n = 6$ and $j = 50i$, then $A \in \Re^{48i \times 50i}$. In this case, the number of rows and columns of A are comparable to each other. Cholesky update procedure takes $O(i^2)$ steps to update the Cholesky factor, whilst the suggested technique takes $O(ij)$ steps to update the Hankel matrices. Because of the simplicity of the suggested technique, it outperforms the Cholesky update method in real time operations. In this regard, the proposed technique is suited more to the identification of mechanical systems, which involves a large number of input and output parameters.

It is proposed that Hankel matrices, T_p, T_f, Y_p, and Y_f, can also be updated using the following simple mathematical relation;

$$\begin{bmatrix} T \\ Y \end{bmatrix}_{k+1} = \begin{bmatrix} T \\ Y \end{bmatrix}_k \begin{bmatrix} \begin{bmatrix} S^*_{j-1} & 0 \end{bmatrix} \end{bmatrix} + \begin{bmatrix} \tau_o \\ \tau \\ y_o \\ y \end{bmatrix}_k \begin{bmatrix} \begin{bmatrix} 0 & 1 \end{bmatrix} \end{bmatrix} \tag{2.32}$$

where $\tau_o = T_{k\{n+1:n(i+1),j\}}$, $y_o = Y_{k\{3n+1:3n(i+1),j\}}$, and

$$S^*_{j-1} = \begin{bmatrix} 0 & 0 & \dots & 0 \\ 1 & 0 & \dots & 0 \\ 0 & 1 & \dots & 0 \\ \vdots & \vdots & \ddots & 0 \\ 0 & 0 & 0 & 1 \end{bmatrix} \in \Re^{j\times(j-1)}$$

$[\bullet]S^*_{j-1}$ truncates the first column of the matrix $[\bullet]$. In (2.32), τ_k is replaced with τ_{excite} during excitation phase, where τ_{excite} is the torque generated by the actuators during the excitation phase.

2.6 Results from Simulations

2.6.1 Experiment 1

A planar robot with two DOF was simulated using MATLAB and Simulink. Torque was applied using actuators mounted on manipulator joints to excite the plant. In order to evaluate the subspace predictor, the following steps were followed to calculate the error between the actual and predicted trajectories;

1. The prediction horizon, i, was chosen and a numerical experiment was performed with a given input vector. The resultant joint trajectory was recorded.

2. From the recorded trajectory, a predictor (L_w, L_τ) was calculated using a subspace projection algorithm.

3. The outputs were calculated using the subspace predictor for the given inputs.

4. The difference (i.e., error) between the calculated values and the actual values were plotted for each joint axis.

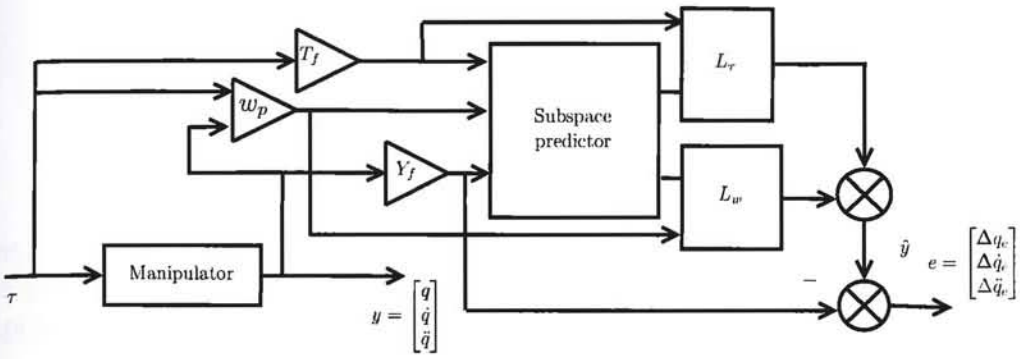

Figure 2.2: A block diagram showing the process followed for predictor identification and error calculation

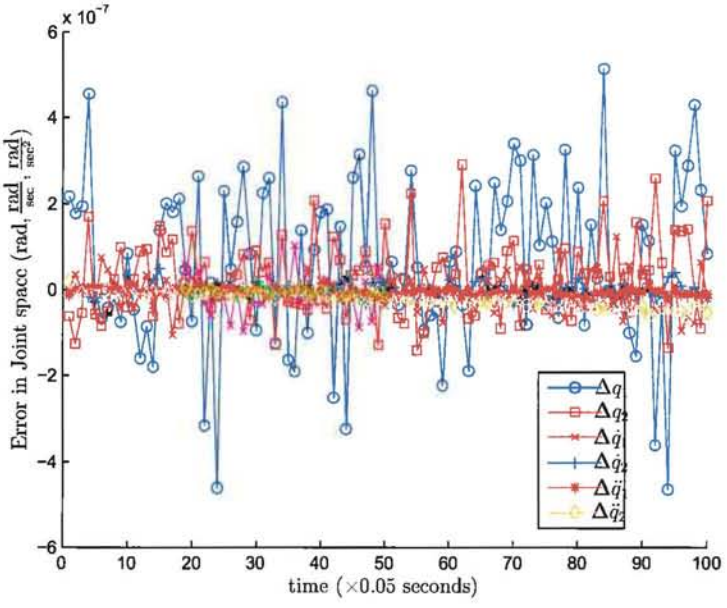

Figure 2.3: The difference between the predicted joint variables and the actual joint variables during the training mode [85]

The process followed to identify the subspace predictor and calculate the error is shown in Figure 2.2. The results from this simulation, which are plotted in Figure 2.3, suggests that the prediction error is in the range of 10^{-7} radians.

2.6.2 Experiment 2

SimMechanics toolbox of MATLAB was employed to simulate a bipedal leg with a torso. One of the challenges in simulations was to simulate foot-ground interaction. Many implementations were found in the literature [44, 72, 109, 116]. A model

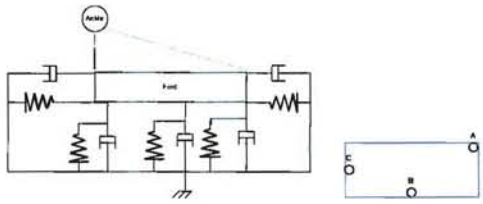

Figure 2.4: On the left is the side view and on the right is the top view of foot model where points A, B, and C are connected to three dampers and springs. Dampers and springs connected on sides are responsible for friction with the ground [84]

with three contact points was devised to simulate the human foot. This is shown in figure 2.4. It was assumed that there are only three points where the foot touches the ground and there is no air friction.

Under the action of normal gravity and exogenous force signals at each joint, the leg falls down, and the joint trajectory of the torso is recorded as shown in Figure 2.5. Using subspace identification, a predictor is found. This predictor is then applied on the input joint signals. The procedure for evaluating the error between the actual and the predicted trajectories is similar to what has been indicated in Section 2.6.1 and depicted in Figure 2.2. The error in joint space was translated to operational space and plotted in Figure 2.6.

It was found that for prediction horizon i less than a certain value, the system simply fails to predict the future outputs. Some suggest that the value of i should be 2 to 3 times the expected order of the system for stable and accurate results [117], however, there is no hard and fast rule. In the experiments performed for this thesis, the prediction horizon more than 10 did not improve the accuracy of the prediction. Increasing the value of i can also be computationally expensive. It can be seen in the simulation and graphs that for movements of more than 1 meter, the error is in the order of micrometers. These results are very encouraging especially when there are multiple rigid bodies which are coupled together with rotatory joints and complex foot-ground interaction.

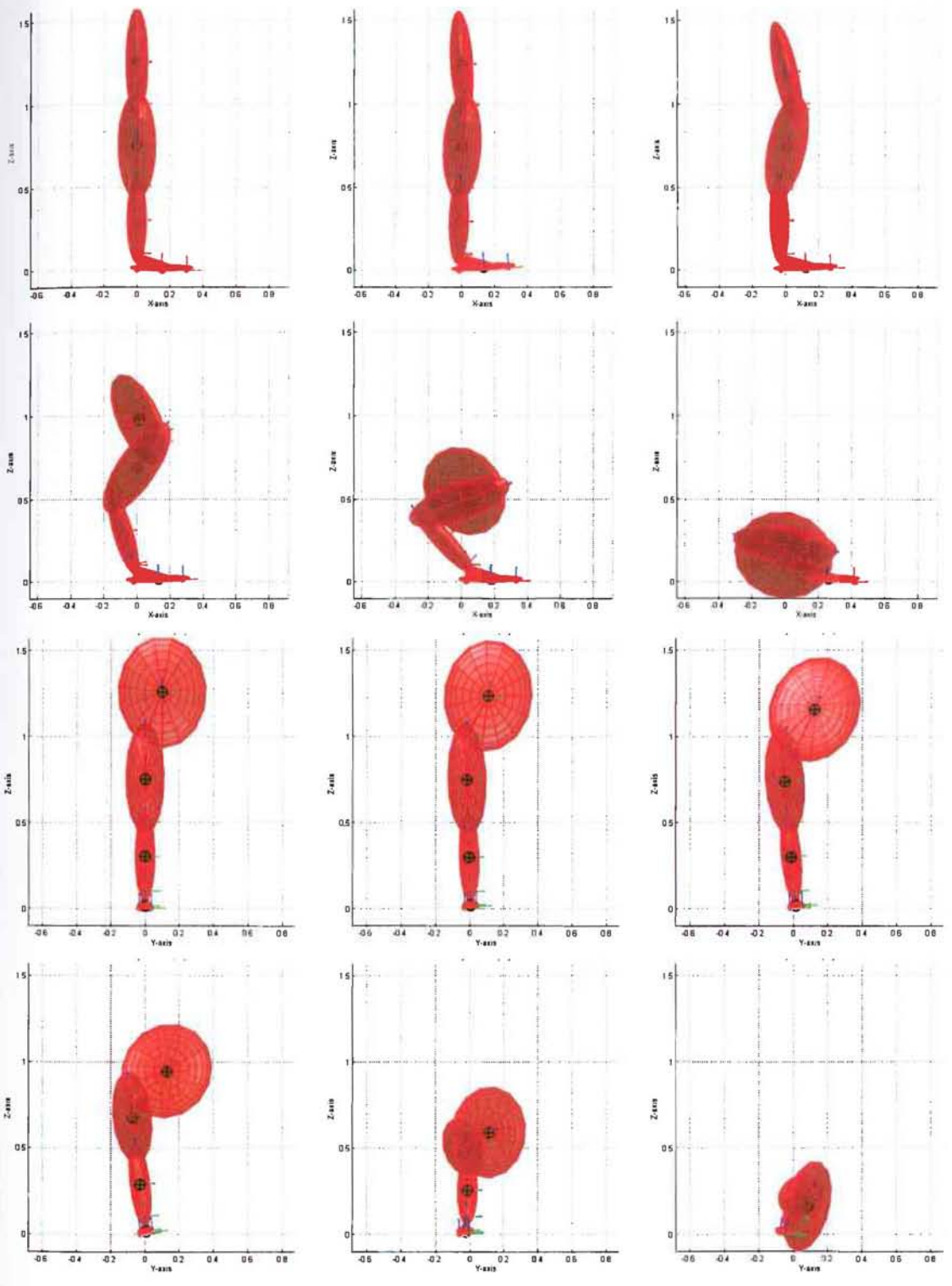

Figure 2.5: Free fall of a biped leg with exogenous force signals acting on its joints. Top six and bottom six shots were taken from the same simulation but from different angles after every 0.1 second [84]

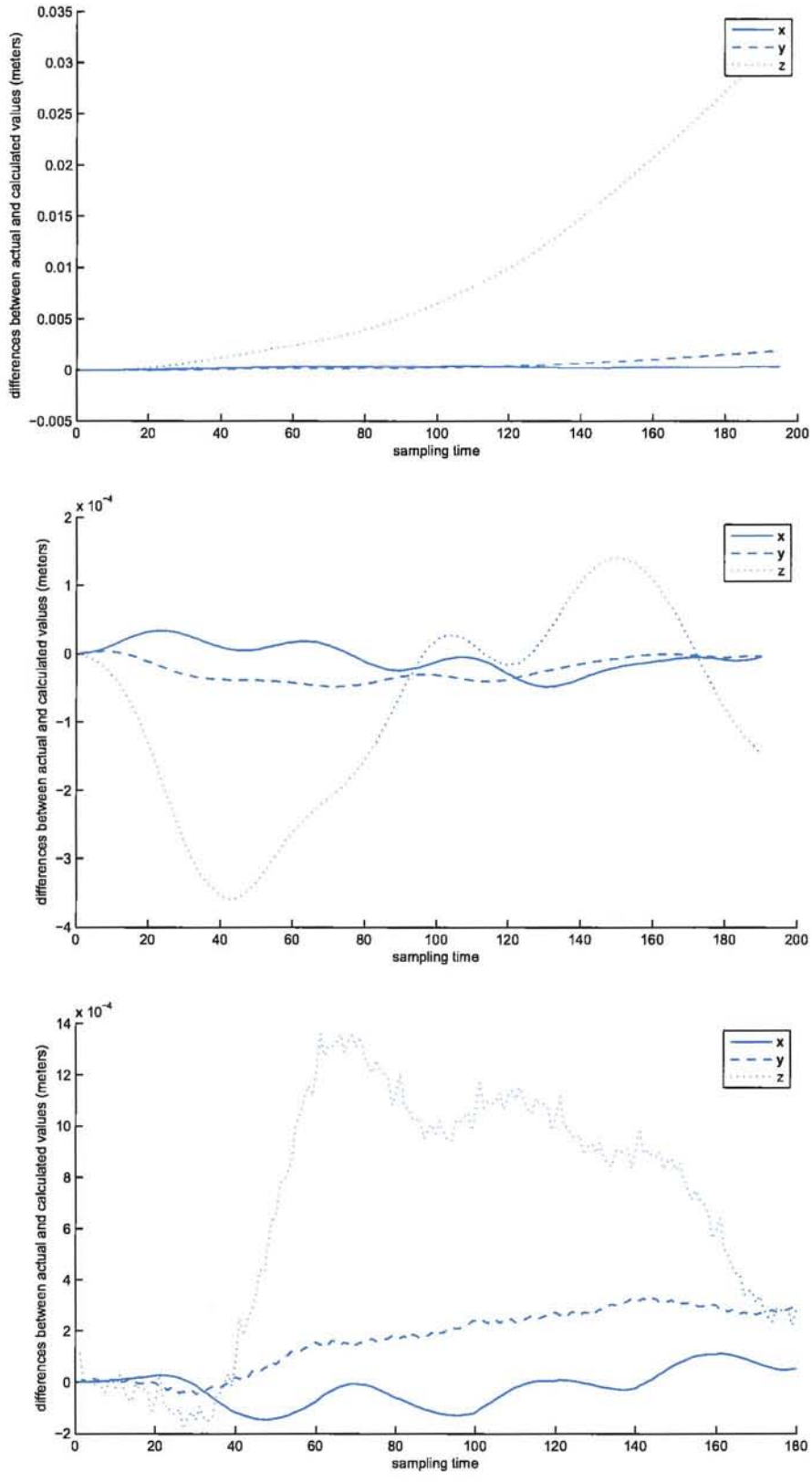

Figure 2.6: Error in the calculation of the torso position. Above graphs are with $i = 5, i = 10$, and $i = 20$ respectively. Note that the largest movement of torso is in the z-direction, the error is also mostly in this direction, which shows that the error is increased when the same value of subspace predictor is used for larger movements of end-effector in operational space [84]

2.7 Summary

The important results of this chapter are:

- A fast method of calculating the subspace predictor L_w, L_τ is presented for rank-deficient matrices (2.27);
- An efficient method of updating the subspace predictor for robot manipulators described in Section 2.5.1;
- A simplified mathematical relation to update the subspace predictor (2.32); and
- Using the method shown in Figure 2.2, results of simulations on different mechanical manipulators are given in Figures 2.6 and 2.5. The latter simulation uses foot-ground interaction shown in Figure 2.4.

Chapter 3

Model Free Operational Space $\mathscr{H}_\infty$ Control

This chapter formulates control laws using the linear subspace models evaluated in Chapter 2. Section 3.1 establishes a framework to incorporate the reference trajectory in operational space. Section 3.2 formulates a model free $\mathscr{H}_\infty$ non-robust control. Section 3.3 deduces non-robust $\mathscr{H}_2$ control law; and lastly, Section 3.4 formulates a model free $\mathscr{H}_\infty$ robust control law with additive uncertainty.

3.1 Operational Space Control

If the task is given in operational space then it becomes inevitable to cater for the non-linearities introduced by the forward and inverse kinematics functions. First, the joint variables are translated into operational space. The resultant is compared to the reference trajectory and the error is then converted back to joint space, as shown in Figure 3.1.

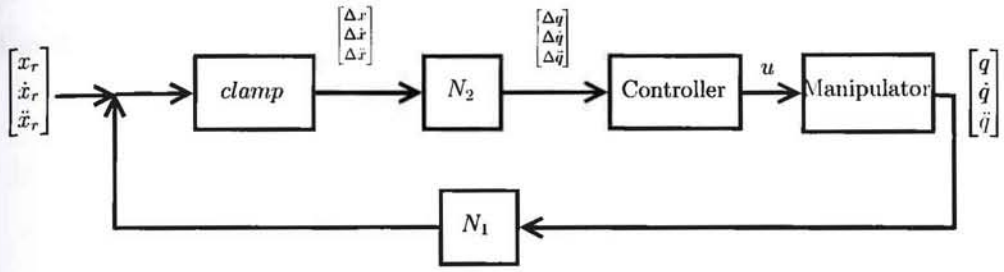

Figure 3.1: Operational space control of an articulated manipulator

If x is the end-effector position and $F(q)$ is the forward kinematic function then its derivatives can be written as

$$x = F(q) \tag{3.1}$$

$$\dot{x} = \frac{F(q)}{\partial q}\frac{\partial q}{\partial t} = J(q)\dot{q} \tag{3.2}$$

$$\ddot{x} = J(q)\ddot{q} + \dot{J}(q,\dot{q})\dot{q} \tag{3.3}$$

where $J(q)$ is the systems Jacobian and $\dot{J}(q)$ is its time-derivate. The Jacobian can be formulated using the differential or pushforward of $F(q)$ [95] as follows;

$$J(q) = \frac{\partial F(q)}{\partial q} = \begin{bmatrix} \frac{\partial f_1(q)}{\partial q_1} & \frac{\partial f_1(q)}{\partial q_2} & \cdots & \frac{\partial f_1(q)}{\partial q_n} \\ \frac{\partial f_2(q)}{\partial q_1} & \frac{\partial f_2(q)}{\partial q_2} & \cdots & \frac{\partial f_2(q)}{\partial q_n} \\ \vdots & \vdots & \ddots & \vdots \\ \frac{\partial f_l(q)}{\partial q_1} & \frac{\partial f_l(q)}{\partial q_2} & \cdots & \frac{\partial f_l(q)}{\partial q_n} \end{bmatrix} \tag{3.4}$$

where l is the number of DOF for the end-effector. The time derivative of a Jacobian column is the sum of the partial derivatives of this column with respect to joint variables, multiplied by the time-derivates of these variables [13]. As such, time-derivative of the i^{th} column of the Jacobian is given by

$$\dot{J}^i(q,\dot{q}) = \sum_{j=1}^{n} \frac{\partial J^i(q)}{\partial q^j}\frac{\partial q^j}{\partial t} = \sum_{j=1}^{n} \frac{\partial J^i(q)}{\partial q^j}\dot{q}^j \tag{3.5}$$

Equations (3.1), (3.2), and (3.3) can be combined as follows;

$$\begin{bmatrix} x \\ \dot{x} \\ \ddot{x} \end{bmatrix} = \begin{bmatrix} \frac{F(q)}{q} & 0 & 0 \\ 0 & J(q) & 0 \\ 0 & \dot{J}(q,\dot{q}) & J(q) \end{bmatrix} \begin{bmatrix} q \\ \dot{q} \\ \ddot{q} \end{bmatrix} \tag{3.6}$$

or

$$\begin{bmatrix} x \\ \dot{x} \\ \ddot{x} \end{bmatrix} = N_1 y \tag{3.7}$$

where $N_1 \in \Re^{3l \times 3n}$ and

$$\frac{F(q)}{q} = \begin{bmatrix} \frac{f_1(q)}{q_1} & 0 & \dots & 0 \\ \frac{f_2(q)}{q_1} & 0 & \dots & 0 \\ \vdots & \vdots & \ddots & 0 \\ \frac{f_l(q)}{q_1} & 0 & 0 & 0 \end{bmatrix} \in \Re^{l \times n} \tag{3.8}$$

The above matrix produces large values for very small values of q_1. To avoid this situation, a limit is imposed here on the value of q_1 so that there is always a valid solution available. The reason for using $\frac{F(q)}{q}$ instead of $F(q)$ in (3.6) is that the output of subspace predictor is $\left[q^T, \dot{q}^T, \ddot{q}^T\right]^T$. Use of (3.6) makes it possible to connect different blocks of the system mathematically.

For conversion of the error from the reference operational space trajectory and the output of the forward kinematics block, a similar approach is adopted. Let $\left[\Delta x, \Delta \dot{x}, \Delta \ddot{x}\right]^T$ be the error in operational space. If the error is small, then (3.2) can be approximated to

$$\Delta x \approx J(q)\Delta q \tag{3.9}$$

However, it can be stated, without any approximation, that

$$\Delta \dot{x} = J(q)\Delta \dot{q} \tag{3.10}$$

$$\Delta \ddot{x} = \dot{J}(q,\dot{q})\Delta \dot{q} + J(q)\Delta \ddot{q} \tag{3.11}$$

It is a common practice that when end-effector trajectory is formulated in operational space, Δx is chosen in (3.9) such that the approximate movement of the end-effector partially matches the target velocities in (3.10) [115]. Equation (3.9) is only valid for a small value of Δx. If the target position is too distant, it is important to bring the target closer. This way, the manipulator reaches its final target in smaller steps. For this reason, Δx needs to be clamped such that

$$clamp(\Delta x, D_{max}) = \begin{cases} \Delta x \text{ if } ||\Delta x|| < D_{max} \\ D_{max} \frac{\Delta x}{||\Delta x||} \text{ otherwise} \end{cases} \tag{3.12}$$

where $||\bullet||$ is the Euclidean norm. The value of the scalar D_{max} should be at least several times larger than what end-effector moves in a single step and less than half the length of a typical link. This heuristic approach has also been reported to reduce oscillations in the system, which allows the designer to use a smaller value for damping constant. This usually results in a quicker response [14]. To calculate the error in joint space, (3.9), (3.10), and (3.11) can be written as

$$\Delta q = J^\dagger(q)\Delta x \tag{3.13}$$

$$\Delta \dot{q} = J^\dagger(q)\Delta \dot{x} \tag{3.14}$$

$$\Delta \ddot{q} = J^\dagger(q)(\Delta \ddot{x} - \dot{J}(q,\dot{q})\Delta \dot{q}) = J^\dagger(q)\Delta \ddot{x} - J^\dagger(q)\dot{J}(q,\dot{q})J^\dagger(q)\Delta \dot{x} \tag{3.15}$$

In matrix form, these equations can be written as

$$\begin{bmatrix} \Delta q \\ \Delta \dot{q} \\ \Delta \ddot{q} \end{bmatrix} = \begin{bmatrix} J^\dagger(q) & 0 & 0 \\ 0 & J^\dagger(q) & 0 \\ 0 & -J^\dagger(q)\dot{J}(q,\dot{q})J^\dagger(q) & J^\dagger(q) \end{bmatrix} \begin{bmatrix} \Delta x \\ \Delta \dot{x} \\ \Delta \ddot{x} \end{bmatrix} \tag{3.16}$$

or alternatively

$$\Delta y = N_2 \begin{bmatrix} \Delta x \\ \Delta \dot{x} \\ \Delta \ddot{x} \end{bmatrix} \tag{3.17}$$

where $J^\dagger(q)$ is the pseudoinverse of $J(q)$. Pseudoinverse is defined for all matrices including the ones which are not square or are not full rank. It also gives the best solution in terms of least squares. The pseudoinverse gives a stable solution even in those cases when the target end-effector position doesn't lie in the work volume of the mechanical manipulator. The resulting solution is closest location to its target which minimizes $||J(q)\Delta q - \Delta x||^2$. However, the pseudoinverse suffers from stability issues near singularities. If a manipulator is at a singular position, the pseudoinverse doesn't tend to move the manipulator in any direction. In the vicinity of singularity, the pseudoinverse creates large changes in joint variables, even for very small changes in the end-effector, resulting in an unstable system. One important feature of pseudoinverse is that the term $(I - J^\dagger(q)J(q))$ projects on the null space of $J(q)$. This feature can be exploited for redundant manipulators. It is possible to generate internal motions in a redundant manipulator, i.e., $\dot{q}_0$, without changing its end-effector position [89]. For redundant manipulators, (3.2) can be written as

$$\dot{x} = J(q)\dot{q} + (I - J^\dagger(q)J(q))\dot{q}_0 \tag{3.18}$$

The damped least-squares (DLS) method, which is also referred to the Levenberg-Marquardt method, solves many problems related to pseudoinverse. The method gives a numerically stable solution near singularities, and was first used in inverse kinematics by Wampler [108] and Nakamura and Hanafusa [70]. It was also used for theodolite calibration by Sultan and Wager [97].

Not only does DLS minimize the term $||J(q)\dot{q} - \dot{x}||^2$ but it also minimizes the joint velocities with a damping factor, i.e., $\lambda^2||\dot{q}||^2$ where $\lambda \in \Re$ and $\lambda \neq 0$. The function to be minimized can be written as

$$\min_{\dot{q}} \left\{ ||J(q)\dot{q} - \dot{x}||^2 + \lambda^2||\dot{q}||^2 \right\} \tag{3.19}$$

The DLS solution is equal to [14]

$$\dot{q} = (J^T(q)J(q) + \lambda^2 I)^{-1} J^T(q)\dot{x} \tag{3.20}$$

or alternatively

$$\dot{q} = J^T(q)(J(q)J^T(q) + \lambda^2 I)^{-1}\dot{x} \tag{3.21}$$

Equation (3.20) requires an inversion of an $n \times n$ matrix, while (3.21) requires an inversion of only an $l \times l$ matrix, which is computationally more efficient. In terms of SVD, the singular values change from $\frac{1}{\sigma^2}$ for $J^\dagger(q)$ to $\frac{\sigma^2}{\sigma^2+\lambda^2}$ for $(J(q)J^T(q) + \lambda^2 I)^{-1}$ [14]. If $\sigma_i \to 0, \frac{1}{\sigma_i} \to \infty$, while in the other case, $\frac{\sigma^2}{\sigma^2+\lambda^2} \to \frac{1}{\lambda^2}$ when $\sigma_i \to 0$. Therefore, a stable solution is observed even near singularities for $\forall\lambda : \lambda \neq 0$. Using (3.21), N_2 can be redefined as

$$N_2 \triangleq \begin{bmatrix} J^*(q) & 0 & 0 \\ 0 & J^*(q) & 0 \\ 0 & -J^*(q)\dot{J}(q,\dot{q})J^*(q) & J^*(q) \end{bmatrix} \in \Re^{3l\times 3n} \tag{3.22}$$

where $J^*(q) = J^T(q)(J(q)J^T(q) + \lambda^2 I)^{-1}$. The value of λ is set by the designer. Large values can result in a slower convergence rate and very small values can reduce the effectiveness of the method. In literature, there are many methods proposed to select the value of λ dynamically [66, 70, 17]. In Chapter 6, different values of λ are tested to examine its effect on the performance and the stability of the system and then a control law is synthesized to find the optimum value of λ.

3.2 Model Free Subspace Based Operational Space $\mathscr{H}_\infty$ Control

Figure 3.2 shows a generalized feedback system. The plant has two inputs, d is the disturbance signal and u is the input from the controller. The variable to be controlled is z, and a certain behaviour is desired from it. The measured output,

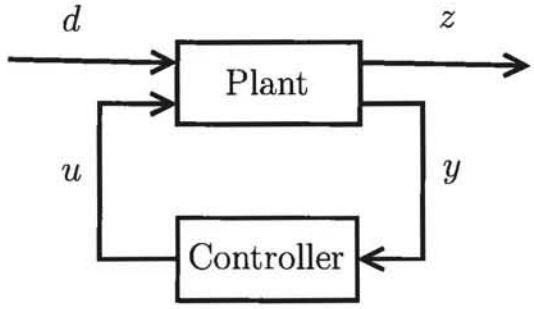

Figure 3.2: Generalized feedback system

y, is fed into the controller. In terms of $\mathscr{H}_\infty$ optimal control, the transfer function from the disturbance signals to the controlled variables is minimized [65] such that

$$||F_{zd}||_\infty < \gamma \tag{3.23}$$

where F_{zd} is the transfer function from disturbance signals d to the controlled variables z, and $\gamma \in \Re : \gamma > 0$. γ is a factor by which the disturbance input vector d bounds to the design output z. $||\bullet||_\infty$ is defined as [40]

$$||F_{zd}||_\infty = \sup_{\substack{d \in \mathscr{L}_2(0,\infty) \\ ||d||_2 = 1}} \frac{||z||_2}{||d||_2} \tag{3.24}$$

where norms $||z||_2$ and $||d||_2$ are defined as

$$||z||_2 = \sqrt{\int_0^\infty z^T(t)z(t)dt}$$

$$||d||_2 = \sqrt{\int_0^\infty d^T(t)d(t)dt}$$

or in terms of $\mathscr{L}^p$ spaces

$$\lim_{p\to\infty} ||F_{zd}||_p = \lim_{p\to\infty} (|F_{zd_1}|^p + |F_{zd_2}|^p + \cdots + |F_{zd_n}|^p)^{\frac{1}{p}} \tag{3.25}$$

$$= \max\{|F_{zd_1}| + |F_{zd_2}| + \cdots + |F_{zd_n}|\} \tag{3.26}$$

$$= ||F_{zd}||_\infty \tag{3.27}$$

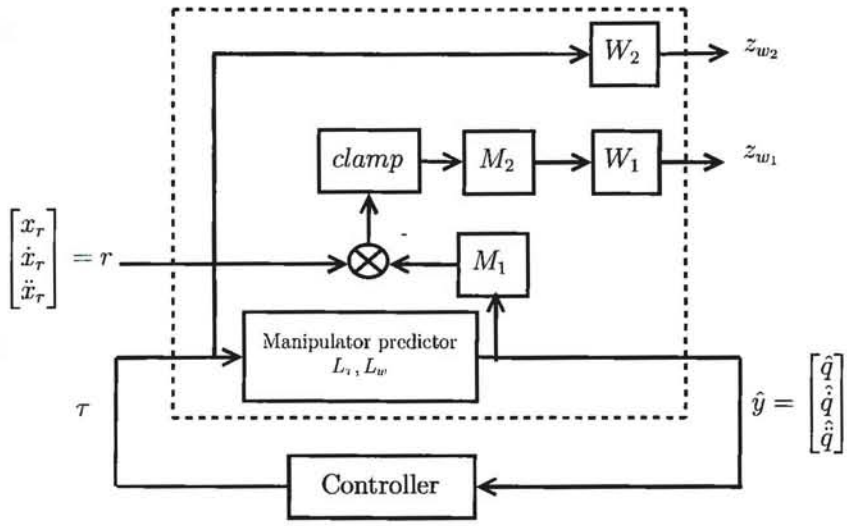

Figure 3.3: Model free subspace based operational space $\mathscr{H}_\infty$ control. Dynamic parameters of the robotic manipulator are unknown and the controller is synthesized in realtime

Intuitively, $||F_{zd}||_\infty < \gamma$ can be interpreted as a $\gamma-$level $\mathscr{H}_\infty$ control scheme in which the effect of disturbances is minimized onto the controlled variables. These controlled variables arise from weighted exogenous signals [29].

Figure 3.3 shows the complete system to be controlled. The *manipulator predictor* is as depicted in Figure 2.1 and r is the reference trajectory in operational space. W_1 and W_2 are frequency dependant performance weights. These weights are chosen by the designer such that W_1 is a low pass filter and W_2 is a high pass or a band-stop filter [102]. Their gain must be finite over all frequencies, and as a consequence, they must have relative McMillan degree 0 [117].

Theorem 3.1. *If measurements of the torque vector (τ), joint vector (y), and reference trajectory (r) in operational space are available for times $\{k-i,\ldots,k-2,k-1\}$, then the strictly causal subspace based, γ-level $\mathscr{H}_\infty$ control for times $\{k,\ldots,k+i,k+i-1\}$ is given by*

$$\tau_{opt} \triangleq \left(L_\tau^T M_1^T \widetilde{Q}_1 M_1 L_\tau + Q_2\right)^{-1} \begin{bmatrix} \left(-L_\tau^T M_1^T \widetilde{Q}_1 M_1 L_w\right)^T \\ \left(L_\tau^T M_1^T (\gamma^{-2}\widetilde{Q}_1 + I) M_2^T H_1^T \Gamma_1\right)^T \\ \left(-H_2^T \Gamma_2\right)^T \end{bmatrix}^T \begin{bmatrix} w_p \\ x_{w_1} \\ x_{w_2} \end{bmatrix}_k \tag{3.28}$$

provided that

$$\gamma > \gamma_{\min} \triangleq \sqrt{\bar{\lambda}[(M_2^T Q_1 M_2)^{-1} + M_1 L_\tau Q_2^{-1} L_\tau^T M_1^T]^{-1}} \tag{3.29}$$

where

- $\widetilde{Q}_1 \triangleq ((M_2^T Q_1 M_2)^{-1} - \gamma^{-2} I)^{-1}$
- *Optimum torque is given by*

$$\tau_{opt} = \begin{bmatrix} \tau_k \\ \vdots \\ \tau_{k+i-1} \end{bmatrix}$$

- *Forward and inverse kinematics matrices for the prediction horizon i is defined using N_1 and N_2, i.e.,*

$$M_1 \triangleq \begin{bmatrix} N_1 & 0 & \dots & 0 \\ 0 & N_1 & \dots & 0 \\ \vdots & \vdots & \ddots & 0 \\ 0 & 0 & \dots & N_1 \end{bmatrix} \in \Re^{3li \times 3ni} \tag{3.30}$$

$$M_2 \triangleq \begin{bmatrix} N_2 & 0 & \dots & 0 \\ 0 & N_2 & \dots & 0 \\ \vdots & \vdots & \ddots & 0 \\ 0 & 0 & \dots & N_2 \end{bmatrix} \in \Re^{3ni \times 3li} \tag{3.31}$$

- *The state of the discrete linear time invariant (LTI) weighting filters W_1 and W_2 can be updated using*

$$\begin{aligned}
(x_{w_1})_{k+1} &= A_{w_1}(x_{w_1})_k + B_{w_1}(M_2(r_k - M_1 y_k)) \\
(z_{w_1})_k &= C_{w_1}(x_{w_1})_k + D_{w_1}(M_2(r_k - M_1 y_k)) \\
(x_{w_2})_{k+1} &= A_{w_2}(x_{w_2})_k + B_{w_2}(\tau_k) \\
(z_{w_2})_k &= C_{w_2}(x_{w_2})_k + D_{w_2}(\tau_k)
\end{aligned} \tag{3.32}$$

- *H_1 and H_2 are the impulse responses of W_1 and W_2, respectively. They are defined as*

$$H_1 \triangleq \begin{bmatrix}
D_{w_1} & 0 & 0 & \cdots & 0 \\
C_{w_1}B_{w_1} & D_{w_1} & 0 & \cdots & 0 \\
C_{w_1}A_{w_1}B_{w_1} & C_{w_1}B_{w_1} & D_{w_1} & \cdots & 0 \\
\vdots & \vdots & \vdots & \ddots & \vdots \\
C_{w_1}A_{w_1}^{i-2}B_{w_1} & C_{w_1}A_{w_1}^{i-3}B_{w_1} & C_{w_1}A_{w_1}^{i-4}B_{w_1} & \cdots & D_{w_1}
\end{bmatrix} \tag{3.33}$$

$$H_2 \triangleq \begin{bmatrix}
D_{w_2} & 0 & 0 & \cdots & 0 \\
C_{w_2}B_{w_2} & D_{w_2} & 0 & \cdots & 0 \\
C_{w_2}A_{w_2}B_{w_2} & C_{w_2}B_{w_2} & D_{w_2} & \cdots & 0 \\
\vdots & \vdots & \vdots & \ddots & \vdots \\
C_{w_2}A_{w_2}^{i-2}B_{w_2} & C_{w_2}A_{w_2}^{i-3}B_{w_2} & C_{w_2}A_{w_2}^{i-4}B_{w_2} & \cdots & D_{w_2}
\end{bmatrix} \tag{3.34}$$

- $Q_1 \triangleq H_1^T H_1, Q_2 \triangleq H_2^T H_2$

- *The extended observability matrices, Γ_1 and Γ_2, formed from the impulse responses of the weighting filters W_1 and W_2 are given as follows;*

$$\Gamma_1 \triangleq \begin{bmatrix} C_{w_1} \\ C_{w_1}A_{w_1} \\ \vdots \\ C_{w_1}A_{w_1}^{i-1} \end{bmatrix} \tag{3.35}$$

$$\Gamma_2 \triangleq \begin{bmatrix} C_{w_2} \\ C_{w_2}A_{w_2} \\ \vdots \\ C_{w_2}A_{w_2}^{i-1} \end{bmatrix} \tag{3.36}$$

- $(w_p)_k$ *is a vector made up of past values of τ and y given by*

$$(w_p)_k \triangleq \begin{bmatrix} \tau_{k-i} \\ \vdots \\ \tau_{k-1} \\ y_{k-i} \\ \vdots \\ y_{k-1} \end{bmatrix}$$

The control law given in (3.28) is a strictly causal controller and doesn't depend on the current value of the reference trajectory. Intuitively, it can be seen that the future optimum torque vector for the robot manipulator depends on the state of the weights and the past values of both torques and joint variables.

To ensure stability, γ is selected such that $\gamma = 1.1\gamma_{\min}$ [117]. Higher value of γ increases the stability of the system at the cost of performance.

The following mathematical results will be used in the proof of Theorem 3.4 [10, 41].

Lemma 3.1. *If* A^{-1}, C^{-1}, $(BAB^T + C)^{-1}$, *and* $(A^{-1} + B^T C^{-1} B)^{-1}$ *exist, then*

$$A - AB^T(BAB^T + C)^{-1}BA = (A^{-1} + B^T C^{-1} B)^{-1} \tag{3.37}$$

$$AB^T(BAB^T + C)^{-1} = (A^{-1} + B^T C^{-1} B)^{-1} B^T C^{-1} \tag{3.38}$$

Lemma 3.2. *If* A_1^{-1}, A_3^{-1}, *and* $\begin{bmatrix} A_1 & A_2 \\ A_2^T & A_3 \end{bmatrix}^{-1}$ *exit, then*

$$\begin{bmatrix} A_1 & A_2 \\ A_2^T & A_3 \end{bmatrix}^{-1} = \begin{bmatrix} (A_1 - A_2 A_3^{-1} A_2^T)^{-1} & -(A_1 - A_2 A_3^{-1} A_2^T)^{-1} A_2 A_3^{-1} \\ -(A_3 - A_2^T A_1^{-1} A_2)^{-1} A_2^T A_1^{-1} & (A_3 - A_2^T A_1^{-1} A_2)^{-1} \end{bmatrix}$$

Lemma 3.3. *If* A_1, A_2^{-1}, *and* A_3^{-1} *exit, then according to Schur decomposition*

$$\begin{bmatrix} A_1 & A_2 \\ A_2^T & A_3 \end{bmatrix} = \begin{bmatrix} I & A_2 A_2^{-1} \\ 0 & I \end{bmatrix} \begin{bmatrix} A_1 - A_2 A_3^{-1} A_2^T & 0 \\ 0 & A_3 \end{bmatrix} \begin{bmatrix} I & 0 \\ A_3^{-1} A_2^T & I \end{bmatrix} \tag{3.39}$$

Lemma 3.4. *If* $\begin{bmatrix} A_1 & A_2 \\ A_2^T & A_3 \end{bmatrix}$ *is a Hessian such that* $A_3 = A_3^T$ *and it has been formulated by double differentiation of* $\begin{bmatrix} a^T, b^T \end{bmatrix}^T$ *for the maximum and minimum values of* a *and* b, *respectively, then*

$$A_1 - A_2 A_3^{-1} A_2^T < 0 \tag{3.40}$$

$$A_3 > 0 \tag{3.41}$$

Proof of Lemma 3.4. From (3.39)

$$\begin{bmatrix} A_1 & A_2 \\ A_2^T & A_3 \end{bmatrix} = \begin{bmatrix} I & A_2 A_3^{-1} \\ 0 & I \end{bmatrix} \begin{bmatrix} A_1 - A_2 A_3^{-1} A_2^T & 0 \\ 0 & A_3 \end{bmatrix} \begin{bmatrix} I & 0 \\ A_3^{-1} A_2^T & I \end{bmatrix} \tag{3.42}$$

The matrices on sides in (3.42) are transpose of each other, hence they do not affect the polarity of the terms in the middle matrix. As the top rows were differentiated by the variable to be maximized, hence

$$A_1 - A_2 A_3^{-1} A_2^T < 0$$

and similarly, the bottom rows were differentiated by the variable to be minimized, hence

$$A_3 > 0$$

□

Proof of Theorem 3.1. The reference signal r is defined as

$$r \triangleq \begin{bmatrix} x_k \\ \dot{x}_k \\ \ddot{x}_k \\ \vdots \\ x_{k+i-1} \\ \dot{x}_{k+i-1} \\ \ddot{x}_{k+i-1} \end{bmatrix} \in \Re^{3il}$$

where l is the number of DOF in operational space. In time domain, W_1 and W_2 can be formulated using their impulse responses (Markov parameters) and extended observability matrices. The output of these weights can be given by

$$\begin{bmatrix} z_{w_1} \\ z_{w_2} \end{bmatrix} = \begin{bmatrix} H_1(e) + \Gamma_1(x_{w_1})_k \\ H_2(\tau) + \Gamma_2(x_{w_2})_k \end{bmatrix} \tag{3.43}$$

where x_{w_1} and x_{w_2} are the state variables for the weighting matrices W_1 and W_2. These weights are normally assigned by the designer.

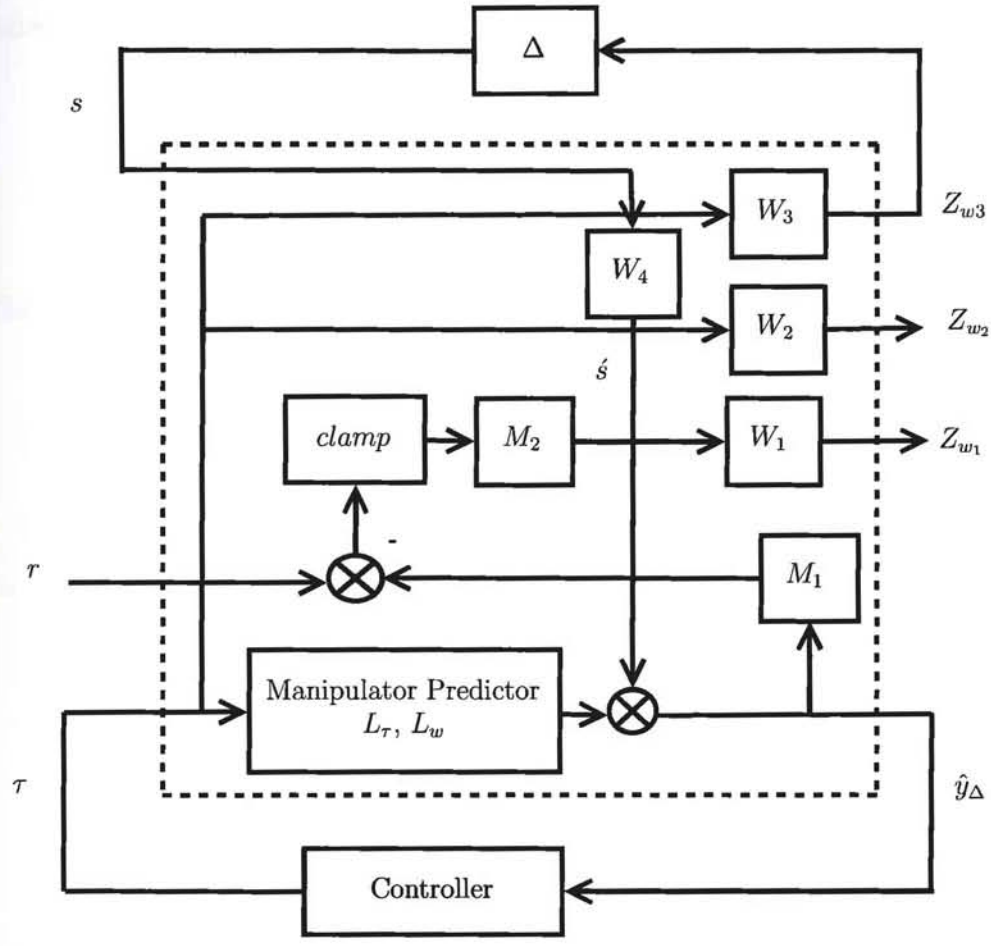

Figure 3.4: Model free subspace based operational space $\mathscr{H}_\infty$ robust control Subspace identification of an articulated manipulator in operational space in the presence of uncertainties

From figure 3.4, $e = M_2(r - M_1\hat{y}_f)$, hence (3.43) becomes

$$\begin{bmatrix} z_{w_1} \\ z_{w_2} \end{bmatrix} = \begin{bmatrix} H_1(M_2(r - M_1\hat{y}_f)) + \Gamma_1(x_{w_1})_k \\ H_2(\tau) + \Gamma_2(x_{w_2})_k \end{bmatrix} \tag{3.44}$$

The cost function to minimize the control effort and the feedback error for the given refence trajectory as bounded by γ is given by

$$L(\gamma) = z_{w_1}^T z_{w_1} + z_{w_2}^T z_{w_2} - \gamma^2 r^T r, \tag{3.45}$$

where the objective is

$$\min_{\tau} \max_{r} L(\gamma) < 0$$

Substituting the cost function in (3.45) gives

$$\min_{\tau}\max_{r}\left(\begin{bmatrix} z_{w_1} \\ z_{w_2} \end{bmatrix}^T \begin{bmatrix} z_{w_1} \\ z_{w_2} \end{bmatrix} - \gamma^2 r^T r\right) < 0 \tag{3.46}$$

The vector of control variables in (3.44) can be rewritten as

$$\begin{bmatrix} z_{w_1} \\ z_{w_2} \end{bmatrix} = \begin{bmatrix} H_1 M_2 & -H_1 M_2 M_1 L_\tau & -H_1 M_2 M_1 L_w & \Gamma_1 & 0 \\ 0 & H_2 & 0 & 0 & \Gamma_2 \end{bmatrix} x \tag{3.47}$$

where

$$x = \begin{bmatrix} r \\ \tau \\ w_p \\ x_{w_1} \\ x_{w_2} \end{bmatrix}$$

. Using (3.47) in (3.46) produces

$$\min_{\tau}\max_{r} x^T \begin{bmatrix} L_1 & L_2 \\ \vdots & \vdots \end{bmatrix} x < 0 \tag{3.48}$$

where

$$L_1 \triangleq \begin{bmatrix} M_2^T Q_1 M_2 - \gamma^2 I & -M_2^T Q_1 M_2 M_1 L_\tau \\ -L_\tau^T M_1^T M_2^T Q_1 M_2 & L_\tau^T M_1^T M_2^T Q_1 M_2 M_1 L_\tau + Q_2 \end{bmatrix} \tag{3.49}$$

$$L_2 \triangleq \begin{bmatrix} -M_2^T Q_1 M_2 M_1 L_w & M_2^T H_1^T \Gamma_1 & 0 \\ L_\tau^T M_1^T M_2^T Q_1 M_2 M_1 L_w & -L_\tau^T M_1^T M_2^T H_1^T \Gamma_1 & H_2^T \Gamma_2 \end{bmatrix} \tag{3.50}$$

To find the point that minimizes τ and maximizes r at the same time, (3.48) is differentiated with respect to $\begin{bmatrix} r^T, \tau^T \end{bmatrix}^T$ and equated to zero. As $x = \begin{bmatrix} r^T, \tau^T, w_p^T, x_{w_1}^T, x_{w_2}^T \end{bmatrix}^T$,

only the first two rows (3.48) will be left as follows;

$$2\begin{bmatrix} L_1 & L_2 \end{bmatrix}\begin{bmatrix} r \\ \tau \\ w_p \\ x_{w_1} \\ x_{w_2} \end{bmatrix} = 0 \tag{3.51}$$

which can be rearranged to

$$L_1\begin{bmatrix} r \\ \tau \end{bmatrix} = -L_2\begin{bmatrix} w_p \\ x_{w_1} \\ x_{w_2} \end{bmatrix}_k \tag{3.52}$$

In order to find the maximum condition for r and minimum condition for τ, (3.52) is differentiated again with respect to $\begin{bmatrix} r^T, \tau^T \end{bmatrix}^T$ that yields

$$H_{hess} \triangleq \begin{bmatrix} M_2^T Q_1 M_2 - \gamma^2 I & -M_2^T Q_1 M_2 M_1 L_\tau \\ -L_\tau^T M_1^T M_2^T Q_1 M_2 & L_\tau^T M_1^T M_2^T Q_1 M_2 M_1 L_\tau + Q_2 \end{bmatrix} \tag{3.53}$$

Let

$$\begin{bmatrix} A_1 & A_2 \\ A_2^T & A_3 \end{bmatrix} \triangleq \begin{bmatrix} M_2^T Q_1 M_2 - \gamma^2 I & -M_2^T Q_1 M_2 M_1 L_\tau \\ -L_\tau^T M_1^T M_2^T Q_1 M_2 & L_\tau^T M_1^T M_2^T Q_1 M_2 M_1 L_\tau + Q_2 \end{bmatrix} \tag{3.54}$$

As $A_3 \in \Re^{3il \times 3il}$ and $r \in \Re^{3il}$, the condition for worst case input reference signal can be stipulated by (3.40). From (3.54) and (3.40), the following can be obtained;

$$M_2^T Q_1 M_2 - \gamma^2 I - M_2^T Q_1 M_2 M_1 L_\tau (L_\tau^T M_1^T M_2^T Q_1 M_2 M_1 L_\tau + Q_2)^{-1} L_\tau^T M_1^T M_2^T Q_1 M_2 < 0 \tag{3.55}$$

From (3.55) and (3.37), the following can be deduced;

$$\left((M_2^T Q_1 M_2)^{-1} + M_1 L_\tau Q_2^{-1} L_\tau^T M_1^T\right)^{-1} < \gamma^2 I$$

or

$$\gamma > \sqrt{\bar{\lambda}[(M_2^T Q_1 M_2)^{-1} + M_1 L_\tau Q_2^{-1} L_\tau^T M_1^T]^{-1}} \equiv \gamma_{\min} \tag{3.56}$$

where $\bar{\lambda}[\bullet]$ is the largest eigenvalue of $\bullet$ and $\gamma_{\min}$ is the minimum value of γ.

As $Q_1 = Q_1^T$ and $Q_2 = Q_2^T$, and both of these matrices are positive definite, then it can be concluded from (3.53), (3.54), and (3.41) that $A_3 > 0$, which satisfies the saddle condition of τ approaching the minimum. Equation (3.52) can be rewritten to calculate the optimum torque τ_{opt} and the worst case reference trajectory r_{wc}, i.e.,

$$\begin{bmatrix} r_{wc} \\ \tau_{opt} \end{bmatrix} = -L_1^{-1} L_2 \begin{bmatrix} w_p \\ x_{w_1} \\ x_{w_2} \end{bmatrix}_k \tag{3.57}$$

or

$$\tau_{opt} = -\begin{bmatrix} 0 & I \end{bmatrix} L_1^{-1} L_2 \begin{bmatrix} w_p \\ x_{w_1} \\ x_{w_2} \end{bmatrix}_k \tag{3.58}$$

Using Lemma 3.2, it can be stated that

$$\begin{bmatrix} 0 & I \end{bmatrix} \begin{bmatrix} A_1 & A_2 \\ A_2^T & A_3 \end{bmatrix}^{-1} = (A_3 - A_2^T A_1^{-1} A_2)^{-1} \begin{bmatrix} -A_2^T A_1^{-1} & I \end{bmatrix} \tag{3.59}$$

Substituting (3.58) and (3.49) in (3.59) yields the following expression;

$$\tau_{opt} = -(L_\tau^T M_1^T M_2^T Q_1 M_2 M_1 L_\tau + Q_2 - L_\tau^T M_1^T M_2^T Q_1 M_2 (M_2^T Q_1 M_2 - \gamma^2 I)^{-1} M_2^T Q_1 M_2 M_1 L_\tau)^{-1}$$
$$\left[L_\tau^T M_1^T M_2^T Q_1 M_2 (M_2^T Q_1 M_2 - \gamma^2 I)^{-1} \quad I \right] L_2 \begin{bmatrix} w_p \\ x_{w_1} \\ x_{w_2} \end{bmatrix}_k \quad (3.60$$

or

$$\tau_{opt} = (L_\tau^T M_1^T (M_2^T Q_1 M_2 - M_2^T Q_1 M_2 (M_2^T Q_1 M_2 - \gamma^2 I)^{-1} M_2^T Q_1 M_2) M_1 L_\tau + Q_2)^{-1} \quad (3.61)$$
$$\begin{bmatrix} (-L_\tau^T M_1^T (M_2^T Q_1 M_2 - M_2^T Q_1 M_2 (M_2^T Q_1 M_2 - \gamma^2 I)^{-1} M_2^T Q_1 M_2) M_1 L_w)^T \\ (-L_\tau^T M_1^T (M_2^T Q_1 M_2 (M_2^T Q_1 M_2 - \gamma^2 I)^{-1} - I) M_2^T H_1^T \Gamma_1)^T \\ (-H_2^T \Gamma_2)^T \end{bmatrix}^T \begin{bmatrix} w_p \\ x_{w_1} \\ x_{w_2} \end{bmatrix}_k$$

If $A \triangleq M_2^T Q_1 M_2$, $B \triangleq I$, and $C \triangleq -\gamma^2 I$ in (3.37), then it can be concluded that

$$M_2^T Q_1 M_2 - M_2^T Q_1 M_2 (M_2^T Q_1 M_2 - \gamma^2 I)^{-1} M_2^T Q_1 M_2 = ((M_2^T Q_1 M_2)^{-1} - \gamma^{-2} I)^{-1} \equiv \widetilde{Q}_1 \quad (3.62)$$

Similarly, (3.38) can be written as

$$M_2^T Q_1 M_2 (M_2^T Q_1 M_2 - \gamma^2 I)^{-1} = -((M_2^T Q_1 M_2)^{-1} - \gamma^{-2} I)^{-1} \gamma^{-2} I = -\gamma^{-2} \widetilde{Q}_1 \quad (3.63)$$

Using (3.62) and (3.63) in (3.61) produces

$$\tau_{opt} \equiv -(L_\tau^T M_1^T \widetilde{Q}_1 M_1 L_\tau + Q_2)^{-1} \begin{bmatrix} (L_\tau^T M_1^T \widetilde{Q}_1 M_1 L_w)^T \\ -(L_\tau^T M_1^T (\gamma^{-2} \widetilde{Q}_1 + I) M_2^T H_1^T \Gamma_1)^T \\ (H_2^T \Gamma_2)^T \end{bmatrix}^T \begin{bmatrix} w_p \\ x_{w_1} \\ x_{w_2} \end{bmatrix}_k \quad (3.64)$$

Equation (3.64) calculates the optimum torque for the joint actuators. It holds as long as the matrix $\left[(M_2^T Q_1 M_2)^{-1} - \gamma^{-2} I \right]$ is not singular. In case the matrix is singular, τ_{opt} can be calculated using (3.58). □

3.3 Model Free Subspace Based Operational Space $\mathscr{H}_2$ Control

$\mathscr{H}_\infty$ control synthesis relates to a worst case synthesis that takes account of the robustness of the feedback system to plant disturbances. On the other hand, $\mathscr{H}_2$ control is a generalization of LQG optimal control [42], in which the disturbance is assumed to be zero. Here, the controlled signals arise from exogenous signals which are fixed or have a fixed power spectrum [29].

Theorem 3.2. *If measurements of the torque vector (τ), joint vector (y), and reference trajectory (r) in operational space are available for times $\{k-i,\ldots,k-2,k-1\}$, then the strictly causal subspace based $\mathscr{H}_2$ control for times $\{k,\ldots,k+i,k+i-1\}$ is given by*

$$\tau_{opt} \triangleq -(L_\tau^T M_1^T M_2^T Q_1 M_2 M_1 L_\tau + Q_2)^{-1} L_\tau^T M_1^T M_2^T Q_1 M_2 M_1 L_w (w_p)_k \tag{3.65}$$

where

- *Q_1 and Q_2 are positive diagonal matrices that can be written as*

$$Q_1 \triangleq \begin{bmatrix} Q & 0 & \ldots & 0 \\ 0 & Q & \ldots & 0 \\ \vdots & \vdots & \ddots & \vdots \\ 0 & 0 & \ldots & Q \end{bmatrix} \in \Re^{3ni\times 3ni} \tag{3.66}$$

$$Q_2 \triangleq \begin{bmatrix} R & 0 & \ldots & 0 \\ 0 & R & \ldots & 0 \\ \vdots & \vdots & \ddots & \vdots \\ 0 & 0 & \ldots & R \end{bmatrix} \in \Re^{ni\times ni} \tag{3.67}$$

- $Q_1 > 0$, $Q_2 > 0$

It can be seen in (3.65) that the system has no dependance on the value of r. This lack of dependence on the value of r is due to the strict causal nature

of the control algorithm, and inability of the weights to retain their states. The performance channels can be formulated using the following relations:

$$z_{w_1} = D_1(M_2(r_k - M_1(y_k))) \tag{3.68}$$

$$z_{w_2} = D_2(\tau) \tag{3.69}$$

Another explanation for this disappearance of r is that when $\gamma \to \infty$ in (3.24), all the disturbances are assumed to be zero.

Proof of Theorem 3.2. In $\mathscr{H}_\infty$, when disturbances are zero or in other words, when $\gamma \to \infty$, $\mathscr{H}_\infty \to \mathscr{H}_2$ [40].

If $\gamma \to \infty$ then (3.62) can be written as

$$\begin{aligned} \lim_{\gamma\to\infty} \widetilde{Q}_1 &= \lim_{\gamma\to\infty} ((M_2^T Q_1 M_2)^{-1} - \gamma^{-2} I)^{-1} \\ &= M_2^T Q_1 M_2 \end{aligned}$$

Similarly, using (3.66) and (3.67)

$$x_{w_1} = 0$$

and

$$x_{w_2} = 0$$

Substituting these values in (3.28) yields

$$\tau_{opt} \equiv -(L_\tau^T M_1^T M_2^T Q_1 M_2 M_1 L_\tau + Q_2)^{-1} L_\tau^T M_1^T M_2^T Q_1 M_2 M_1 L_w (w_p)_k \tag{3.70}$$

□

3.4 Robust Control

There are two ways to incorporate model uncertainty in small gain theorem, additive uncertainty and multiplicative uncertainty (for details on small gain theorem, reference is made to [65]). Additive uncertainty counts for high frequency dynamics and nonlinearities neglected in the control design model, while multiplicative uncertainty caters for input modeling errors and imperfections in the linearized actuator model [49]. As shown in Chapter 1, linear control techniques for mechanical manipulators approximate the non-linear model using Taylor series expansion. For this negligence of non-linear components, $\gamma_\Delta-$ level $\mathscr{H}_\infty$ robust control law with additive uncertainty is proposed. Additive uncertainty also deals with high frequency noise from sensors, which are used to measure joint accelerations. This increases the overall robustness of the system.

Theorem 3.3. *If measurements of torque vector (τ), joint vector (y), and reference trajectory (r) in operational space are available for times $\{k-i,\ldots,k-2,k-1\}$, then the strictly causal subspace based, γ_Δ-level $\mathscr{H}_\infty$ control for times $\{k,\ldots,k+i,k+i-1\}$ is given by*

$$\tau_{opt_\Delta} \triangleq -L_{1_\Delta}^{-1} L_{2_\Delta} \begin{bmatrix} w_p \\ x_{w_1} \\ x_{w_2} \\ x_{w_3} \end{bmatrix} \tag{3.71}$$

where

$$L_{1_\Delta} \triangleq \begin{bmatrix} M_2^T Q_1 M_2 - \gamma^2 I & -M_2^T Q_1 M_2 M_1 H_4 & -M_2^T Q_1 M_2 M_1 L_\tau \\ -H_4^T M_1^T M_2^T Q_1 M_2 & H_4^T M_1^T M_2^T Q_1 M_2 M_1 H_4 - \gamma^2 I & H_4^T M_1^T M_2^T Q_1 M_2 M_1 L_\tau \\ -L_\tau^T M_1^T M_2^T Q_1 M_2 & L_\tau^T M_1^T M_2^T Q_1 M_2 M_1 H_4 & L_\tau^T M_1^T M_2^T Q_1 M_2 M_1 L_\tau + Q_2 + Q_3 \end{bmatrix}$$

$$L_{2_\Delta} \triangleq \begin{bmatrix} -M_2^T Q_1 M_2 M_1 L_w & M_2^T H_1^T \Gamma_1 & 0 & 0 & -M_2^T Q_1 M_2 M_1 \Gamma_4 \\ H_4^T M_1^T M_2^T Q_1 M_2 M_1 L_w & -H_4^T M_1^T M_2^T H_1^T \Gamma_1 & 0 & 0 & H_4^T M_1^T M_2^T Q_1 M_2 M_1 \Gamma_4 \\ L_\tau^T M_1^T M_2^T Q_1 M_2 M_1 L_w & -L_\tau^T M_1^T M_2^T H_1^T \Gamma_1 & H_2^T \Gamma_2 & H_3^T \Gamma_3 & L_\tau^T M_1^T M_2^T Q_1 M_2 M_1 \Gamma_4 \end{bmatrix} \tag{3.72}$$

provided that

$$\gamma_\Delta > \gamma_{\min_\Delta} \triangleq \sqrt{\bar{\lambda}[(I + M_1 Q_4 M_1^T)(M_2^T Q_1 M_2 + M_1 L_\tau (Q_2 + Q_3)^{-1} L_\tau M_1^T)^{-1}]} \tag{3.73}$$

where

- *The state of discrete LTI weighting filters W_3 and W_4 can be updated using*

$$\begin{aligned} (x_{w_3})_{k+1} &= A_{w_3}(x_{w_3})_k + B_{w_3}(M_2(r_k - M_1 y_k)) \\ (z_{w_3})_k &= C_{w_3}(x_{w_3})_k + D_{w_3}(M_2(r_k - M_1 y_k)) \\ (x_{w_4})_{k+1} &= A_{w_4}(x_{w_4})_k + B_{w_4}(s)_k \\ (\acute{s})_k &= C_{w_4}(x_{w_4})_k + D_{w_4}(s)_k \end{aligned}$$

- *H_3 and H_4 are the impulse responses of W_3 and W_4, respectively. They are defined as*

$$H_3 \triangleq \begin{bmatrix} D_{w_3} & 0 & 0 & \cdots & 0 \\ C_{w_3}B_{w_3} & D_{w_3} & 0 & \cdots & 0 \\ C_{w_3}A_{w_3}B_{w_3} & C_{w_3}B_{w_3} & D_{w_3} & \cdots & 0 \\ \vdots & \vdots & \vdots & \ddots & \vdots \\ C_{w_3}A_{w_3}^{i-2}B_{w_3} & C_{w_3}A_{w_3}^{i-3}B_{w_3} & C_{w_3}A_{w_3}^{i-4}B_{w_3} & \cdots & D_{w_3} \end{bmatrix} \tag{3.74}$$

$$H_4 \triangleq \begin{bmatrix} D_{w_4} & 0 & 0 & \cdots & 0 \\ C_{w_4}B_{w_4} & D_{w_4} & 0 & \cdots & 0 \\ C_{w_4}A_{w_4}B_{w_4} & C_{w_4}B_{w_4} & D_{w_4} & \cdots & 0 \\ \vdots & \vdots & \vdots & \ddots & \vdots \\ C_{w_4}A_{w_4}^{i-2}B_{w_4} & C_{w_4}A_{w_4}^{i-3}B_{w_4} & C_{w_4}A_{w_4}^{i-4}B_{w_4} & \cdots & D_{w_4} \end{bmatrix} \tag{3.75}$$

- $Q_3 \triangleq H_3^T H_3, Q_4 \triangleq H_4^T H_4$

- *The extended observability matrices, Γ_3 and Γ_3, formed from the impulse responses of the weighting filters W_3 and W_4, are given as follows;*

$$\Gamma_3 \triangleq \begin{bmatrix} C_{w_3} \\ C_{w_3}A_{w_3} \\ \vdots \\ C_{w_3}A_{w_3}^{i-1} \end{bmatrix} \tag{3.76}$$

$$\Gamma_4 \triangleq \begin{bmatrix} C_{w_4} \\ C_{w_4}A_{w_4} \\ \vdots \\ C_{w_4}A_{w_4}^{i-1} \end{bmatrix} \tag{3.77}$$

The following mathematical result will be used in the proof of Theorem 3.3.

Lemma 3.5. *If* $A_a, A_b, A_c, A_d, A_e, A_f, A_f^{-1}$, *and* $(A_c - A_e A_f^{-1} A_e^T)^{-1}$ *exist and* $\begin{bmatrix} A_a & A_b & A_d \\ A_b^T & A_c & A_e \\ A_d^T & A_e^T & A_f \end{bmatrix}$ *is a Hessian such that* $A_f = A_f^T$ *and it was formulated by double differentiation of* $\begin{bmatrix} a^T & b^T & c^T \end{bmatrix}^T$ *for the maximum values of* a *and* b *and minimum value of* c *then*

$$A_f > 0 \tag{3.78}$$

$$A_c - A_e A_f^{-1} A_e^T < 0 \tag{3.79}$$

$$A_a - A_d A_f^{-1} A_d^T - (A_b - A_d A_f^{-1} A_e^T)(A_c - A_e A_f^{-1} A_e^T)^{-1}(A_b^T - A_e A_f^{-1} A_d^T) < 0 \tag{3.80}$$

Proof of Lemma 3.5. Let

$$A_1 \triangleq \begin{bmatrix} A_a & A_b \\ A_b^T & A_c \end{bmatrix},$$

$$A_2 \triangleq \begin{bmatrix} A_d \\ A_e \end{bmatrix},$$

and

$$A_3 \triangleq A_f$$

then from (3.41)

$$A_f > 0$$

Using Lemma 3.4 for above inequality, it can be stated that

$$A_1 - A_2 A_3^{-1} A_2^T < 0$$

Substituting values of A_1, A_2, and A_3 in the above expression yields

$$\begin{bmatrix} A_a & A_b \\ A_b^T & A_d \end{bmatrix} - \begin{bmatrix} A_d \\ A_e \end{bmatrix} A_f^{-1} \begin{bmatrix} A_d^T & A_e^T \end{bmatrix} < 0$$

which can be expanded to

$$\begin{bmatrix} A_a - A_d A_f^{-1} A_d^T & A_b - A_d A_f^{-1} A_e^T \\ A_b^T - A_e A_f^{-1} A_d^T & A_c - A_e A_f^{-1} A_e^T \end{bmatrix} < 0$$

It can be deduced from Schur decomposition, in Lemma 3.4, for above inequality that

$$A_c - A_e A_f^{-1} A_e^T < 0$$

and

$$A_a - A_d A_f^{-1} A_d^T - (A_b - A_d A_f^{-1} A_e^T)(A_c - A_e A_f^{-1} A_e^T)^{-1}(A_b^T - A_e A_f^{-1} A_d^T) < 0$$

□

Proof of Theorem 3.3. From Figure 3.4, control variables z_{w_1}, z_{w_2}, and z_{w_3} can be written as

$$\begin{bmatrix} z_{w_1} \\ z_{w_2} \\ z_{w_3} \end{bmatrix} = \begin{bmatrix} H_1(e) + \Gamma_1(x_{w_1})_k \\ H_2(\tau) + \Gamma_2(x_{w_2})_k \\ H_3(\tau) + \Gamma_3(x_{w_3})_k \end{bmatrix} \tag{3.81}$$

where x_{w_1}, x_{w_2}, and x_{w_3} are the state variables for the weighting matrices W_1, W_2, and W_3. From Figure 3.4, $e = M_2(r - M_1\hat{y}_f)$, hence (3.81) can be re-expressed as

$$\begin{bmatrix} z_{w_1} \\ z_{w_2} \\ z_{w3} \end{bmatrix} = \begin{bmatrix} H_1(M_2(r - M_1(\hat{y} + H_4(s) + \Gamma_4(x_{w4})_k))) + \Gamma_1(x_{w_1})_k \\ H_2(\tau) + \Gamma_2(x_{w_2})_k \\ H_3(\tau) + \Gamma_3(x_{w_3})_k \end{bmatrix} \tag{3.82}$$

The cost function to minimize the control effort and the feedback error for the given refence trajectory bounded by γ_Δ is given by

$$L_\Delta(\gamma_\Delta) = z_{w_1}^T z_{w_1} + z_{w_2}^T z_{w_2} + z_{w_3}^T z_{w_3} - \gamma_\Delta^2 r^T r, \tag{3.83}$$

where the objective is

$$\min_{\tau} \max_{r,s} L_\Delta(\gamma_\Delta) < 0$$

Substituting objective in (3.83) gives

$$\min_{\tau} \max_{r,s} \left(\begin{bmatrix} z_{w_1} \\ z_{w_2} \\ z_{w_3} \end{bmatrix}^T \begin{bmatrix} z_{w_1} \\ z_{w_2} \\ z_{w_3} \end{bmatrix} - \gamma_\Delta^2 r^T r \right) < 0 \tag{3.84}$$

From (3.30), (3.31), and (3.82), the following can be concluded;

$$\begin{bmatrix} z_{w_1} \\ z_{w_2} \\ z_{w3} \end{bmatrix} = \begin{bmatrix} H_1M_2 & -H_1M_2M_1H_4 & -H_1M_2M_1L_\tau & -H_1M_2M_1L_w & \Gamma_1 & 0 & 0 & -H_1M_2M_1\Gamma_4 \\ 0 & 0 & H_2 & 0 & 0 & \Gamma_2 & 0 & 0 \\ 0 & 0 & H_3 & 0 & 0 & 0 & \Gamma_3 & 0 \end{bmatrix} \tag{3.85}$$

where

$$x_\Delta = \begin{bmatrix} r \\ s \\ \tau \\ w_p \\ x_{w_1} \\ x_{w_2} \\ x_{w3} \end{bmatrix}$$

Substituting (3.85) in (3.84) produces

$$\min_{\tau} \max_{r,s} x_\Delta^T \begin{bmatrix} L_1 & L_2 \\ \vdots & \vdots \end{bmatrix} x_\Delta < 0 \tag{3.86}$$

where

$$L_{1_\Delta} \equiv \begin{bmatrix} M_2^T Q_1 M_2 - \gamma_\Delta^2 I & -M_2^T Q_1 M_2 M_1 H_4 & -M_2^T Q_1 M_2 M_1 L_\tau \\ -H_4^T M_1^T M_2^T Q_1 M_2 & H_4^T M_1^T M_2^T Q_1 M_2 M_1 H_4 - \gamma_\Delta^2 I & H_4^T M_1^T M_2^T Q_1 M_2 M_1 L_\tau \\ -L_\tau^T M_1^T M_2^T Q_1 M_2 & L_\tau^T M_1^T M_2^T Q_1 M_2 M_1 H_4 & L_\tau^T M_1^T M_2^T Q_1 M_2 M_1 L_\tau + Q_2 + Q_3 \end{bmatrix} \tag{3.87}$$

and

$$L_{2_\Delta} \equiv \begin{bmatrix} -M_2^T Q_1 M_2 M_1 L_w & M_2^T H_1^T \Gamma_1 & 0 & 0 & -M_2^T Q_1 M_2 M_1 \Gamma_4 \\ H_4^T M_1^T M_2^T Q_1 M_2 M_1 L_w & -H_4^T M_1^T M_2^T H_1^T \Gamma_1 & 0 & 0 & H_4^T M_1^T M_2^T Q_1 M_2 M_1 \Gamma_4 \\ L_\tau^T M_1^T M_2^T Q_1 M_2 M_1 L_w & -L_\tau^T M_1^T M_2^T H_1^T \Gamma_1 & H_2^T \Gamma_2 & H_3^T \Gamma_3 & L_\tau^T M_1^T M_2^T Q_1 M_2 M_1 \Gamma_4 \end{bmatrix} \tag{3.88}$$

To find the saddle point that minimizes τ and maximizes r at the same time, (3.86) is differentiated with respect to $\begin{bmatrix} r^T, s^T, \tau^T \end{bmatrix}^T$ and equated to zero. As $x_\Delta = \begin{bmatrix} r^T, s^T, \tau^T, w_p^T, x_{w_1}^T, x_{w_2}^T, x_{w3}^T \end{bmatrix}^T$, only the top three rows from (3.86) will be left. Rearranging the equation yields

$$L_{1_\Delta} \begin{bmatrix} r \\ s \\ \tau \end{bmatrix} = -L_{2_\Delta} \begin{bmatrix} w_p \\ x_{w_1} \\ x_{w_2} \\ x_{w_3} \end{bmatrix} \tag{3.89}$$

In order to find the maximum condition for r and s, and minimum condition for τ, (3.89) is differentiated again with respect to $\begin{bmatrix} r^T, s^T, \tau^T \end{bmatrix}^T$, which yields

$$H_{hess_\Delta} \triangleq \begin{bmatrix} M_2^T Q_1 M_2 - \gamma_\Delta^2 I & -M_2^T Q_1 M_2 M_1 H_4 & -M_2^T Q_1 M_2 M_1 L_\tau \\ -H_4^T M_1^T M_2^T Q_1 M_2 & H_4^T M_1^T M_2^T Q_1 M_2 M_1 H_4 - \gamma_\Delta^2 I & H_4^T M_1^T M_2^T Q_1 M_2 M_1 L_\tau \\ -L_\tau^T M_1^T M_2^T Q_1 M_2 & L_\tau^T M_1^T M_2^T Q_1 M_2 M_1 H_4 & L_\tau^T M_1^T M_2^T Q_1 M_2 M_1 L_\tau + Q_2 + Q_3 \end{bmatrix} \tag{3.90}$$

Comparing the Hessian in Lemma 3.5 with (3.90) and then substituting these values in (3.80) produces

$$X - \gamma_\Delta^2 I - X M_1 H_4 (H_4^T M_1^T X M_1 H_4 - \gamma_\Delta^2 I)^{-1} H_4^T M_1^T < 0 \tag{3.91}$$

where

$$X \triangleq M_2^T Q_1 M_2 - M_2^T Q_1 M_2 M_1 L_\tau (H_4^T M_1^T M_2^T Q_1 M_2 M_1 L_\tau + Q_2 + Q_3)^{-1} L_\tau M_1^T M_2^T Q_1 M_2$$

Using (3.37), the above relation can be rewritten as

$$X = ((M_2^T Q_1 M_2)^{-1} + M_1 L_\tau (Q_2 + Q_3)^{-1} L_\tau M_1^T)^{-1} \tag{3.92}$$

If $A \triangleq X$, $B \triangleq H_4^T M_1^T$, and $C \triangleq \gamma_\Delta^2 I$, then using (3.37) produces

$$\gamma_\Delta^2 I > (X^{-1} - \gamma_\Delta^{-2} M_1 Q_4 M_1^T)^{-1} \tag{3.93}$$

which can be rearranged to

$$\gamma_\Delta^2 X^{-1} - M_1 Q_4 M_1^T > I$$

or

$$\gamma_\Delta^2 I > (I + M_1 Q_4 M_1^T) X$$

Using the value of X from (3.92) in the above inequality for the minimum value of γ yields

$$\gamma_\Delta > \sqrt{\bar{\lambda}[(I + M_1 Q_4 M_1^T)((M_2^T Q_1 M_2)^{-1} + M_1 L_\tau (Q_2 + Q_3)^{-1} L_\tau M_1^T)^{-1}]} \equiv \gamma_{\min_\Delta} \tag{3.94}$$

The minimum condition for the torque is stipulated by applying the condition mentioned in (3.78) onto (3.90), i.e.,

$$L_\tau^T M_1^T M_2^T Q_1 M_2 M_1 L_\tau + Q_2 + Q_3 > 0$$

As, $Q_1 > 0, Q_2 > 0$, and $Q_3 > 0$, the above inequality proves the minimum saddle condition for the torque. From (3.89), τ_{opt_Δ} can be written as

$$\tau_{opt_\Delta} \equiv -L_{1_\Delta}^{-1} L_{2_\Delta} \begin{bmatrix} w_p \\ x_{w_1} \\ x_{w_2} \\ x_{w_3} \end{bmatrix} \tag{3.95}$$

where L_{1_Δ} and L_{2_Δ} are defined in (3.87) and (3.88), respectively.

□

The control law presented in (3.71) gives a robust solution at the cost of performance. The following theorem proves this hypothesis.

Theorem 3.4. *If $\gamma_{\min_\Delta}$ is as defined in (3.73) and $\gamma_{\min}$ is as defined in (3.29) then*

$$\gamma_{\min_\Delta} > \gamma_{\min} \tag{3.96}$$

The following mathematical result will be used in the proof of Theorem 3.4.

Lemma 3.6. *If A^{-1}, B^{-1}, and C^{-1} exist then*

$$(ABC)^{-1} = C^{-1} B^{-1} A^{-1} \tag{3.97}$$

Proof of Theorem 3.4. Applying the condition in (3.78) to (3.90) yields

$$\begin{aligned} L_\tau^T M_1^T M_2^T Q_1 M_2 M_1 L_\tau + Q_2 + Q_3 &> 0 \\ M_2^T Q_1 M_2 + (L_\tau^T M_1^T)^{-1}(Q_2 + Q_3)(M_1 L_\tau)^{-1} &> 0 \\ -(L_\tau^T M_1^T)^{-1}(Q_2 + Q_3)(M_1 L_\tau)^{-1} &< M_2^T Q_1 M_2 \end{aligned}$$

Taking the inverse on both sides of the equation and then using (3.97) produces

$$\begin{aligned} M_1 L_\tau (Q_2 + Q_3)^{-1} L_\tau^T M_1^T &> -(M_2^T Q_1 M_2)^{-1} \\ (M_2^T Q_1 M_2)^{-1} + M_1 L_\tau (Q_2 + Q_3)^{-1} L_\tau^T M_1^T &> 0 \end{aligned}$$

As $Q_3 > 0$

$$(M_2^T Q_1 M_2)^{-1} + M_1 L_\tau (Q_2 + Q_3)^{-1} L_\tau^T M_1^T < (M_2^T Q_1 M_2)^{-1} + M_1 L_\tau (Q_2)^{-1} L_\tau^T M_1^T$$

or

$$((M_2^T Q_1 M_2)^{-1} + M_1 L_\tau (Q_2 + Q_3)^{-1} L_\tau^T M_1^T)^{-1} > ((M_2^T Q_1 M_2)^{-1} + M_1 L_\tau (Q_2)^{-1} L_\tau^T M_1^T)^{-1}$$

As $Q_4 > 0$ and $M_1^T M_1 > 0$, hence

$$\begin{aligned} & (I + M_1 Q_4 M_1^T)((M_2^T Q_1 M_2)^{-1} + M_1 L_\tau (Q_2 + Q_3)^{-1} L_\tau^T M_1^T)^{-1} \\ > \; & ((M_2^T Q_1 M_2)^{-1} + M_1 L_\tau (Q_2)^{-1} L_\tau^T M_1^T)^{-1} \end{aligned}$$

or

$$\begin{aligned} & \sqrt{\bar{\lambda}[(I + M_1 Q_4 M_1^T)((M_2^T Q_1 M_2)^{-1} + M_1 L_\tau (Q_2 + Q_3)^{-1} L_\tau^T M_1^T)^{-1}]} \\ > \; & \sqrt{\bar{\lambda}[((M_2^T Q_1 M_2)^{-1} + M_1 L_\tau (Q_2)^{-1} L_\tau^T M_1^T)^{-1}]} \end{aligned}$$

that equates to

$$\gamma_{\min_\Delta} > \gamma_{\min}$$

□

3.5 Summary

The important results of this chapter are:

- Formulation of a basic framework to cater for the kinematic constraints (3.6) – (3.22);
- Model free operational space $\mathscr{H}_\infty$ control for rigid robot manipulators (3.28) – (3.29);
- Model free operational space $\mathscr{H}_2$ control for rigid robot manipulators (3.65);
- Model free operational space $\mathscr{H}_\infty$ robust control with additive uncertainties (3.71) – (3.73); and
- Reduction in performance of model free robust control at the cost of robustness (3.96).

Chapter 4

Interaction Control

One of the most important requirements of a manipulator is its ability to interact with the environment. There are many applications in industrial robots where the end-effector of the manipulator interacts with the environment. Some of the examples are available in applications that involve polishing, deburring, machining, or assembly. It is important that a control algorithm used for these applications caters for the *contact force*, otherwise the job can be detrimental to both the manipulator and the work piece.

Since the interaction between the environment and the manipulator is described in operational space, it is natural to design the control strategy in operational space. The control laws, described in Chapter 3, can be adapted to cater for the contact forces that interact with the end-effector. These forces can be related to the reactive joint force through the following relation [94];

$$f_n = J^T f_l$$

where $f_l \in \Re^l$ is a force vector in operational space and $f_n \in \Re^n$ is either a force vector or a torque vector depending on whether the joints are prismatic or rotatory. This relation will be used in the formulation of different control schemes for serial manipulators.

Interaction control schemes are generally categorized into two groups [19]. The first group is referred to as the *hybrid position/force control.* Section 4.1 proposes a control scheme under this category. The second group is called *impedance control,* and it implies the use of a controller that regulates the stiffness of the joints of a manipulator. This is formulated in Section 4.2. Section 4.3 discusses the effect of scaling of the force vector for different cases.

4.1 Hybrid Interaction Control

This control scheme is based on the observation that when a manipulator is in contact with the environment, some of its force and position subspaces vary to keep the manipulator free to move despite being constrained by the environment. The controller is designed to mimic these variations by involving two disturbance signals, one to guide the position of the end-effector and one to signify the force signal, as shown in Figure 4.1. The controller tries to minimize the control effort for the worst case value of the reference trajectory and the force vector.

For a given job, if a desired force is required to be applied, whilst following a given trajectory, the force vector can be expressed as

$$f = \begin{cases} f_e - f_d \text{ if } f_e > f_d \\ 0 \text{ otherwise} \end{cases} \tag{4.1}$$

where f_d is the desired contact force, and f_e is the actual recorded force from the sensor mounted on the end-effector.

Theorem 4.1. *If measurements of the torque vector (τ), joint vector (y), force vector on the end-effector (f) and reference trajectory (r) in operational space are available for times $\{k-i,\ldots,k-2,k-1\}$, then the strictly causal subspace based, γ_f-level $\mathscr{H}_\infty$ hybrid force/position control for times $\{k,\ldots,k+i,k+i-1\}$ is given*

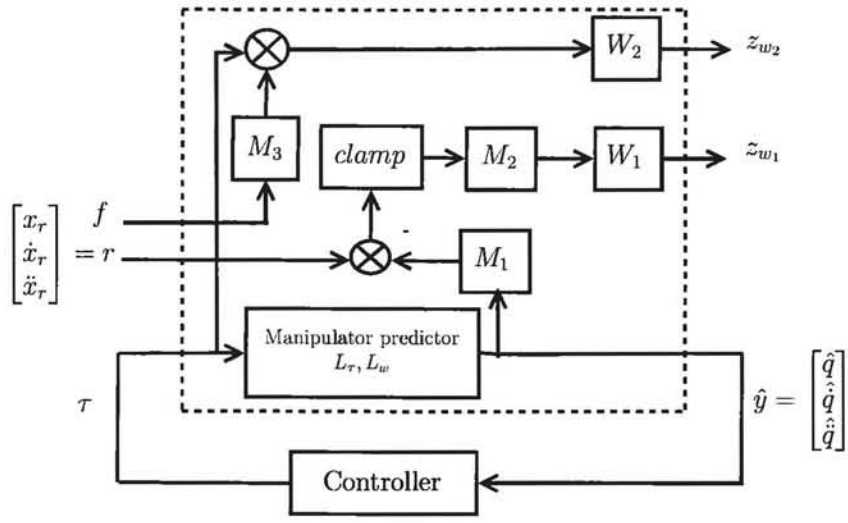

Figure 4.1: Model free subspace based operational space $\mathscr{H}_\infty$ hybrid force/position control. f is measured from sensors attached to the end-effector

by

$$\tau_{opt_f} \triangleq -(L_\tau^T M_1^T \widetilde{Q}_1 M_1 L_\tau + \widetilde{Q}_{2_f})^{-1} \begin{bmatrix} (L_\tau^T M_1^T \widetilde{Q}_1 M_1 L_w)^T \\ -(L_\tau^T M_1^T (\gamma_f^{-2} \widetilde{Q}_1 + I) M_2^T H_1^T \Gamma_1)^T \\ ((I + \gamma_f^{-2} \widetilde{Q}_{2_f} M_3 M_3^T) H_2^T \Gamma_2)^T \end{bmatrix}^T \begin{bmatrix} w_p \\ x_{w_1} \\ x_{w_2} \end{bmatrix}_k \tag{4.2}$$

provided that

$$\gamma_f > \gamma_{\min_f} \triangleq \sqrt{\bar{\lambda}[(I + M_1 L_\tau M_3 M_3^T L_\tau^T M_1^T)((M_2^T Q_1 M_2)^{-1} + M_1 L_\tau Q_2^{-1} L_\tau^T M_1^T)^{-1}]} \tag{4.3}$$

where

- $\widetilde{Q}_{2_f} \triangleq (Q_2^{-1} - \gamma_f^{-2} M_3 M_3^T)^{-1}$
- *Forces acting on the end-effector in operational space can be projected onto joint space using*

$$M_3 \triangleq \begin{bmatrix} J^T & 0 & \dots & 0 \\ 0 & J^T & \dots & 0 \\ \vdots & \vdots & \ddots & 0 \\ 0 & 0 & \dots & J^T \end{bmatrix} \in \Re^{ni \times li} \tag{4.4}$$

The following mathematical results will be used in the proof of Theorem 4.1.

Lemma 4.1.

$$\begin{bmatrix} A_1 & 0 \\ 0 & A_2 \end{bmatrix}^{-1} = \begin{bmatrix} A_1^{-1} & 0 \\ 0 & A_2^{-1} \end{bmatrix} \tag{4.5}$$

Lemma 4.2. *If* A_a^{-1}, A_c^{-1}, *and* $\begin{bmatrix} A_a & 0 & A_d \\ 0 & A_c & A_e \\ A_d^T & A_e^T & A_f \end{bmatrix}^{-1}$ *exist, then*

$$\begin{bmatrix} 0 \\ 0 \\ I \end{bmatrix}^T \begin{bmatrix} A_a & 0 & A_d \\ 0 & A_c & A_e \\ A_d^T & A_e^T & A_f \end{bmatrix}^{-1} = (A_f - A_d^T A_a^{-1} A_d - A_e^T A_c^{-1} A_e)^{-1} \begin{bmatrix} -A_d^T A_a^{-1} & -A_e^T A_c^{-1} & I \end{bmatrix} \tag{4.6}$$

Proof of Lemma 4.2. Let

$$A_1 \triangleq \begin{bmatrix} A_a & 0 \\ 0 & A_c \end{bmatrix},$$

$$A_2 \triangleq \begin{bmatrix} A_d \\ A_e \end{bmatrix},$$

and

$$A_3 \triangleq A_f$$

$$\Rightarrow \quad \begin{bmatrix} 0 & I \end{bmatrix} \begin{bmatrix} A_1 & A_2 \\ A_2^T & A_3 \end{bmatrix}^{-1} = \begin{bmatrix} 0 & 0 & I \end{bmatrix} \begin{bmatrix} A_a & 0 & A_d \\ 0 & A_c & A_e \\ A_d^T & A_e^T & A_f \end{bmatrix}^{-1}$$

then from (3.59)

$$\begin{aligned}
&\begin{bmatrix} 0 & 0 & I \end{bmatrix} \begin{bmatrix} A_a & 0 & A_d \\ 0 & A_c & A_e \\ A_d^T & A_e^T & A_f \end{bmatrix}^{-1} \\
&= (A_3 - A_2^T A_1^{-1} A_2)^{-1} \begin{bmatrix} -A_2^T A_1^{-1} & I \end{bmatrix} \\
&= \left(A_f - \begin{bmatrix} A_d^T & A_e^T \end{bmatrix} \begin{bmatrix} A_a & 0 \\ 0 & A_c \end{bmatrix}^{-1} \begin{bmatrix} A_d \\ A_e \end{bmatrix} \right)^{-1} \begin{bmatrix} - \begin{bmatrix} A_d^T & A_e^T \end{bmatrix} \begin{bmatrix} A_a & 0 \\ 0 & A_c \end{bmatrix}^{-1} & I \end{bmatrix}
\end{aligned}$$

Using (4.5) in the expression above yields

$$\begin{aligned}
&\left(A_f - \begin{bmatrix} A_d^T & A_e^T \end{bmatrix} \begin{bmatrix} A_a^{-1} & 0 \\ 0 & A_c^{-1} \end{bmatrix} \begin{bmatrix} A_d \\ A_e \end{bmatrix} \right)^{-1} \begin{bmatrix} - \begin{bmatrix} A_d^T & A_e^T \end{bmatrix} \begin{bmatrix} A_a^{-1} & 0 \\ 0 & A_c^{-1} \end{bmatrix} & I \end{bmatrix} \\
&= (A_f - A_d^T A_a^{-1} A_d - A_e^T A_c^{-1} A_e)^{-1} \begin{bmatrix} -A_d^T A_a^{-1} & -A_e^T A_c^{-1} & I \end{bmatrix}
\end{aligned}$$

□

Proof of Theorem 4.1. The force signal f in operational space is defined as

$$f \triangleq \begin{bmatrix} f_k \\ f_{k+1} \\ \vdots \\ f_{k+i-1} \end{bmatrix} \in \Re^{il}$$

From (3.23) and (3.24), γ_f−level $\mathscr{H}_\infty$ control with d disturbances and z control variables can be written as

$$\sup_{\substack{d \in \mathscr{L}_2(0,\infty) \\ ||d||_2 = 1}} \frac{||z||_2}{||d||_2} < \gamma_f \tag{4.7}$$

From Figure 4.1, it can be seen that the disturbance signals consist of the reference trajectory and the force signal acting on the end-effector. Squaring the performance objective for the force control for the system described in (4.7) produces

$$\frac{z_{w_1}^T z_{w_1} + z_{w_2}^T z_{w_2}}{r^T r + f^T f} < \gamma_f^2 \tag{4.8}$$

or

$$z_{w_1}^T z_{w_1} + z_{w_2}^T z_{w_2} - \gamma_f^2 r^T r - \gamma_f^2 f^T f < 0 \tag{4.9}$$

The force f acting on the end-effector in operational space projects onto the torque in joint space with a factor of J^T. The control variables can be re-written as

$$\begin{bmatrix} z_{w_1} \\ z_{w_2} \end{bmatrix} = \begin{bmatrix} H_1(e) + \Gamma_1(x_{w_1})_k \\ H_2(\tau + M_3 f) + \Gamma_2(x_{w_2})_k \end{bmatrix} \tag{4.10}$$

where M_3 is a diagonal matrix with J^T on its diagonal. Substituting the value of e from Figure 4.1 yields

$$\begin{bmatrix} z_{w_1} \\ z_{w_2} \end{bmatrix} = \begin{bmatrix} H_1(M_2(r - M_1\hat{y}_f)) + \Gamma_1(x_{w_1})_k \\ H_2(\tau + M_3 f) + \Gamma_2(x_{w_2})_k \end{bmatrix} \tag{4.11}$$

The cost function to minimize the control effort and the feedback error, for the given reference trajectory and force on the end-effector bounded by γ_f, is given by

$$L_f(\gamma_f) = z_{w_1}^T z_{w_1} + z_{w_2}^T z_{w_2} - \gamma_f^2 r^T r - \gamma_f^2 f^T f \tag{4.12}$$

where the objective is

$$\min_{\tau} \max_{r,f} L(\gamma_f) < 0$$

A controller for the maximum force f and the reference trajectory r will now be formulated to cater for the worst case scenario. Substituting the cost function given

in (4.12) in the above objective gives

$$\min_{\tau} \max_{r,f} \left(\begin{bmatrix} z_{w_1} \\ z_{w_2} \end{bmatrix}^T \begin{bmatrix} z_{w_1} \\ z_{w_2} \end{bmatrix} - \gamma_f^2 (r^T r + f^T f) \right) < 0 \tag{4.13}$$

Substituting the values of z_{w_1} and z_{w_2} in (4.11) yields

$$\begin{bmatrix} z_{w_1} \\ z_{w_2} \end{bmatrix} = \begin{bmatrix} H_1 M_2 & 0 & -H_1 M_2 M_1 L_\tau & -H_1 M_2 M_1 L_w & \Gamma_1 & 0 \\ 0 & H_2 M_3 & H_2 & 0 & 0 & \Gamma_2 \end{bmatrix} x_f \tag{4.14}$$

where

$$x_f \triangleq \begin{bmatrix} r \\ f \\ \tau \\ w_p \\ x_{w_1} \\ x_{w_2} \end{bmatrix} \tag{4.15}$$

Using (4.14) in the performance objective described in (4.13) produces

$$\min_{\tau} \max_{r,f} x_f^T \begin{bmatrix} L_{1_f} & L_{2_f} \\ \vdots & \vdots \end{bmatrix} x_f < 0 \tag{4.16}$$

where

$$L_{1_f} \triangleq \begin{bmatrix} M_2^T Q_1 M_2 - \gamma_f^2 I & 0 & -M_2^T Q_1 M_2 M_1 L_\tau \\ 0 & M_3^T Q_2 M_3 - \gamma_f^2 I & M_3^T Q_2 \\ -L_\tau^T M_1^T M_2^T Q_1 M_2 & Q_2 M_3 & L_\tau^T M_1^T M_2^T Q_1 M_2 M_1 L_\tau + Q_2 \end{bmatrix} \tag{4.17}$$

and

$$L_{2_f} \triangleq \begin{bmatrix} -M_2^T Q_1 M_2 M_1 L_w & M_2^T H_1^T \Gamma_1 & 0 \\ 0 & 0 & M_3^T H_2^T \Gamma_2 \\ L_\tau^T M_1^T M_2^T Q_1 M_2 M_1 L_w & -L_\tau^T M_1^T M_2^T H_1^T \Gamma_1 & H_2^T \Gamma_2 \end{bmatrix} \tag{4.18}$$

To find the saddle point that minimizes τ, and maximizes r and f at the same time, (4.16) is differentiated with respect to $\left[r^T, f^T, \tau^T\right]^T$ and equated to zero. As $x_f = \left[r^T, f^T, \tau^T, w_p^T, x_{w_1}^T, x_{w_2}^T\right]^T$, only the first three rows from (4.16) will remain. After differentiation, (4.16) can be written as

$$L_{1_f} \begin{bmatrix} r \\ f \\ \tau \end{bmatrix} = -L_{2_f} \begin{bmatrix} w_p \\ x_{w_1} \\ x_{w_2} \end{bmatrix} \tag{4.19}$$

In order to find the maximum condition for r and f, and minimum condition for τ, (4.19) is differentiated again with respect to $\left[r^T, f^T, \tau^T\right]^T$. This yields the following;

$$H_{hess_f} \triangleq \begin{bmatrix} M_2^T Q_1 M_2 - \gamma_f^2 I & 0 & -M_2^T Q_1 M_2 M_1 L_\tau \\ 0 & M_3^T Q_2 M_3 - \gamma_f^2 I & M_3^T Q_2 \\ -L_\tau^T M_1^T M_2^T Q_1 M_2 & Q_2 M_3 & L_\tau^T M_1^T M_2^T Q_1 M_2 M_1 L_\tau + Q_2 \end{bmatrix} \tag{4.20}$$

To evaluate the value of γ_f for the worst case situation, (3.80) can be written as

$$M_2^T Q_1 M_2 - \gamma_f^2 I - M_2^T Q_1 M_2 M_1 L_\tau X_f L_\tau^T M_1^T M_2^T Q_1 M_2 < 0 \tag{4.21}$$

where

$$X_f \triangleq A - AB^T(BAB^T + C)^{-1}BA \tag{4.22}$$

where $A \triangleq (L_\tau^T M_1^T M_2^T Q_1 M_2 M_1 L_\tau + Q_2)^{-1}$, $B \triangleq M_3^T Q_2$, and $C \triangleq \gamma_f^2 - M_3^T Q_2 M_3$. Using (3.37) in (4.22) produces

$$X_f = (L_\tau^T M_1^T M_2^T Q_1 M_2 M_1 L_\tau + Q_2 - Q_2 M_3(-\gamma_f^2 + M_3^T Q_2 M_3)^{-1} M_3^T Q_2)^{-1} \tag{4.23}$$

If $A \triangleq Q_2$, $B \triangleq M_3^T$, and $C \triangleq -\gamma_f^2 I$, then using (3.37) gives

$$X_f = (L_\tau^T M_1^T M_2^T Q_1 M_2 M_1 L_\tau + (Q_2^{-1} - \gamma_f^{-2} M_3 M_3^T)^{-1})^{-1} \tag{4.24}$$

Substituting X_f in (4.21) results in

$$A - \gamma_f^2 I - AB^T(BAB^T + C)^{-1}BA < 0$$

where $A \triangleq M_2^T Q_1 M_2$, $B \triangleq L_\tau^T M_1^T$, and $C \triangleq (Q_2^{-1} - \gamma_f^{-2} M_3 M_3^T)^{-1}$. Simplification of the above inequality using (3.37) produces

$$\gamma_f^2 I > ((M_2^T Q_1 M_2)^{-1} + M_1 L_\tau (Q_2^{-1} - \gamma_f^{-2} M_3 M_3^T) L_\tau^T M_1^T)^{-1}$$

or

$$\gamma_f^{-2} I < (M_2^T Q_1 M_2)^{-1} + M_1 L_\tau (Q_2^{-1} - \gamma_f^{-2} M_3 M_3^T) L_\tau^T M_1^T$$

or

$$\gamma_f^{-2}(I + M_1 L_\tau M_3 M_3^T L_\tau^T M_1^T) < (M_2^T Q_1 M_2)^{-1} + M_1 L_\tau Q_2^{-1} L_\tau^T M_1^T$$

The above inequality can be rearranged to

$$\gamma_f^2 > (I + M_1 L_\tau M_3 M_3^T L_\tau^T M_1^T)((M_2^T Q_1 M_2)^{-1} + M_1 L_\tau Q_2^{-1} L_\tau^T M_1^T)^{-1}$$

or

$$\gamma_f > \sqrt{\bar{\lambda}[(I + M_1 L_\tau M_3 M_3^T L_\tau^T M_1^T)((M_2^T Q_1 M_2)^{-1} + M_1 L_\tau Q_2^{-1} L_\tau^T M_1^T)^{-1}]} \equiv \gamma_{\min_f}$$

As $Q_1 > 0$ and $Q_2 > 0$, hence

$$L_\tau^T M_1^T M_2^T Q_1 M_2 M_1 L_\tau + Q_2 > 0,$$

By comparing (4.20) and the Hessian in Lemma 3.5, the above relation satisfies the minimum condition for τ as per the criteria described in (3.78). Equation (4.19) can be rewritten to calculate the optimum torque τ_{opt_f} and the worst case reference trajectory r_{wc}, i.e.,

$$\begin{bmatrix} r_{wc} \\ f_{wc} \\ \tau_{opt_f} \end{bmatrix} = -L_{1_f}^{-1} L_{2_f} \begin{bmatrix} w_p \\ x_{w_1} \\ x_{w_2} \end{bmatrix}_k \tag{4.25}$$

or

$$\tau_{opt_f} = -\begin{bmatrix} 0 & 0 & I \end{bmatrix} L_{1_f}^{-1} L_{2_f} \begin{bmatrix} w_p \\ x_{w_1} \\ x_{w_2} \end{bmatrix}_k \tag{4.26}$$

Using (4.6)

$$\tau_{opt_f} = -(L_\tau^T M_1^T X_{f_1} M_1 L_\tau + X_{f_2})^{-1} X_{f_3} L_{2_f} \begin{bmatrix} w_p \\ x_{w_1} \\ x_{w_2} \end{bmatrix}_k \tag{4.27}$$

where

$$X_{f_1} \triangleq M_2^T Q_1 M_2 - M_2^T Q_1 M_2 (M_2^T Q_1 M_2 + (-\gamma_f^2 I))^{-1} M_2^T Q_1 M_2,$$

$$X_{f_2} \triangleq Q_2 - Q_2 M_3 (M_3^T Q_2 M_3 + (-\gamma_f^2 I))^{-1} M_3^T Q_2,$$

and

$$X_{f_3} \triangleq \begin{bmatrix} L_\tau^T M_1^T M_2^T Q_1 M_2 (M_2^T Q_1 M_2 + (-\gamma_f^2 I))^{-1} & -Q_2 M_3 (M_3^T Q_2 M_3 + (-\gamma_f^2 I))^{-1} & I \end{bmatrix} \tag{4.28}$$

X_{f_1} and X_{f_2} can be simplified using (3.37), i.e.,

$$X_{f_1} = ((M_2^T Q_1 M_2)^{-1} - \gamma_f^{-2})^{-1} \equiv \widetilde{Q}_1 \tag{4.29}$$

$$X_{f_2} = (Q_2^{-1} - \gamma_f^{-2} M_3 M_3^T)^{-1} \equiv \widetilde{Q}_{2_f} \tag{4.30}$$

From (4.18) and (4.28)

$$X_{f_3} L_{2_f} = \begin{bmatrix} (L_\tau^T M_1^T (M_2^T Q_1 M_2 - M_2^T Q_1 M_2 (M_2^T Q_1 M_2 - \gamma_f^2 I)^{-1} M_2^T Q_1 M_2) M_1 L_w)^T \\ (L_\tau^T M_1^T (M_2^T Q_1 M_2 (M_2^T Q_1 M_2 - \gamma_f^2 I)^{-1} - I) M_2^T H_1^T \Gamma_1)^T \\ (H_2^T \Gamma_2 - Q_2 M_3 (M_3^T Q_2 M_3 - \gamma_f^2 I)^{-1} M_3^T H_2^T \Gamma_2)^T \end{bmatrix}^T \tag{4.31}$$

If $A \triangleq Q_2$, $B \triangleq M_3^T$, and $C \triangleq -\gamma^2 I$ in (3.38), then it can be written that

$$\begin{aligned} & H_2^T \Gamma_2 - Q_2 M_3 (M_3^T Q_2 M_3 - \gamma_f^2 I)^{-1} M_3^T H_2^T \Gamma_2 \\ = \; & H_2^T \Gamma_2 + \gamma_f^{-2} (Q_2^{-1} - \gamma_f^{-2} M_3 M_3^T)^{-1} M_3 M_3^T H_2^T \Gamma_2 \\ = \; & (I + \gamma_f^{-2} \widetilde{Q}_{2_f} M_3 M_3^T) H_2^T \Gamma_2 \end{aligned} \tag{4.32}$$

Using (4.32), (3.62), and (3.63) in (4.31) produces

$$X_{f_3} L_{2_f} = \begin{bmatrix} (L_\tau^T M_1^T \widetilde{Q}_1 M_1 L_w)^T \\ -(L_\tau^T M_1^T (\gamma_f^{-2} \widetilde{Q}_1 + I) M_2^T H_1^T \Gamma_1)^T \\ ((I + \gamma_f^{-2} \widetilde{Q}_{2_f} M_3 M_3^T) H_2^T \Gamma_2)^T \end{bmatrix}^T \tag{4.33}$$

Substituting the value of $X_{f_3} L_{2_f}$ obtained above and the values of X_{f_1} and X_{f_2} from (4.29) and (4.30) in (4.27), respectively, yields

$$\tau_{opt_f} \equiv -(L_\tau^T M_1^T \widetilde{Q}_1 M_1 L_\tau + \widetilde{Q}_{2_f})^{-1} \begin{bmatrix} (L_\tau^T M_1^T \widetilde{Q}_1 M_1 L_w)^T \\ -(L_\tau^T M_1^T (\gamma_f^{-2} \widetilde{Q}_1 + I) M_2^T H_1^T \Gamma_1)^T \\ ((I + \gamma_f^{-2} \widetilde{Q}_{2_f} M_3 M_3^T) H_2^T \Gamma_2)^T \end{bmatrix}^T \begin{bmatrix} w_p \\ x_{w_1} \\ x_{w_2} \end{bmatrix}_k \tag{4.34}$$

□

The hybrid control law stated in (4.2) provides a robust solution when an external force is exerted on the end-effector. This robustness comes at the cost of performance. The following proposition proves this hypothesis.

Proposition 4.1. *If $\gamma_{\min_\Delta}$ is defined in (3.73) and $\gamma_{\min}$ is defined in (3.29) then from Theorem 3.4*

$$\gamma_{\min_\Delta} > \gamma_{\min}$$

and if $\gamma_{\min_f}$ is defined in (4.3), it can be stated from comparing (3.73) to (4.3) that

$$\gamma_{\min_f} > \gamma_{\min} \tag{4.35}$$

Proof of Proposition 4.1. If $Q_3 = I$ and $Q_4 = L_\tau M_3 M_3^T L_\tau^T$ in (3.73), then rest of the proof is analogous to the proof of Theorem 3.4. □

4.2 Impedance Control

In impedance control, the impedance, or stiffness, of the joints of the mechanical manipulator is regulated. The main idea in this control scheme is not to follow a certain trajectory but to maintain a desired dynamic relation of the contact forces between the end-effector and the environment. Unlike the hybrid control scheme given in Section 4.1, the control effort is minimized only for the worst case value of the given trajectory in operational space. This way, the controller tries to follow the trajectory as much as possible without countering the effect of the applied force. The controller passes the effect of the applied force onto the joints, and as a consequence it seems to an observer as if the stiffness of joints has been compromised.

Theorem 4.2. *If measurements of the torque vector (τ), joint vector (y), force vector on the end-effector (f) and reference trajectory (r) in operational space are available for times $\{k-i, \ldots, k-2, k-1\}$, then the strictly causal subspace based,*

γ_i-level $\mathscr{H}_\infty$ impedance control for times $\{k, \ldots, k+i, k+i-1\}$ is given by

$$\tau_{opt_i} \triangleq -\left(L_\tau^T M_1^T \widetilde{Q}_1 M_1 L_\tau + Q_2\right)^{-1} \begin{bmatrix} (Q_2 M_3)^T \\ \left(L_\tau^T M_1^T \widetilde{Q}_1 M_1 L_w\right)^T \\ -\left(L_\tau^T M_1^T (\gamma_i^{-2} \widetilde{Q}_1 + I) M_2^T H_1^T \Gamma_1\right)^T \\ \left(H_2^T \Gamma_2\right)^T \end{bmatrix}^T \begin{bmatrix} f \\ w_p \\ x_{w_1} \\ x_{w_2} \end{bmatrix}_k \tag{4.36}$$

provided that

$$\gamma_i > \gamma_{\min_i} \triangleq \sqrt{\bar{\lambda}[((M_2^T Q_1 M_2)^{-1} + M_1 L_\tau Q_2^{-1} L_\tau^T M_1^T)^{-1}]} \equiv \gamma_{\min} \tag{4.37}$$

Proof of Theorem 4.2. Following the proof of Theorem 4.1 for the same system described in Figure 4.1, the objective is given as

$$\min_\tau \max_r \left(\begin{bmatrix} z_{w_1} \\ z_{w_2} \end{bmatrix}^T \begin{bmatrix} z_{w_1} \\ z_{w_2} \end{bmatrix} - \gamma_i^2 r^T r \right) < 0 \tag{4.38}$$

where the vector of control variables is given by

$$\begin{bmatrix} z_{w_1} \\ z_{w_2} \end{bmatrix} = \begin{bmatrix} H_1 M_2 & -H_1 M_2 M_1 L_\tau & 0 & -H_1 M_2 M_1 L_w & \Gamma_1 & 0 \\ 0 & H_2 & H_2 M_3 & 0 & 0 & \Gamma_2 \end{bmatrix} x_i \tag{4.39}$$

where

$$x_i \triangleq \begin{bmatrix} r \\ \tau \\ f \\ w_p \\ x_{w_1} \\ x_{w_2} \end{bmatrix}$$

Using the vector of control variables in (4.39) and expanding the objective described in (4.38) yields

$$\min_{\tau} \max_{r} x_i^T \begin{bmatrix} L_{1_i} & L_{2_i} \\ \vdots & \vdots \end{bmatrix} x_i < 0 \tag{4.40}$$

where

$$L_{1_i} \triangleq \begin{bmatrix} M_2^T Q_1 M_2 - \gamma_i^2 I & -M_2^T Q_1 M_2 M_1 L_\tau \\ -L_\tau^T M_1^T M_2^T Q_1 M_2 & L_\tau^T M_1^T M_2^T Q_1 M_2 M_1 L_\tau + Q_2 \end{bmatrix} \tag{4.41}$$

and

$$L_{2_i} \triangleq \begin{bmatrix} 0 & -M_2^T Q_1 M_2 M_1 L_w & M_2^T H_1^T \Gamma_1 & 0 \\ Q_2 M_3 & L_\tau^T M_1^T M_2^T Q_1 M_2 M_1 L_w & -L_\tau^T M_1^T M_2^T H_1^T \Gamma_1 & H_2^T \Gamma_2 \end{bmatrix} \tag{4.42}$$

The differentiation of (4.40) with respect to $\left[r^T, \tau^T\right]^T$, and then equating it to zero gives the saddle point for the maximum r and minimum τ, i.e.,

$$2 \begin{bmatrix} L_{1_i} & L_{2_i} \end{bmatrix} x_i = 0$$

or

$$L_{1_i} \begin{bmatrix} r_{wc} \\ \tau_{\min_i} \end{bmatrix} = -L_{2_i} \begin{bmatrix} f \\ w_p \\ x_{w_1} \\ x_{w_2} \end{bmatrix} \tag{4.43}$$

The performance objective ($\gamma_{\min_i}$) can be found by differentiating the above expression one more time by $\left[r^T, \tau^T\right]^T$. This results in

$$H_{hess_i} \triangleq \begin{bmatrix} M_2^T Q_1 M_2 - \gamma_i^2 I & -M_2^T Q_1 M_2 M_1 L_\tau \\ -L_\tau^T M_1^T M_2^T Q_1 M_2 & L_\tau^T M_1^T M_2^T Q_1 M_2 M_1 L_\tau + Q_2 \end{bmatrix} \tag{4.44}$$

which is the same expression as (3.53). Following the steps in (3.54) – (3.56), the performance objective is found to be

$$\gamma_i > \gamma_{\min_i} \equiv \sqrt{\bar{\lambda}[(M_2^T Q_1 M_2)^{-1} + M_1 L_\tau Q_2^{-1} L_\tau^T M_1^T]^{-1}} \equiv \gamma_{\min} \tag{4.45}$$

Similar to (3.58), optimum torque for impedance control is given as

$$\tau_{opt_i} = -\begin{bmatrix} 0 & I \end{bmatrix} L_{1_i}^{-1} L_{2_i} \begin{bmatrix} f \\ w_p \\ x_{w_1} \\ x_{w_2} \end{bmatrix}_k$$

Substituting the value of L_{2_i} from (4.42) produces

$$\begin{aligned} \tau_{opt_i} &= -\begin{bmatrix} 0 & I \end{bmatrix} L_{1_i}^{-1} \begin{bmatrix} 0 & -M_2^T Q_1 M_2 M_1 L_w & M_2^T H_1^T \Gamma_1 & 0 \\ Q_2 M_3 & L_\tau^T M_1^T M_2^T Q_1 M_2 M_1 L_w & -L_\tau^T M_1^T M_2^T H_1^T \Gamma_1 & H_2^T \Gamma_2 \end{bmatrix} \begin{bmatrix} f \\ w_p \\ x_{w_1} \\ x_{w_2} \end{bmatrix}_k \\ &= -\begin{bmatrix} 0 & I \end{bmatrix} L_{1_i}^{-1} \begin{bmatrix} 0 \\ Q_2 M_3 \end{bmatrix} f_k - \\ &\quad \begin{bmatrix} 0 & I \end{bmatrix} L_{1_i}^{-1} \begin{bmatrix} -M_2^T Q_1 M_2 M_1 L_w & M_2^T H_1^T \Gamma_1 & 0 \\ L_\tau^T M_1^T M_2^T Q_1 M_2 M_1 L_w & -L_\tau^T M_1^T M_2^T H_1^T \Gamma_1 & H_2^T \Gamma_2 \end{bmatrix} \begin{bmatrix} w_p \\ x_{w_1} \\ x_{w_2} \end{bmatrix}_k \end{aligned} \tag{4.46}$$

According to (3.50)

$$L_2 \equiv \begin{bmatrix} -M_2^T Q_1 M_2 M_1 L_w & M_2^T H_1^T \Gamma_1 & 0 \\ L_\tau^T M_1^T M_2^T Q_1 M_2 M_1 L_w & -L_\tau^T M_1^T M_2^T H_1^T \Gamma_1 & H_2^T \Gamma_2 \end{bmatrix}$$

As L_1 is defined in (3.49) and it can be seen that $L_{1_i} \equiv L_1$, hence

$$\begin{aligned}\tau_{opt_i} &= -\begin{bmatrix}0 & I\end{bmatrix} L_1^{-1} \begin{bmatrix}0 \\ Q_2 M_3\end{bmatrix} f_k - \begin{bmatrix}0 & I\end{bmatrix} L_1^{-1} L_2 \begin{bmatrix}w_p \\ x_{w_1} \\ x_{w_2}\end{bmatrix}_k \\ &= -\begin{bmatrix}0 & I\end{bmatrix} L_1^{-1} \begin{bmatrix}0 \\ Q_2 M_3\end{bmatrix} f_k + \tau_{opt} \end{aligned} \tag{4.47}$$

where τ_{opt} is defined in (3.28). Using results from (3.60) – (3.63) in above equation yields

$$\tau_{opt_i} = -(L_\tau^T M_1^T \widetilde{Q}_1 M_1 L_\tau + Q_2)^{-1} Q_2 M_3 f_k + \tau_{opt} \tag{4.48}$$

or

$$\tau_{opt_i} \equiv -(L_\tau^T M_1^T \widetilde{Q}_1 M_1 L_\tau + Q_2)^{-1} \begin{bmatrix} (Q_2 M_3)^T \\ (L_\tau^T M_1^T \widetilde{Q}_1 M_1 L_w)^T \\ -(L_\tau^T M_1^T (\gamma_i^{-2} \widetilde{Q}_1 + I) M_2^T H_1^T \Gamma_1)^T \\ (H_2^T \Gamma_2)^T \end{bmatrix}^T \begin{bmatrix} f \\ w_p \\ x_{w_1} \\ x_{w_2} \end{bmatrix}_k \tag{4.49}$$

where the lower bound of γ_i is as defined in (4.45). □

It can be seen in (4.48) that the force (f) is linearly related to the torque in joint space. The direct relation of the applied force onto the generated torque enables the manipulator to reduce its stiffness.

4.3 Scaling of the Force Vector

This section explores the properties of the force control when the force vector is scaled, as shown in Figure 4.2. One of the interesting property of the following theorem is that the expression for the optimum torque and the performance objective remains the same. This property has been used in Section 5.2 to simplify the expression for the optimum torque and the performance objective.

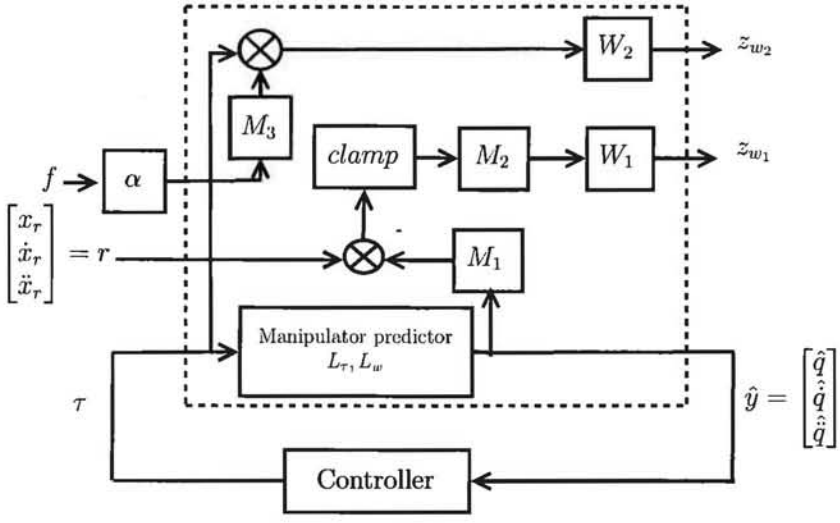

Figure 4.2: Scaling of the force vector. The scaling factor α is *not* part of the plant

Theorem 4.3. *If τ_{opt_f} is defined in (4.2) and $\gamma_{\min_f}$ is defined in (4.3) for the force vector (f) acting on the end-effector of the manipulator in operational space, then the optimum torque vector ($\tau_{opt_{\alpha f}}$) for the force vector (αf) is given by*

$$\tau_{opt_{\alpha f}} \equiv \tau_{opt_f} \tag{4.50}$$

provided that

$$\gamma_{\min_{\alpha f}} \equiv \gamma_{\min_f} \tag{4.51}$$

and

$$(x_{w_1})_{k+1} = A_{w_1}(x_{w_1})_k + B_{w_1}(\alpha f + \tau)_k \tag{4.52}$$

Proof of Theorem 4.3. Following the proof of Theorem 4.1, the objective in (4.13) can be written as

$$\min_{\tau} \max_{r,f} \left(\begin{bmatrix} z_{w_1} \\ z_{w_2} \end{bmatrix}^T \begin{bmatrix} z_{w_1} \\ z_{w_2} \end{bmatrix} - \gamma_{\alpha f}^2 (r^T r + \alpha^2 f^T f) \right) < 0 \tag{4.53}$$

and the vector of control variables in (4.14) becomes

$$\begin{bmatrix} z_{w_1} \\ z_{w_2} \end{bmatrix} = \begin{bmatrix} H_1M_2 & 0 & -H_1M_2M_1L_\tau & -H_1M_2M_1L_w & \Gamma_1 & 0 \\ 0 & \alpha H_2M_3 & H_2 & 0 & 0 & \Gamma_2 \end{bmatrix} x_f \quad (4.54)$$

where x_f is defined in (4.15). Substituting (4.54) in (4.53) yields

$$\min_{\tau} \max_{r,f} x_f^T \begin{bmatrix} L_{1_{\alpha f}} & L_{2_{\alpha f}} \\ \vdots & \vdots \end{bmatrix} x_f < 0 \quad (4.55)$$

where

$$L_{1_{\alpha f}} \triangleq \begin{bmatrix} M_2^TQ_1M_2 - \gamma_f^2 I & 0 & -M_2^TQ_1M_2M_1L_\tau \\ 0 & \alpha^2M_3^TQ_2M_3 - \alpha^2\gamma_f^2 I & \alpha M_3^TQ_2 \\ -L_\tau^TM_1^TM_2^TQ_1M_2 & \alpha Q_2M_3 & L_\tau^TM_1^TM_2^TQ_1M_2M_1L_\tau + Q_2 \end{bmatrix} \quad (4.56)$$

and

$$L_{2_{\alpha f}} \triangleq \begin{bmatrix} -M_2^TQ_1M_2M_1L_w & M_2^TH_1^T\Gamma_1 & 0 \\ 0 & 0 & \alpha M_3^TH_2^T\Gamma_2 \\ L_\tau^TM_1^TM_2^TQ_1M_2M_1L_w & -L_\tau^TM_1^TM_2^TH_1^T\Gamma_1 & H_2^T\Gamma_2 \end{bmatrix} \quad (4.57)$$

Following the steps (4.19) – (4.21) to find the performance objective, (4.22) can be written as

$$X_{\alpha f} \triangleq A - AB^T(BAB^T + C)^{-1}BA \quad (4.58)$$

where $A \triangleq (L_\tau^TM_1^TM_2^TQ_1M_2M_1L_\tau + Q_2)^{-1}$, $B \triangleq \alpha M_3^TQ_2$, and $C \triangleq \alpha^2\gamma_f^2 - \alpha^2M_3^TQ_2M_3$. Using (3.37) in (4.58) produces

$$X_{\alpha f} = (L_\tau^TM_1^TM_2^TQ_1M_2M_1L_\tau + Q_2 - Q_2M_3(-\gamma_f^2 + M_3^TQ_2M_3)^{-1}M_3^TQ_2)^{-1} \quad (4.59)$$

that is equivalent to (4.23) which leads to

$$\gamma_{\min_{\alpha f}} \equiv \gamma_{\min_f} \equiv \sqrt{\bar{\lambda}[(I + M_1L_\tau M_3M_3^TL_\tau^TM_1^T)((M_2^TQ_1M_2)^{-1} + M_1L_\tau Q_2^{-1}L_\tau^TM_1^T)^{-1}]}$$

Similarly, following steps (4.25) – (4.26) and using (4.6)

$$\tau_{opt_{\alpha f}} = -(L_\tau^T M_1^T X_{\alpha f_1} M_1 L_\tau + X_{\alpha f_2})^{-1} X_{\alpha f_3} L_{2_{\alpha f}} \begin{bmatrix} w_p \\ x_{w_1} \\ x_{w_2} \end{bmatrix}_k \tag{4.60}$$

where

$$\begin{aligned} X_{\alpha f_1} &\triangleq M_2^T Q_1 M_2 - M_2^T Q_1 M_2 (M_2^T Q_1 M_2 + (-\gamma_{\alpha f}^2 I))^{-1} M_2^T Q_1 M_2 \equiv X_{f_1}, \\ X_{\alpha f_2} &\triangleq Q_2 - \alpha^2 Q_2 M_3 (\alpha^2 M_3^T Q_2 M_3 + (-\alpha^2 \gamma_{\alpha f}^2 I))^{-1} M_3^T Q_2 \\ &= Q_2 - Q_2 M_3 (M_3^T Q_2 M_3 + (-\gamma_{\alpha f}^2 I))^{-1} M_3^T Q_2 \equiv X_{f_2}, \end{aligned}$$

and

$$X_{\alpha f_3} \triangleq \left[L_\tau^T M_1^T M_2^T Q_1 M_2 (M_2^T Q_1 M_2 + (-\gamma_{\alpha f}^2 I))^{-1} \quad -\alpha Q_2 M_3 (\alpha^2 M_3^T Q_2 M_3 + (-\alpha^2 \gamma_{\alpha f}^2 I))^{-1} \quad I \right] \tag{4.61}$$

$X_{\alpha f_1}$ and $X_{\alpha f_2}$ can be simplified using (3.37), i.e.,

$$X_{\alpha f_1} = ((M_2^T Q_1 M_2)^{-1} - \gamma_{\alpha f}^{-2})^{-1} \equiv \widetilde{Q}_1 \tag{4.62}$$

$$X_{\alpha f_2} = (Q_2^{-1} - \gamma_{\alpha f}^{-2} M_3 M_3^T)^{-1} \equiv \widetilde{Q}_{2_{\alpha f}} \tag{4.63}$$

Using (4.57) and (4.61)

$$X_{\alpha f_3} L_{2_{\alpha f}} = \begin{bmatrix} (L_\tau^T M_1^T (M_2^T Q_1 M_2 - M_2^T Q_1 M_2 (M_2^T Q_1 M_2 - \gamma_{\alpha f}^2 I)^{-1} M_2^T Q_1 M_2) M_1 L_w)^T \\ (L_\tau^T M_1^T (M_2^T Q_1 M_2 (M_2^T Q_1 M_2 - \gamma_{\alpha f}^2 I)^{-1} - I) M_2^T H_1^T \Gamma_1)^T \\ (H_2^T \Gamma_2 - \alpha Q_2 M_3 (\alpha^2 M_3^T Q_2 M_3 - \alpha^2 \gamma_{\alpha f}^2 I)^{-1} (\alpha M_3^T H_2^T \Gamma_2))^T \end{bmatrix}^T \tag{4.64}$$

or

$$X_{\alpha f_3} L_{2_{\alpha f}} = \begin{bmatrix} (L_\tau^T M_1^T (M_2^T Q_1 M_2 - M_2^T Q_1 M_2 (M_2^T Q_1 M_2 - \gamma_{\alpha f}^2 I)^{-1} M_2^T Q_1 M_2) M_1 L_w)^T \\ (L_\tau^T M_1^T (M_2^T Q_1 M_2 (M_2^T Q_1 M_2 - \gamma_{\alpha f}^2 I)^{-1} - I) M_2^T H_1^T \Gamma_1)^T \\ (H_2^T \Gamma_2 - Q_2 M_3 (M_3^T Q_2 M_3 - \gamma_{\alpha f}^2 I)^{-1} M_3^T H_2^T \Gamma_2)^T \end{bmatrix}^T \tag{4.65}$$

which is equivalent to (4.31). Substituting the value of $X_{\alpha f_3} L_{2_{\alpha f}}$, $X_{\alpha f_1}$, and $X_{\alpha f_2}$ from (4.33), (4.29), and (4.30) in (4.60), respectively, yields

$$\tau_{opt_{\alpha f}} = -(L_\tau^T M_1^T \widetilde{Q}_1 M_1 L_\tau + \widetilde{Q}_{2_{\alpha f}})^{-1} \begin{bmatrix} (L_\tau^T M_1^T \widetilde{Q}_1 M_1 L_w)^T \\ -(L_\tau^T M_1^T (\gamma_{\alpha f}^{-2} \widetilde{Q}_1 + I) M_2^T H_1^T \Gamma_1)^T \\ ((I + \gamma_{\alpha f}^{-2} \widetilde{Q}_{2_{\alpha f}} M_3 M_3^T) H_2^T \Gamma_2)^T \end{bmatrix}^T \begin{bmatrix} w_p \\ x_{w_1} \\ x_{w_2} \end{bmatrix}_k$$

As $\gamma_f \equiv \gamma_{\alpha f}$, hence

$$\tau_{opt_{\alpha f}} \equiv \tau_{opt_f}$$

□

For the scaled disturbance vector, the expressions for the optimum torque and the performance objective remain the same. However, scaling affects the updating procedure for the weight state as given in (4.52). The expressions for torque and performance objective remain unchanged because (4.2) and (4.3) are not directly affected by the value of f. The following two corollaries utilize these properties.

Corollary 4.1. *If τ_{opt_f} is defined in (4.2), $\gamma_{\min_f}$ in (4.3), $\tau_{opt_{\alpha f}}$ in (4.50), and $\gamma_{\min_{\alpha f}}$ in (4.51) such that*

$$\tau_{opt_{\alpha f}} \equiv \tau_{opt_f} \tag{4.66}$$

provided that

$$\gamma_{\min_{\alpha f}} \equiv \gamma_{\min_f} \tag{4.67}$$

and

$$(x_{w_1})_{k+1} = A_{w_1} (x_{w_1})_k + B_{w_1} (\alpha f + \tau)_k \tag{4.68}$$

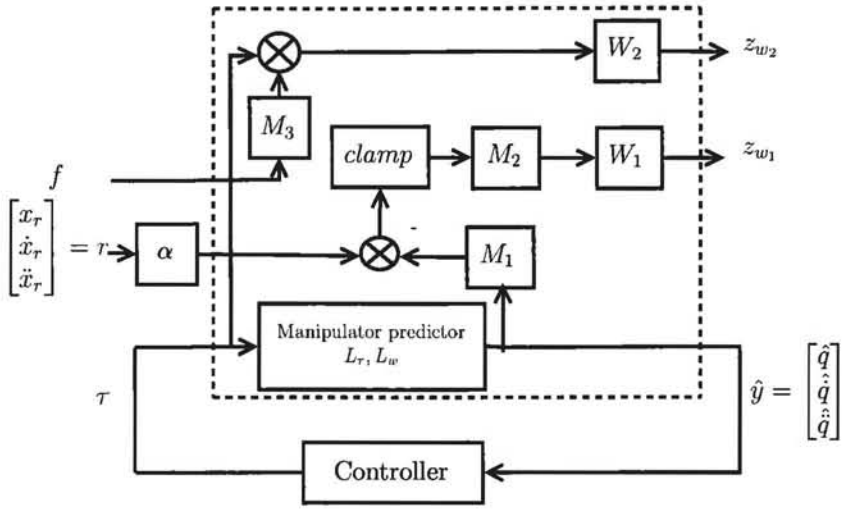

Figure 4.3: Scaling of the reference trajectory

then the strictly causal subspace based, $\gamma_{\alpha r}$-level $\mathscr{H}_\infty$ hybrid force/position control with scaled reference trajectory (αr) for times $\{k, \ldots, k+i, k+i-1\}$, as shown in Figure 4.3, is

$$\tau_{opt_{\alpha r}} \equiv \tau_{opt_f} \tag{4.69}$$

provided that

$$\gamma_{\min_{\alpha r}} \equiv \gamma_{\min_f} \tag{4.70}$$

and

$$(x_{w_2})_{k+1} = A_{w_1}(x_{w_2})_k + B_{w_1}(M_2(\alpha r_k - M_1 y_k)) \tag{4.71}$$

Corollary 4.2. *If $\tau_{opt_f} = g(w_p, x_{w_1}, x_{w_2})$ is defined in (4.2) and $\gamma_{\min_f}$ in (4.3) for the force vector (f) in operational space on the end-effector such that*

$$\tau_{opt_{\alpha f}} \equiv \tau_{opt_f} \tag{4.72}$$

provided that

$$\gamma_{\min_{\alpha f}} \equiv \gamma_{\min_f} \tag{4.73}$$

and

$$(x_{w_1})_{k+1} = A_{w_1}(x_{w_1})_k + B_{w_1}(\alpha f + \tau)_k \tag{4.74}$$

then $\tau_{opt_i} = g(f, w_p, x_{w_1}, x_{w_2})$ *defined in (4.36) for the force vector (f) in operational space can be re-written for the scaled force vector* (αf) *as*

$$\begin{aligned}\tau_{opt_{\alpha i}} &= g(\alpha f, w_p, x_{w_1}, x_{w_2}) \\ &= -(L_\tau^T M_1^T \widetilde{Q}_1 M_1 L_\tau + Q_2)^{-1} \begin{bmatrix} (\alpha Q_2 M_3)^T \\ (L_\tau^T M_1^T \widetilde{Q}_1 M_1 L_w)^T \\ -(L_\tau^T M_1^T (\gamma_i^{-2} \widetilde{Q}_1 + I) M_2^T H_1^T \Gamma_1)^T \\ (H_2^T \Gamma_2)^T \end{bmatrix}^T \begin{bmatrix} f \\ w_p \\ x_{w_1} \\ x_{w_2} \end{bmatrix}_k \end{aligned} \tag{4.75}$$

provided that

$$\gamma_{\min_{\alpha i}} \triangleq \gamma_{\min_i}$$

and

$$(x_{w_1})_{k+1} = A_{w_1}(x_{w_1})_k + B_{w_1}(\alpha f + \tau)_k \tag{4.76}$$

where $\gamma_{\min_i}$ *is defined in (4.37).*

4.4 Summary

The important results of this chapter are:

- Model free subspace based operational space $\mathscr{H}_\infty$ hybrid force/position control (4.2) – (4.3);
- Reduction in performance in the hybrid control (4.35);
- Model free subspace based operational space $\mathscr{H}_\infty$ impedance control (4.36) – (4.37);
- Effect of the scaling of the force vector in hyrbrid force/position control (4.50) – (4.52);
- Effect of the scaling of the reference trajectory (4.69) – (4.71); and

- Effect of the scaling of the force vector in impedance control (4.75) – (4.76).

Chapter 5

Special Cases of Interaction Control

This chapter proposes two control schemes which can be considered extension to interaction control. The control scheme proposed in Section 5.1 removes the bias from the dynamic behaviour of the system to compensate for gravity effects. The control scheme proposed in Section 5.2 formulates a control law for parallel manipulators.

5.1 Bias Removal Control

In this section, interaction control as presented in Section 4.1 is adapted to remove the bias from the dynamic behaviour of the system. In isolation, if an actuator is driving a single joint, the torque produced by the actuator should be equal to the measurement of a strain gauge mounted on the joint. In the presence of exogenous forces such as gravity, the strain gauge senses the combined torque of both the actuator and these forces. If τ_g is the measurement of the torque from strain gauges and τ is the torque produced by the actuators, then

$$f \triangleq \tau_g - \tau \tag{5.1}$$

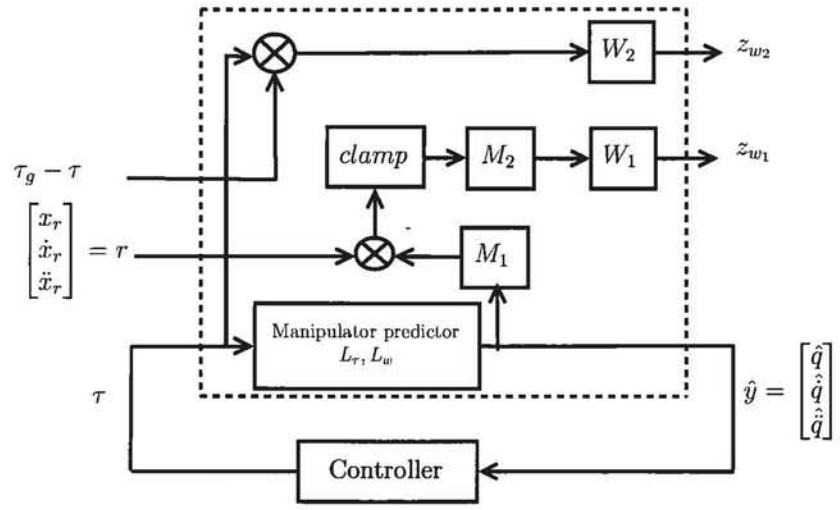

Figure 5.1: Model free subspace based operational space $\mathscr{H}_\infty$ control with bias removal. τ_g is the torque vector measured from strain gauges

is the disturbance vector that needs to be minimized, as shown in Figure 5.1. The actuator torque data, τ, is obtained through actuator current measurements [101]. The relationship between current and torque for an actuator can be determined through a separate experiment.

Such a technique has been used by Koivo [57] and Raibert and Craig [82], in which the manipulator follows a torque trajectory. Hashimoto [43] proposed the use of *joint-torque sensory feedback* (JTF) control to remove the effect of external disturbances such as gravitational force. Aghili et al. [3] proposed an adaptive implementation of JTF control.

It has been reported that the bias in the dynamic behaviour of the manipulator is mainly due to gravity [57, 26], hence the proposed control scheme can be used to compensate the gravitational pull on the structure. Examples of torque-measuring techniques that employ strain gauges are given in [82], [78], and [2].

Here, it should be noted that the impedance control cannot be used with the bias removal control because the whole structure would lose its stiffness and simply collapse as a result of the torque measured at joints being mainly due to the gravitational force.

Proposition 5.1. *If measurements of the calculated torque vector (τ), joint vector (y), torque vector from strain gauges (τ_g), and reference trajectory (r) in operational space are available for times $\{k-i,\ldots,k-2,k-1\}$, then the strictly causal subspace based, γ_g-level $\mathscr{H}_\infty$ bias removal control for times $\{k,\ldots,k+i,k+i-1\}$ is given by*

$$\tau_{opt_g} \triangleq -(L_\tau^T M_1^T \widetilde{Q}_1 M_1 L_\tau + \widetilde{Q}_2)^{-1} \begin{bmatrix} (L_\tau^T M_1^T \widetilde{Q}_1 M_1 L_w)^T \\ -(L_\tau^T M_1^T (\gamma_g^{-2}\widetilde{Q}_1 + I) M_2^T H_1^T \Gamma_1)^T \\ ((\gamma_g^{-2}\widetilde{Q}_2 + I) H_2^T \Gamma_2)^T \end{bmatrix}^T \begin{bmatrix} w_p \\ x_{w_1} \\ x_{w_2} \end{bmatrix}_k \tag{5.2}$$

provided that

$$\gamma_g > \gamma_{\min_g} \triangleq \sqrt{\bar{\lambda}[(I + M_1 L_\tau L_\tau^T M_1^T)((M_2^T Q_1 M_2)^{-1} + M_1 L_\tau Q_2^{-1} L_\tau^T M_1^T)^{-1}]} \tag{5.3}$$

where

$$\widetilde{Q}_2 \triangleq (Q_2^{-1} - \gamma_g^{-2} I)^{-1} \tag{5.4}$$

Proof of Proposition 5.1. Substituting I for M_3 in Theorem 4.1 as the torque vector (τ_g) is in joint space. $\widetilde{Q}_{2_f}$ can be re-written as

$$(\widetilde{Q}_{2_f})_{M_3=I} = (Q_2^{-1} - \gamma_f^{-2})^{-1} \equiv \widetilde{Q}_2$$

Using new values of $\widetilde{Q}_{2_f}$ and M_3 in (4.2) and (4.3) yields

$$\tau_{opt_g} \equiv -(L_\tau^T M_1^T \widetilde{Q}_1 M_1 L_\tau + \widetilde{Q}_2)^{-1} \begin{bmatrix} (L_\tau^T M_1^T \widetilde{Q}_1 M_1 L_w)^T \\ -(L_\tau^T M_1^T (\gamma_g^{-2}\widetilde{Q}_1 + I) M_2^T H_1^T \Gamma_1)^T \\ ((\gamma_g^{-2}\widetilde{Q}_2 + I) H_2^T \Gamma_2)^T \end{bmatrix}^T \begin{bmatrix} w_p \\ x_{w_1} \\ x_{w_2} \end{bmatrix}_k \tag{5.5}$$

and

$$\gamma_g > \gamma_{\min_g} \equiv \sqrt{\bar{\lambda}[(I + M_1 L_\tau L_\tau^T M_1^T)((M_2^T Q_1 M_2)^{-1} + M_1 L_\tau Q_2^{-1} L_\tau^T M_1^T)^{-1}]} \tag{5.6}$$

□

The state vector of the performance weight W_2 can be updated using

$$(x_{w_2})_{k+1} = A_{w_2}(x_{w_2})_k + B_{w_2}(\underbrace{\tau_g - \tau}_{f} + \tau)_k$$

or

$$(x_{w_2})_{k+1} = A_{w_2}(x_{w_2})_k + B_{w_2}(\tau_g)_k \tag{5.7}$$

5.2 Parallel Manipulators

The end-effector of a parallel manipulator is connected to its *base* via a number of serial manipulators in parallel. In these manipulators, there are always more joints than the number of DOF of the end-effector. This places constraints on the structure such that all the joints cannot be actuated at the same time. If the end-effector has l DOF, then there are l active joints where $l \leq 6$. All the other joints are passive and their motion is dependant on the motion of the active joints. The most famous family of such manipulators are called *Stewart-Gough* platforms [11]. These platforms are widely used in simulators [120], low impact docking systems for space vehicles [104], and in form of a hexapod for precise machining [110].

Figure 5.2 shows a 3-R$\underline{\text{P}}$R robot, which has three joints in each serial link. R stands for a rotatory joint and P stands for a prismatic joint whereby the underline signifies the joint which is actuated [91].

The forward kinematics function of a parallel has been studied in detail in the literature, especially for a 3-R$\underline{\text{P}}$R robot. Kong [59] derived algebraic expressions for the forward kinematics of a 3-R$\underline{\text{P}}$R robot and analyzed its singularities. Collins [20] used planar quaternions to formulate kinematic constraints in equations for a 3-R$\underline{\text{P}}$R robot. Murray et al. [69] used coefficients of a *constraint manifold*, which are functions of the locations of the base and platform joints and the distance between them, for the kinematics synthesis of a 3-R$\underline{\text{P}}$R robot. Wenger et al. [112] studied the *degeneracy* in the forward kinematics of a 3-R$\underline{\text{P}}$R robot. Kim et al. [55] and Dutre et al. [31] found the analytical Jacobian for a parallel manipulator. However, there

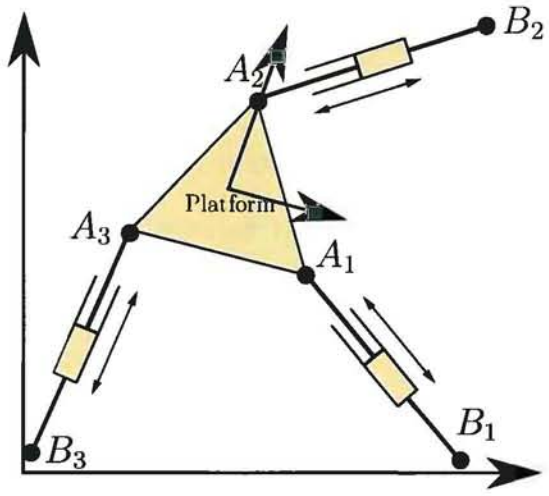

Figure 5.2: A 3-RPR planar parallel manipulator. B_1, B_2, and B_3 are connected to a stationary base

is no attempt in literature to formulate analytically the forward kinematics function for non-redundant parallel manipulators.

In the following, the forward kinematics function of a parallel manipulator is evaluated analytically using the position-closure property to relate the joint variables of the active joints to the position of the end-effector. The analytical Jacobian of a parallel manipulator is also obtained as described in the literature. The following section formulates, N_{1_c} and N_{2_c}, matrices for the forward and inverse kinematics operations followed by a control scheme for the manipulator.

5.2.1 Forward Kinematics Function

In order to formulate the forward and inverse kinematics matrices such as (3.6) and (3.22), it is important to formulate *analytically* the forward kinematics function of a parallel manipulator. The derivation is somewhat similar to the derivation of the analytic Jacobian of a parallel manipulator by Dutre et al. [31], which was derived using the velocity-closure property. The derivation is given as follows;

As all the manipulators are connected to the same end-effector, it can be stated, using the position-closure property, that

$$F_c q_a = F_1 q_1 = F_2 q_2 = \cdots = F_n q_n \tag{5.8}$$

where q_j is the vector of joint variables of j^{th} manipulator and $F_j(q) \triangleq \frac{F_j(q)}{q_j}$ is the forward kinematics function of the j^{th} manipulator.

Each column of the function F_c corresponds to rotational angle or displacement of an active joint, depending on whether the joint is rotatory or prismatic. Hence

$$F_c^i = F_j q_j^i \tag{5.9}$$

where $F_c^i \in \Re^{n_a}$ is the i^{th} column of F_c and q_j^i is a vector of joint variables of the j^{th} manipulator when the i^{th} active joint is moved one unit while all the other active joints are locked. If q_c is the vector of all the joint variables, i.e.,

$$q_c = \begin{bmatrix} q_1 \\ q_2 \\ \vdots \\ q_{n_c} \end{bmatrix} \in \Re^{n_c} \tag{5.10}$$

then (5.9) can be written as

$$F_c^i = F_j S_j q_c^i \tag{5.11}$$

where q_c^i is a vector of all the joints when the i^{th} active joint is moved one unit while all the other active joints are locked and S_j is a selection matrix to select the variables of the j^{th} manipulator, i.e.,

$$S_j = \begin{bmatrix} 0 & \dots & 1 & 0 & \dots & 0 & \dots & 0 \\ 0 & \dots & 0 & 1 & \dots & 0 & \dots & 0 \\ \vdots & \ddots & \vdots & \vdots & \ddots & \vdots & \ddots & \vdots \\ 0 & \dots & 0 & 0 & \dots & 1 & \dots & 0 \end{bmatrix} \in \Re^{n_j \times n_c}$$

where n_j is the number of joints in the j^{th} manipulator. Let q_p be the vector of passive joint variables and q_a be the vector of active joint variables such that

$$q_p = S_p q_c \tag{5.12}$$

$$q_a = S_a q_c \tag{5.13}$$

where $q_p \in \Re^{n_p}$ and $q_a \in \Re^{n_a}$ and S_p and S_a are selection matrices for passive and active joints, respectively. Typical values of S_p and S_a can be written as

$$S_p = \begin{bmatrix} \dots & 0 & 1 & 0 & \dots & 0 & 0 & 0 & \dots \\ \vdots & \vdots & \vdots & \vdots & \vdots & \vdots & \vdots & \vdots & \vdots \\ \dots & 0 & 0 & 0 & \dots & 0 & 1 & 0 & \dots \end{bmatrix} \in \Re^{n_p \times n_c}$$

and

$$S_a = \begin{bmatrix} \dots & 0 & 0 & 0 & \dots & 0 & 1 & 0 & \dots \\ \vdots & \vdots & \vdots & \vdots & \vdots & \vdots & \vdots & \vdots & \vdots \\ \dots & 0 & 1 & 0 & \dots & 0 & 0 & 0 & \dots \end{bmatrix} \in \Re^{n_a \times n_c}$$

Both of these matrices are sparse and orthogonal, i.e., $S_p S_p^T = I$ and $S_a S_a^T = I$, which implies

$$q_{c_p} = S_p^T q_p \tag{5.14}$$

$$q_{c_a} = S_a^T q_a \tag{5.15}$$

where q_{c_p} is equivalent to q_c except that the active joints are set to zero and similarly, q_{c_a} is equivalent to q_c except that the passive joints are set to zero such that

$$q_c = q_{c_p} + q_{c_a} \tag{5.16}$$

Substituting (5.14) and (5.15) in (5.16) yields

$$q_c = S_p^T q_p + S_a^T q_a \tag{5.17}$$

In reference to the position-closure property (5.8), let

$$Aq_c = 0 \tag{5.18}$$

where

$$A = \begin{bmatrix} \frac{F_1}{q_1} & -\frac{F_2}{q_2} & 0 & \dots & 0 \\ \frac{F_1}{q_1} & 0 & -\frac{F_3}{q_3} & \dots & 0 \\ \vdots & \vdots & \vdots & \ddots & \vdots \\ \frac{F_1}{q_1} & 0 & 0 & \dots & -\frac{F_n}{q_n} \end{bmatrix} \in \Re^{n_a(n-1)\times n_c} \tag{5.19}$$

Substituting the value of q_c from (5.17) gives

$$\begin{aligned} Aq_c &= A(q_{c_p} + q_{c_a}) \\ &= AS_p^T q_p + AS_a^T q_a \\ &= A_p q_p + A_a q_a \end{aligned} \tag{5.20}$$

Applying (5.18)

$$q_p = -A_p^\dagger A_a q_a \tag{5.21}$$

Substituting this expression in (5.17) yields

$$q_c = S_a^T q_a - S_p^T A_p^\dagger A_a q_a \tag{5.22}$$

As q_c^i is defined for a unit displacement of the i^{th} active joint, hence, q_a can be replaced with a column of S_a which corresponds to the i^{th} active joint, denoted by $(S_a)^i$, to evaluate q_c^i, i.e.,

$$q_c^i = S_a^T (S_a)^i - S_p^T A_p^\dagger A_a (S_a)^i \tag{5.23}$$

Substituting the above value in (5.11) gives

$$F_c^i = F_j S_j q_c^i \tag{5.24}$$

or

$$F_c = F_j S_j \begin{bmatrix} q_c^1 & q_c^2 & \dots & q_c^{n_a} \end{bmatrix} \tag{5.25}$$

Example

As the proposed kinematics framework is evaluated analytically, it can be applied on any non-redundant parallel manipulator. However, in this section, for the sake of demonstration, a simple case of a 3-RPR robot is presented, shown in Figure 5.2.

The forward kinematics function for the first manipulator can be stated as

$$F_1 = \begin{bmatrix} (x_{1,1} + q_{1,2} + x_{1,2})\cos(q_{1,1}) + x_{1,3}\cos(q_{1,1} + q_{1,3}) \\ (x_{1,1} + q_{1,2} + x_{1,2})\sin(q_{1,1}) + x_{1,3}\sin(q_{1,1} + q_{1,3}) \\ q_{1,1} + q_{1,3} \end{bmatrix} \tag{5.26}$$

where $x_{1,2}$ and $q_{1,2}$ denote the length of the second link and the second joint variable, respectively. The expressions for other links can be written in the same way.

Table 5.1: Assumed values for a 3-RPR robot

Manipulator 1	Manipulator 2	Manipulator 3
$q_{1,1} = \pi/3$	$q_{2,1} = 2\pi/3$	$q_{3,1} = 4\pi/3$
$q_{1,2} = 1$	$q_{2,2} = 1$	$q_{3,2} = 1$
$q_{1,3} = 0$	$q_{2,3} = -\pi/3$	$q_{3,3} = -\pi$
$x_{1,1} = 0.5$	$x_{2,1} = 0.5$	$x_{3,1} = 0.5$
$x_{1,2} = 0.5$	$x_{2,2} = 0.5$	$x_{3,2} = 0.5$
$x_{1,3} = 1$	$x_{2,3} = 1$	$x_{3,3} = 1$

Using this kinematic model for the values given in Table 5.1, the end-effector position was found to be at

$$x_{end_c} = \begin{bmatrix} 1.5 \\ 2.5981 \\ 1.0472 \end{bmatrix}$$

where the first two elements represent the position in $x - y$ plane and the third element represents the angular rotation of the end-effector.

The forward kinematics function, F_c, gives the following end-effector position for the active joints $\begin{bmatrix}1,1,1\end{bmatrix}^T$ [87];

$$x_{end} = \begin{bmatrix}1.498\\2.597\\1.048\end{bmatrix}$$

5.2.2 Analytical Jacobian and its Derivative

Dutre et al. [31] evaluated the analytical Jacobian for a parallel manipulator using the velocity-closure property. The Jacobian can also be derived by replacing F_c in (5.25) by J_c and q_c^i by $\dot{q}_c^i$, i.e.,

$$J_c = J_j S_j \begin{bmatrix}\dot{q}_c^1 & \dot{q}_c^2 & \dots & \dot{q}_c^{n_a}\end{bmatrix} \tag{5.27}$$

where J_c is the analytical Jacobian that relates the velocities of the active joints to the end-effector velocity. J_j and $\dot{q}_j$ are the Jacobian and the vector of joint velocities of the j^{th} manipulator, respectively. $\dot{q}_c^i$ can be stated using (5.23) as follows;

$$\dot{q}_c^i = S_a^T (S_a)^i - S_p^T B_p^\dagger B_a (S_a)^i \tag{5.28}$$

where $B_p = BS_p^T$, $B_a = BS_a^T$, and

$$B = \begin{bmatrix}J_1 & -J_2 & 0 & \dots & 0\\ J_1 & 0 & -J_3 & \dots & 0\\ \vdots & \vdots & \vdots & \ddots & \vdots\\ J_1 & 0 & 0 & 0 & -J_n\end{bmatrix} \in \Re^{n_a(n-1)\times n_c} \tag{5.29}$$

Using B, the velocity-closure property of a parallel manipulator can be written as

$$B\dot{q}_c = 0$$

The derivative of the closed-loop Jacobian (J_c) given in (5.27) is

$$\dot{J}_c = \dot{J}_j S_j \begin{bmatrix} \ddot{q}_c^1 & \ddot{q}_c^2 & \dots & \ddot{q}_c^{n_a} \end{bmatrix} \tag{5.30}$$

where

$$\ddot{q}_c^i = -S_p^T \left(\frac{\partial B_p^\dagger}{\partial q_i} B_a + B_p^\dagger \frac{\partial B_a}{\partial q_i} \right) (S_a)^i \tag{5.31}$$

The derivative of the Jacobian of each manipulator of a parallel manipulator can be expressed using (3.5), i.e.,

$$\dot{J}_j = \sum_{i=1}^{n_a} \frac{\partial J_j}{\partial q_i} \dot{q}_i = \sum_{i=1}^{n_a} \left(\sum_{k=1}^{n_j} \frac{\partial J_j}{\partial q_{j,k}} \frac{\partial q_{j,k}}{\partial q_i} \right) \dot{q}_i \tag{5.32}$$

where k is a joint of the j^{th} manipulator and $\frac{\partial J_j}{\partial q_{j,k}}$ represents Jacobian derivative of the j^{th} serial manipulator. The factor, $\frac{\partial q_{j,k}}{\partial q_i}$ in (5.32), is the k^{th} component in $S_j \ddot{q}_c^i$.

5.2.3 Forward and Inverse Kinematics Matrices

The forward kinematics matrix N_{1_c} for a parallel manipulator can now be expressed using (3.6), (5.25), (5.30), and (5.27)

$$N_{1_c} \triangleq \begin{bmatrix} F_c & 0 & 0 \\ 0 & J_c & 0 \\ 0 & \dot{J}_c & J_c \end{bmatrix} \in \Re^{3n_c \times 3l} \tag{5.33}$$

Similarly, the inverse kinematics matrix N_{2_c} for a parallel manipulator can be written using (3.22) as follows;

$$N_{2_c} \triangleq \begin{bmatrix} J_c^* & 0 & 0 \\ 0 & J_c^* & 0 \\ 0 & -J_c^* \dot{J}_c J_c^* & J_c^* \end{bmatrix} \in \Re^{3l \times 3n_c} \tag{5.34}$$

where $J_c^* = J_c^T (J_c J_c^T + \lambda_c^2 I)^{-1}$. The value of λ_c is set by the designer.

5.2.4 Model Free Operational Space Control

It can be proven that, like serial manipulators, the dynamic parameters of parallel manipulators are linearly related to the applied torque [1, 39], i.e.,

$$\tau_a = W_c(q, \dot{q}, \ddot{q})\Theta_c \tag{5.35}$$

where τ_a is the torque of active joints and Θ_c is a vector of the dynamic parameters of a parallel manipulator.

The relationship between the torque of active joints and passive joints is given by the following relation [16];

$$\tau_c = \tau_a + \left(\frac{\partial q_p}{\partial q_a}\right)^T \tau_p \tag{5.36}$$

where $\tau_p \in \Re^{n_p}$ is the torque measured from strain gauges on passive joints, $\tau_a \in \Re^{n_a}$ is the torque produced by the actuators in active joints, and $\tau_c \in \Re^{n_a}$ is the torque measured from the strain gauges mounted on active joints. From [31], it can be inferred that

$$\frac{\partial q_p}{\partial q_a} = B_p^{\dagger} B_a$$

Using the above value in (5.36) yields

$$\tau_c = \tau_a - (B_p^{\dagger} B_a)^T \tau_p$$

or

$$\tau_c = \tau_a - B_a^T (B_p^{\dagger})^T \tau_p \tag{5.37}$$

The passive joints project torque onto the active joints with a factor of $-B_a^T(B_p^{\dagger})^T$. This will be used as the exogenous force disturbance signal in the hybrid controller, as shown in Figure 5.3.

Proposition 5.2. *If measurements of the calculated torque vector for active joints (τ_a), joint vector of active joints (y_a), torque vector from passive joints (τ_p), and*

reference trajectory (r) in operational space are available for times $\{k-i,\ldots,k-2,k-1\}$, *then the strictly causal subspace based,* γ_c*-level* $\mathscr{H}_\infty$ *parallel manipulator control for times* $\{k,\ldots,k+i,k+i-1\}$ *is given by*

$$\tau_{opt_c} \triangleq -(L_\tau^T M_1^T \widetilde{Q}_1 M_1 L_\tau + \widetilde{Q}_2)^{-1} \begin{bmatrix} (L_\tau^T M_1^T \widetilde{Q}_1 M_1 L_w)^T \\ -(L_\tau^T M_1^T (\gamma_c^{-2}\widetilde{Q}_1 + I) M_2^T H_1^T \Gamma_1)^T \\ ((\gamma_c^{-2}\widetilde{Q}_2 + I) H_2^T \Gamma_2)^T \end{bmatrix}^T \begin{bmatrix} w_p \\ x_{w_1} \\ x_{w_2} \end{bmatrix}_k \tag{5.38}$$

provided that

$$\gamma_c > \gamma_{\min_c} \triangleq \sqrt{\bar{\lambda}[(I + M_1 L_\tau L_\tau^T M_1^T)((M_2^T Q_1 M_2)^{-1} + M_1 L_\tau Q_2^{-1} L_\tau^T M_1^T)^{-1}]} \tag{5.39}$$

and

$$(x_{w_1})_{k+1} = A_{w_1}(x_{w_1})_k + B_{w_1}\left(\tau - B_a^T (B_p^\dagger)^T \tau_p\right)_k \tag{5.40}$$

where

- *The torque of the passive joints projects onto the active joints with a factor of*

$$M_4 \triangleq \begin{bmatrix} -B_a^T(B_p^\dagger)^T & 0 & \ldots & 0 \\ 0 & -B_a^T(B_p^\dagger)^T & \ldots & 0 \\ \vdots & \vdots & \ddots & \vdots \\ 0 & 0 & \ldots & -B_a^T(B_p^\dagger)^T \end{bmatrix} \in \Re^{n_a i \times n_p i} \tag{5.41}$$

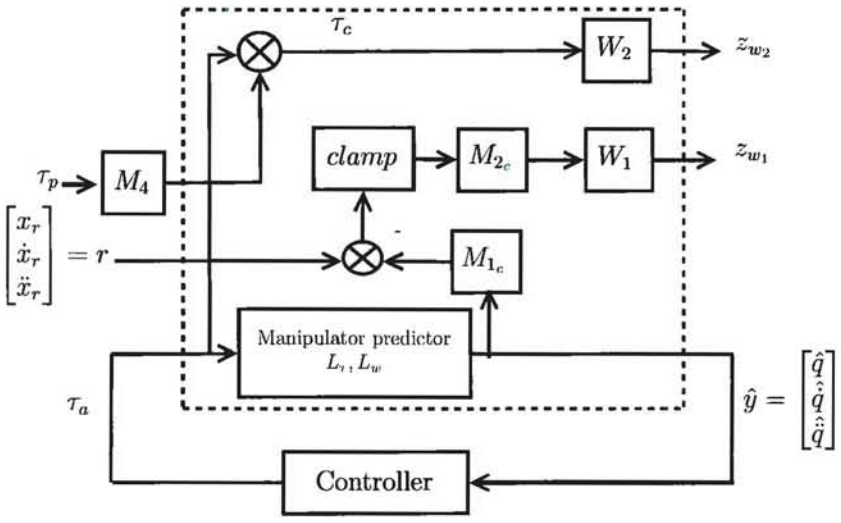

Figure 5.3: Model free subspace based operational space $\mathscr{H}_\infty$ control for parallel manipulators. τ_p is a torque vector from passive joints

- *Forward and inverse kinematics matrices for the parallel manipulator can be given by*

$$M_{1_c} \triangleq \begin{bmatrix} N_{1_c} & 0 & \dots & 0 \\ 0 & N_{1_c} & \dots & 0 \\ \vdots & \vdots & \ddots & 0 \\ 0 & 0 & \dots & N_{1_c} \end{bmatrix} \in \Re^{3li \times 3n_a i} \tag{5.42}$$

$$M_{2_c} \triangleq \begin{bmatrix} N_{2_c} & 0 & \dots & 0 \\ 0 & N_{2_c} & \dots & 0 \\ \vdots & \vdots & \ddots & 0 \\ 0 & 0 & \dots & N_{2_c} \end{bmatrix} \in \Re^{3n_a i \times 3li} \tag{5.43}$$

Proof of Proposition 5.2. Using Theorem 4.3, M_3 is taken out of the plant and substituted with M_4 that is a factor by which the torque of passive joints is superimposed onto the torque acting on the active joints for the prediction horizon i.

M_3 is taken out of the plant by equating it to I and incorporating M_4 in the update procedure of x_{w_1} for a single update results in

$$(x_{w_1})_{k+1} = A_{w_1}(x_{w_1})_k + B_{w_1}\left(\tau - B_a^T(B_p^\dagger)^T\tau_p\right)_k \tag{5.44}$$

Substituting M_3 by I in (5.5), the optimum torque is given by

$$\tau_{opt_c} \equiv -(L_\tau^T M_1^T \widetilde{Q}_1 M_1 L_\tau + \widetilde{Q}_2)^{-1} \begin{bmatrix} (L_\tau^T M_1^T \widetilde{Q}_1 M_1 L_w)^T \\ -(L_\tau^T M_1^T (\gamma_c^{-2} \widetilde{Q}_1 + I) M_2^T H_1^T \Gamma_1)^T \\ ((\gamma_c^{-2} \widetilde{Q}_2 + I) H_2^T \Gamma_2)^T \end{bmatrix}^T \begin{bmatrix} w_p \\ x_{w_1} \\ x_{w_2} \end{bmatrix}_k$$

Using (4.51), for the torque vector τ_p and the scaling factor M_4, it can be stated that

$$\gamma_{\min_{M_4 \tau_p}} \equiv \gamma_{\min_{\tau_p}}$$

Hence, applying $M_3 = I$ to (4.3) yields

$$\gamma_{\min_c} \equiv \sqrt{\bar{\lambda}[(I + M_1 L_\tau L_\tau^T M_1^T)((M_2^T Q_1 M_2)^{-1} + M_1 L_\tau Q_2^{-1} L_\tau^T M_1^T)^{-1}]}$$

□

5.3 Summary

The important results of this chapter are:

- Model free subspace based operational space bias removal $\mathscr{H}_\infty$ control (5.2) – (5.3);
- Forward kinematics function of a parallel manipulator (5.23) – (5.25);
- Framework to cater for kinematic constraints of a parallel manipulator (5.33) – (5.34); and
- Model free subspace based operational space $\mathscr{H}_\infty$ control for a parallel manipulator (5.38) – (5.40).

Chapter 6

Implementation Details & Simulations

This chapter presents implementation details and simulation results of the model free subspace based operational space $\mathscr{H}_\infty$ controllers as proposed in Chapter 3. Implementation details for the robust control, $\mathscr{H}_2$ optimal control, and other controllers proposed in Chapter 4 and 5 are similar.

In this chapter, Section 6.1 presents implementation details for a serial mechanical manipulator. Section 6.2 presents results of simulations conducted with *bang-bang* trajectory [52] for different values of the damping factor. Section 6.3 proposes a control law that finds the optimum value of the damping factor.

6.1 Implementation

Figure 6.1 depicts the implementation of a model free subspace based operational space $\mathscr{H}_\infty$ controller for a serial manipulator. Before running the software, the prediction horizon (i) and the number of prediction problems (j) are selected. In a typical system, i is selected 2 or 3 fold the expected order of the system and j is selected such that $j >> i$. There are $13n$ unknown parameters in a serial manipulator [52] and many of these parameters are linear combination of other

parameters. Hence, an order of $p < 13n$ suffices as long as there is no extra load on the end-effector that can increase the order of the system.

Reference trajectory is generated such that the system is properly excited and all its properties appear in the output. In subspace identification, it is ensured that at all times, the rank of $T^T T = 2 \times 3n \times i$ [74]. The value of i is generally assigned twice the expected order of the system. Hence, for a mechanical manipulators, its value can be set to $2p$. However, if a higher value is selected higher for i to increase the fidelity, the algorithm proposed in Section 2.5 will be used as it can calculate subspace predictor for rank deficient matrices with an added advantage of the increase in performance. Rank deficiency can also occur if the exciting trajectories are badly selected or if i and j are assigned too high values. However, it has been coded in the program that at any time stamp, when the subspace predictor is calculated, the rank of $T^T T$ should not fall below $2 \times 3n \times p$. If it happens, then the calculation of a new subspace predictor is postponed until the condition of minimum rank is met.

If previous states of W_1 and W_2 are unknown then x_{w_1} and x_{w_2} can initially be assigned the value of 0. The current values of q and $\dot{q}$ are observed and $F(q)$, $J(q)$, $\dot{J}(q, \dot{q})$, $J^*(q) = J^T(q)(J(q)J^T(q) + \lambda^2 I)^{-1}$ for the selected value of λ, are calculated to assemble N_1 and N_2 using (3.16) and (3.22), respectively. M_1 and M_2 are calculated using (3.30) and (3.31) for the same value of q and $\dot{q}$, provided that the assumption in (3.9) is not violated for i steps. In MATLAB, `blkdiag` command can be used to create M_1 and M_2 from N_1 and N_2 respectively, when the same value of q is used to initialize M_1 and M_2.

W_1 and W_2 are square positive definite frequency dependant weights to be selected by the designer for different values of $\gamma_{\min}$. W_1 has the property of having a large absolute value for small frequencies, whereas the absolute value tends to a limit for large frequencies. On the other hand, W_2 is typically a high pass filter to remove biases from the inputs to the plant [65]. In MATLAB, these weights can be designed in the $s-$domain (where s is the Laplace operator) and then transferred into $z-$domain with a sampling rate equal to the sampling rate chosen in Simulink

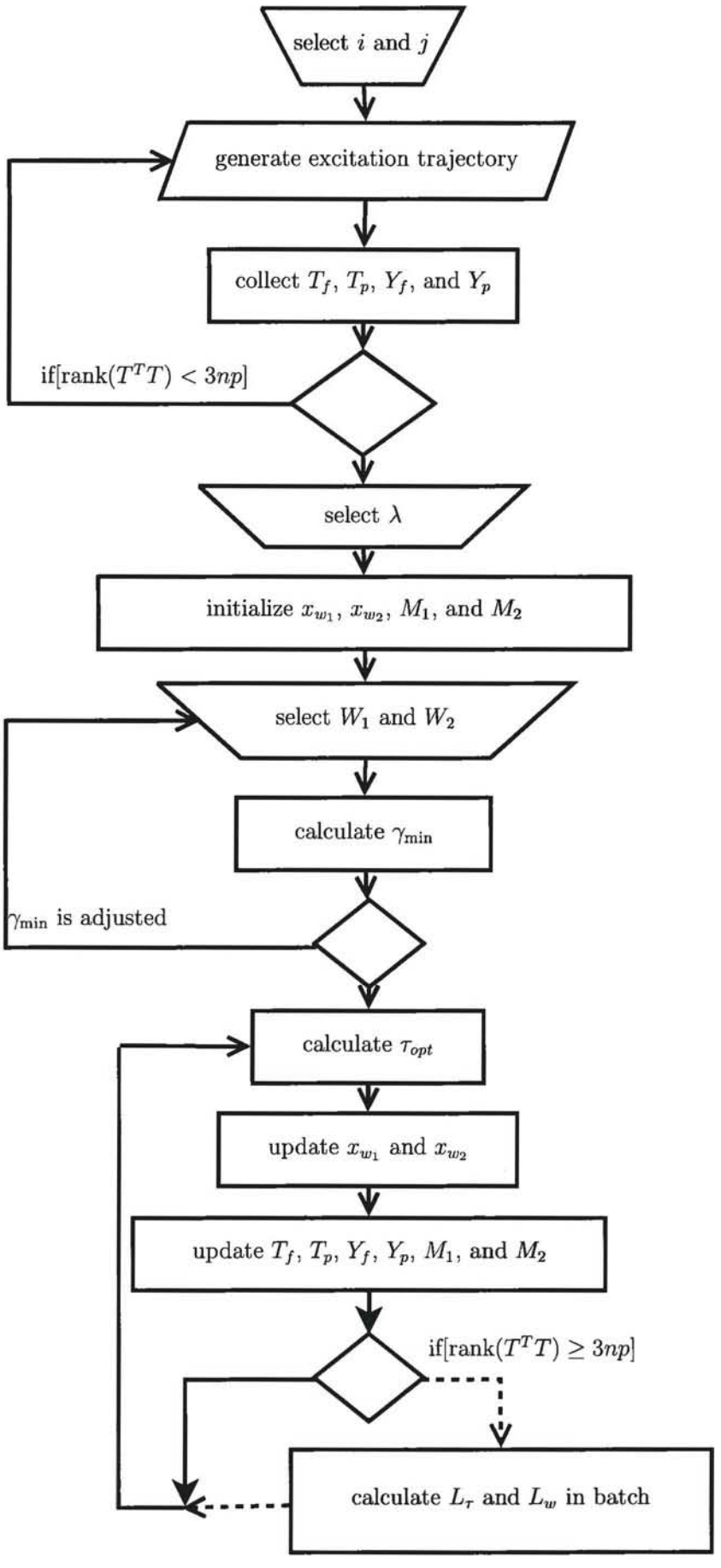

Figure 6.1: Software flow for the model free control of an articulated manipulator

for a fixed-step solver. It has been noticed that variable-step solvers produce erratic results as these weights are not regularly updated after equal intervals of time.

Optimum torque for a manipulator, i.e., $\tau_{opt} = f(x_{w_1}, x_{w_2}, \gamma, L_w, L_\tau, w_p)$, is calculated using (3.28). Current values of r_k and y_k are observed, and x_{w_1}, x_{w_2}, T_p, T_f, Y_p, and Y_f are updated. The values of x_{w_1} and x_{w_2} are calculated using

$$x_{w_1} := A_{w_1} x_{w_1} + B_{w_1}(N_2(r_k - N_1 y_k)) \tag{6.1}$$

$$x_{w_2} := A_{w_2} x_{w_2} + B_{w_2} \tau_k \tag{6.2}$$

The above steps can be simplified into two equations. Using (3.28), let

$$\begin{bmatrix} k_1 & k_2 \end{bmatrix} = \left\{ -(L_\tau^T M_1^T \tilde{Q}_1 M_1 L_\tau + Q_2)^{-1} L_\tau^T M_1^T \tilde{Q}_1 M_1 L_w \right\}_{1:n} \tag{6.3}$$

$$k_3 = \left\{ (L_\tau^T M_1^T \tilde{Q}_1 M_1 L_\tau + Q_2)^{-1} L_\tau^T M_1^T (\gamma^{-2} \tilde{Q}_1 + I) M_2^T H_1^T \Gamma_1 \right\}_{1:n} \tag{6.4}$$

$$k_4 = \left\{ -(L_\tau^T M_1^T \tilde{Q}_1 M_1 L_\tau + Q_2)^{-1} H_2^T \Gamma_2 \right\}_{1:n} \tag{6.5}$$

where $\{\bullet\}_{1:n}$ is the extract of first n rows from the $\bullet$ matrix, and $k_1 \in \Re^{n \times in}$, $k_2 \in \Re^{n \times 3in}$, $k_3 \in \Re^{n \times n_{w_1}}$, $k_4 \in \Re^{n \times n_{w_2}}$. The vector $\left[\tau_p^T, y_p^T, x_{w_1}^T, x_{w_2}^T \right]^T$ can be

calculated in a single step using

$$\begin{bmatrix} \tau_p \\ y_p \\ x_{w_1} \\ x_{w_2} \end{bmatrix}_{k+1} = \begin{bmatrix} \begin{bmatrix} S_n \\ k_1 \end{bmatrix} & \begin{bmatrix} 0 \\ k_2 \end{bmatrix} & \begin{bmatrix} 0 \\ k_3 \end{bmatrix} & \begin{bmatrix} 0 \\ k_4 \end{bmatrix} \\ 0 & \begin{bmatrix} S_{3n} \\ 0 \end{bmatrix} & 0 & 0 \\ 0 & 0 & A_{w_1} & 0 \\ B_{w_2}k_1 & B_{w_2}k_2 & B_{w_2}k_3 & A_{w_2} + B_{w_3}k_4 \end{bmatrix} \begin{bmatrix} \tau_p \\ y_p \\ x_{w_1} \\ x_{w_2} \end{bmatrix}_k + \begin{bmatrix} \begin{bmatrix} 0 \\ I_n \end{bmatrix} & 0 & 0 \\ 0 & 0 & \begin{bmatrix} 0 \\ I_{3n} \end{bmatrix} \\ 0 & B_{w_1}N_2 & -B_{w_1}N_2N_1 \\ 0 & 0 & 0 \end{bmatrix} \begin{bmatrix} \tau_{\text{excite}} \\ r \\ y \end{bmatrix}_k \tag{6.6}$$

where τ_{excite} is the excitation signal during the initial phase of exciting the system to get a starting value for the predictor. Its value is set equal to 0 in the normal mode of operation. I_n and I_{3n} are $n \times n$ and $3n \times 3n$ identity matrices respectively, and

$$S_n = \begin{bmatrix} 0 & I_n & 0 & \dots & 0 \\ 0 & 0 & I_n & \dots & 0 \\ \vdots & \vdots & \vdots & \ddots & 0 \\ 0 & 0 & 0 & \dots & I_n \end{bmatrix} \in \Re^{(i-1)n \times in}$$

$$S_{3n} = \begin{bmatrix} 0 & I_{3n} & 0 & \dots & 0 \\ 0 & 0 & I_{3n} & \dots & 0 \\ \vdots & \vdots & \vdots & \ddots & 0 \\ 0 & 0 & 0 & \dots & I_{3n} \end{bmatrix} \in \Re^{(i-1)3n \times 3in}$$

$S_3[\bullet]$ and $S_{3n}[\bullet]$ truncates the first n and $3n$ rows of the matrix $[\bullet]$, respectively. Equation (6.6) features the general formula to find the optimum torque for

the manipulator. A similar procedure has also been used in [118] to simplify the implementation.

Equation (6.6) requires direct input from the reference trajectory, r, which is calculated using

$$r_k = clamp(r_{original} - M_1 y_k) + M_1 y_k \tag{6.7}$$

where $clamp(\bullet)$ is defined in (3.12). The calculated torque τ_{opt} can be generated by controlling the current in the actuators. The relationship between the current and the torque for a given actuator is modeled using polynomials [100] whose parameters are either provided by the manufacturer or identified experimentally [21, 101].

6.2 Results

The proposed control technique has been implemented using MATLAB and Simulink. In the simulation, gravity and joint friction have been neglected. In the presence of gravity, the manipulator is pulled out of the region of operation. The predictor is trained only for a subset of the total operational space, therefore the system behaves erratically when the manipulator moves far from the region for which the predictor was calculated. In a real life situation, gravity compensators can be used. For the sake of simplicity, the controller is implemented on a two link planar robot. The forward kinematics function for a two link planar robot is

$$F(q) = \begin{bmatrix} x_1 \cos(q_1) + x_2 \cos(q_1 + q_2) \\ x_1 \sin(q1) + x_2 \sin(q_1 + q_2) \end{bmatrix}$$

where x_1 and x_2 are the link lengths. Using (3.4) and (3.5), the Jacobian and its derivative is given by

$$J(q) = \begin{bmatrix} -x_1 \sin(q_1) - x_2 \sin(q_1 + q_2) & -x_2 \sin(q_1 + q_2) \\ x_1 \cos(q_1) + x_2 \cos(q_1 + q_2) & x_2 \cos(q_1 + q_2) \end{bmatrix} \tag{6.8}$$

$$\dot{J}(q, \dot{q}) = \begin{bmatrix} L_{j_1} & L_{j_2} \end{bmatrix} \tag{6.9}$$

where

$$L_{j_1} = \begin{bmatrix} -\dot{q}_2 x_2 \cos(q_1 + q_2) + \dot{q}_1(-x_1 \cos(q_1) - x_2 \cos(q_1 + q_2)) \\ -\dot{q}_2 x_2 \sin(q_1 + q_2) + \dot{q}_1(-x_1 \sin(q_1) - x_2 \sin(q_1 + q_2)) \end{bmatrix} \tag{6.10}$$

$$L_{j_2} = \begin{bmatrix} -\dot{q}_2 x_2 \cos(q_1 + q_2) - \dot{q}_1 x_2 \cos(q_1 + q_2) \\ -\dot{q}_2 x_2 \sin(q_1 + q_2) - \dot{q}_1 x_2 \sin(q_1 + q_2 \end{bmatrix} \tag{6.11}$$

Similarly

$$\frac{F(q)}{q} = \begin{bmatrix} \frac{x_1 \cos(q_1) + x_2 \cos(q_1 + q_2)}{q_1} & 0 \\ \frac{x_1 \sin(q_1) + x_2 \sin(q_1 + q_2)}{q_1} & 0 \end{bmatrix}$$

where $\forall q_1 < 0.1 : q_1 = 0.1$, to avoid very large values of $\frac{F(q)}{q}$. N_1 and N_2 can be calculated by substituting the above equations in (3.6) and (3.22).

Figure 6.2 shows the actual and the calculated values of end-effector coordinates and their derivatives. It can be seen that in the beginning, the limit on the value of q_1 results in a value of x_1 different from the actual value.

Figure 6.3 shows the smooth conversion of the error signals from the joint space to the operational space. The smooth conversion is due to the use of DLS in the definition of N_1 (3.22). In the given example, λ is set equal to 5. λ has a significant impact on the response of the system as it can be seen in the context of Figure 6.5.

A *Bode plot* of the frequency dependant weights is shown in Figure 6.4. The selection of these weights has a direct effect on the performance. The estimated response of the manipulator should be below $||W_1^{-1}||$ for the operating frequency range. In the case presented here, these weights were selected by trial and error. If

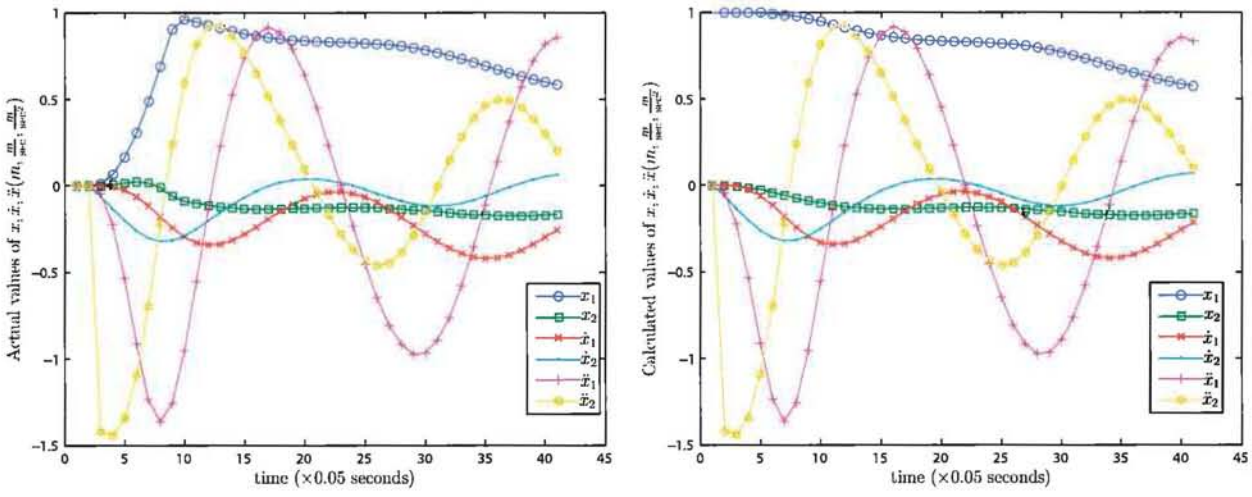

Figure 6.2: The left figure shows the actual end-effector position during excitation mode and the right figure shows the end-effector position calculated using N_1 matrix

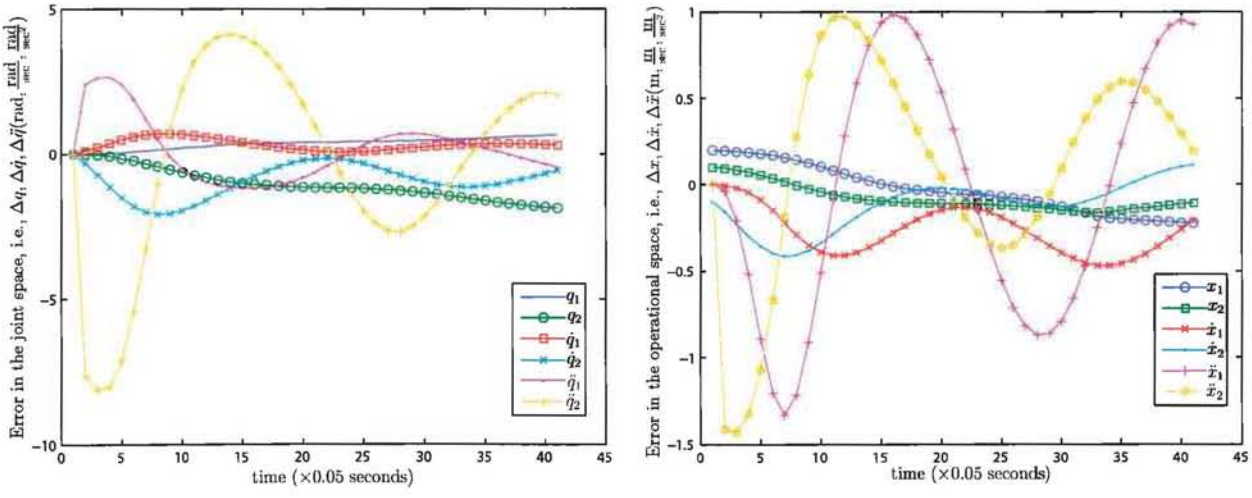

Figure 6.3: The left figure is the error signal in joint space and the right figure shows the error signal in operational space. DLS provides a smooth solution to inverse kinematics

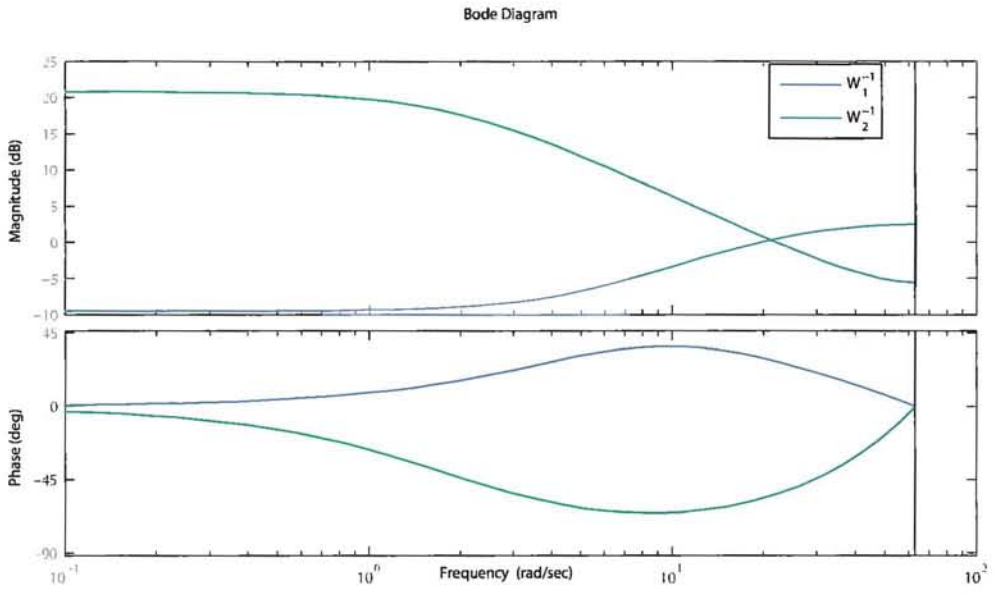

Figure 6.4: $||W_1^{-1}||$ should be more than the expected response of the system for all operating frequencies

the dynamics of a mechanical manipulator exhibit changes considerably beyond the initial values, the weights need to be re-adjusted.

Figure 6.5 shows the position of the end-effector of a 2-DOF planar robot on one axis along with the desired end-effector trajectory against time. A *bang-bang* trajectory is used as the reference signal that was originally designed for the joint space control [52]. The right hand side shows the response of a mechanical manipulator whose dynamics were greatly tempered. In real life, such a situation can arise when W_1 and W_2 are properly chosen for a given robotic arm, but the arm then tries to lift a weight which is many times more than the value it was trained with. Figure 6.5 also shows that an increase in the value of λ dampens the system response and a decrease increases the perturbations in the system. It was noticed that below a certain value of λ, the system becomes unstable.

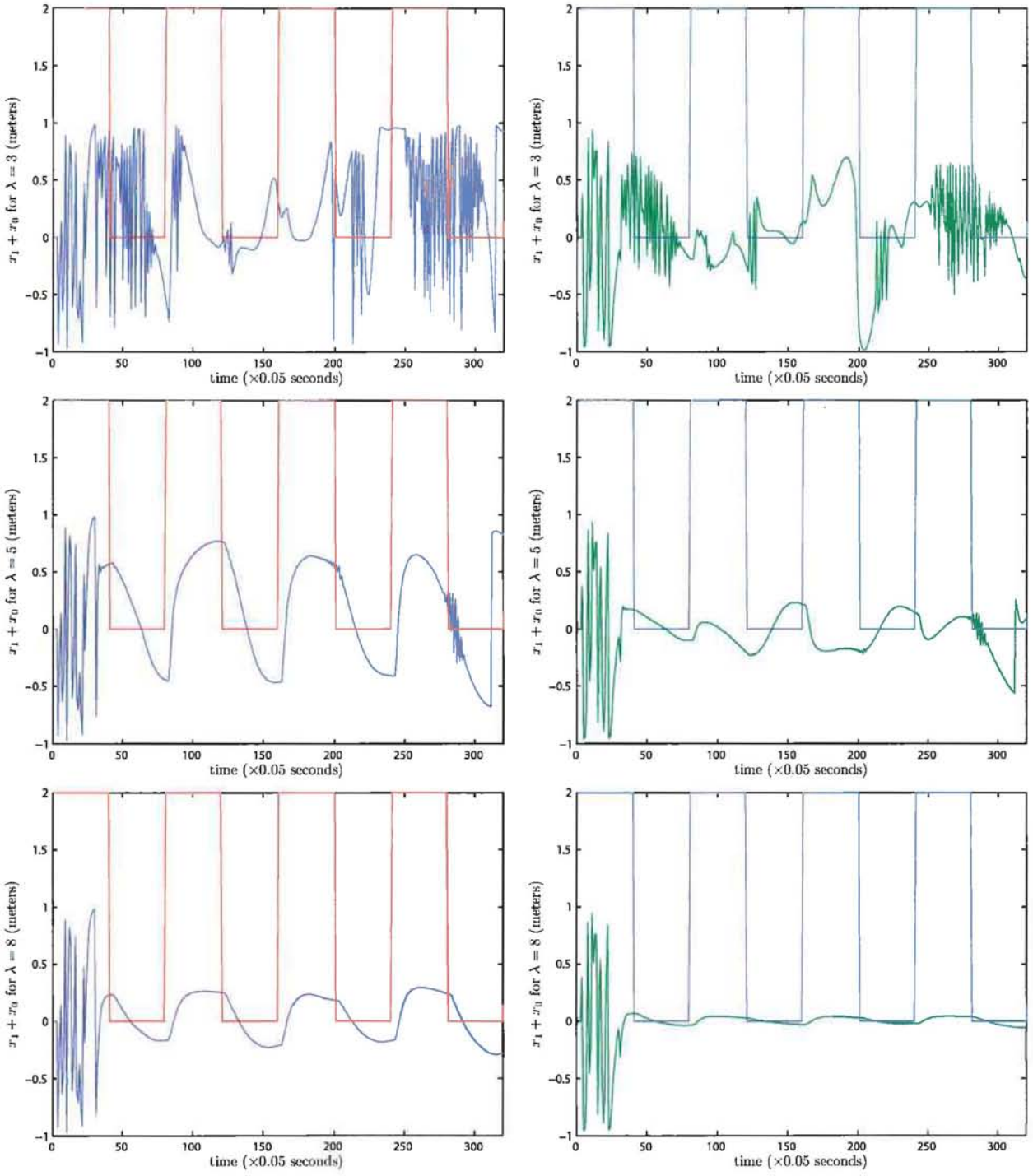

Figure 6.5: Figures on the left side show the end-effector position on *x-axis* for a given trajectory with different values of the damping factor λ. The figures on the right side show the same response with extra mass on the end-effector for the same frequency weights [86]

6.3 Optimum Damping

It can be seen in Figure 6.5 that the value of the damping factor has a significant effect on the behaviour of the system, which makes it imperative to find its optimum value. In this section, optimum value of the damping factor will be derived.

The optimum value of the damping factor, $\lambda_{\min}$, can be defined as the lowest value of λ permitted by the performance objective γ_d. Decreasing the value of λ beyond this limit would make the system unstable.

In DLS, it can be seen in (3.19) that instead of minimizing only $||J(q)\dot{q} - \dot{x}||^2$, the second term ,$\lambda^2||\dot{q}||^2$, is also minimized. This can be achieved by adding another weighted output from the plant that minimizes the error between a disturbance signal (l) and $\dot{q}$. Let

$$l \approx \dot{q}$$

or

$$l + \lambda l = \Delta_d + \dot{q} \tag{6.12}$$

where Δ_d is a vector in which all the elements have the same positive scalar value. For a given performance objective (γ_d), the worst case value of the disturbance signal (l_{wc}) is calculated and used to workout the damping factor using the relation

$$\lambda = \begin{cases} \left| (S_d M_2 x_e + \Delta_d) \otimes \frac{1}{l_{wc}} - 1 \right| & \text{if } |l_{wc} - S_d M_2 x_e| \geq \Delta_d \\ 0 \text{ otherwise} \end{cases} \tag{6.13}$$

where $\otimes$ is an operator of element-wise multiplication, and S_d is a selection matrix to extract $\dot{q}$ from y. S_d is given as follows;

$$S_d = \begin{bmatrix} 0 & 1 & 0 & 0 & 0 & 0 & \dots & 0 \\ 0 & 0 & 0 & 0 & 1 & 0 & \dots & 0 \\ \vdots & \vdots & \vdots & \vdots & \vdots & \vdots & \vdots & \vdots \\ 0 & 0 & 0 & 0 & \dots & 0 & 1 & 0 \end{bmatrix} \in \Re^{in \times 3in} \tag{6.14}$$

The end-effector position in operational space is given by

$$x_e = \begin{bmatrix} x_1 \\ \dot{x}_1 \\ \ddot{x}_1 \\ \vdots \\ x_i \\ \dot{x}_i \\ \ddot{x}_i \end{bmatrix} \in \Re^{3il} \tag{6.15}$$

Near singularity, $\dot{q}$ increases even more than the worst case value of l permitted by the performance objective (γ_d). The value of λ needs to be increased such that the difference in (6.13) is equal to or less than Δ_d. The increase in λ will affect the response of the system indirectly by changing the behaviour of the inverse kinematics block (M_3) near singularities.

It is worth noting here that $\dot{q}$ in (6.12) is calculated using the subspace predictor but in (6.13), $\dot{q}$ is calculated from the inverse kinematics block (M_2) for the worst case value of l (l_{wc}). The reason being that the increase in $\dot{q}$ is due to a very non-linear behavior of M_2 near singularities. In this case $\dot{q}$ needs to be compared with the worst case value of l so that the minimum value of the damping factor could be found. It also ensures that the performance of the controller is bounded by γ_d.

A controller is proposed in the following theorem that adjusts the damping factor in realtime for the system shown in Figure 6.6.

Theorem 6.1. *If measurements of the torque vector (τ), joint vector (y), reference trajectory (r) in operational space are available for times $\{k-i, \ldots, k-2, k-1\}$, then the strictly causal subspace based, γ_d-level $\mathscr{H}_\infty$ optimally damped control for*

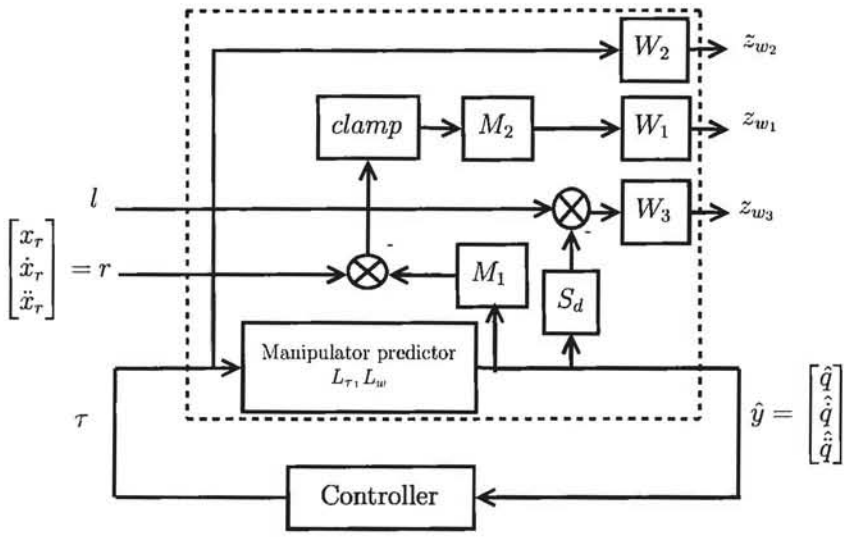

Figure 6.6: Model free subspace based operational space $\mathscr{H}_\infty$ control with optimum damping

times $\{k, \ldots, k+i, k+i-1\}$ *is given by*

$$\tau_{opt_d} \triangleq - \begin{bmatrix} 0 \\ 0 \\ I \end{bmatrix}^T L_{1_d}^{-1} L_{2_d} \begin{bmatrix} w_p \\ x_{w_1} \\ x_{w_2} \\ x_{w_3} \end{bmatrix}_k \tag{6.16}$$

where

$$L_{1_d} \triangleq \begin{bmatrix} Q_3 - \gamma_d^2 I & 0 & -Q_3 S_d L_\tau \\ 0 & M_2^T Q_1 M_2 - \gamma_d^2 I & -M_2^T Q_1 M_2 M_1 L_\tau \\ -L_\tau^T S_d^T Q_3 & -L_\tau^T M_1^T M_2^T Q_1 M_2 & L_\tau^T M_1^T M_2^T Q_1 M_2 M_1 L_\tau + L_\tau^T S_d^T Q_3 S_d L_\tau + Q_2 \end{bmatrix} \tag{6.17}$$

and

$$L_{2_d} \triangleq \begin{bmatrix} -Q_3 S_d L_w & 0 & 0 & H_3^T \Gamma_3 \\ M_2^T Q_1 M_2 M_1 L_w & M_2^T H_1^T \Gamma_1 & 0 & 0 \\ L_\tau^T M_1^T M_2^T Q_1 M_2 M_1 L_w + L_\tau^T S_d^T Q_3 S_d L_w & -L_\tau^T M_1^T M_2^T H_1^T \Gamma_1 & H_2^T \Gamma_2 & -L_\tau^T S_d^T H_3^T \Gamma_3 \end{bmatrix} \tag{6.18}$$

provided that

$$\gamma_d > \gamma_{\min_d} \triangleq \sqrt{\bar{\lambda}[(M_2^T Q_1 M_2)^{-1} + M_1 L_\tau (L_\tau^T S_d^T Q_3 S_d L_\tau + Q_2)^{-1} L_\tau^T M_1^T]^{-1}}, \quad (6.19)$$

$$\lambda > \lambda_{\min} \triangleq \begin{cases} \left| (S_d M_2 x_e + \Delta_d) \otimes \frac{1}{l_{wc}} - 1 \right| & \text{if } |l_{wc} - S_d M_2 x_e| \geq \Delta_d \\ 0 \text{ otherwise} \end{cases}, \quad (6.20)$$

and

$$l_{wc} \triangleq - \begin{bmatrix} I \\ 0 \\ 0 \end{bmatrix}^T L_{1_d}^{-1} L_{2_d} \begin{bmatrix} w_p \\ x_{w_1} \\ x_{w_2} \\ x_{w_3} \end{bmatrix}_k \quad (6.21)$$

Using Theorem 3.4 and Proposition 4.1, it can be proven that

$$\gamma_{\min_d} > \gamma_{\min} \quad (6.22)$$

where $\gamma_{\min_d}$ is defined in (3.29). This decrease in the performance is due to the added optimization criterion in the cost function that is used in regulating the damping factor. In $\mathscr{H}_\infty$ control, the stability of a system is ensured for a given performance objective. Hence, a value of λ below $\lambda_{\min}$ would make the system unstable. Increasing its value would increase the stability but the system will be over damped.

Proof of Theorem 6.1. From Figure 6.6 and using (4.7), it can be stated that

$$z_{w_1}^T z_{w_1} + z_{w_2}^T z_{w_2} + z_{w_3}^T z_{w_3} - \gamma_d^2 r^T r - \gamma_d^2 l^T l < 0 \quad (6.23)$$

The vector l contains the disturbance signal. Its worst case value for the given performance objective will be used to find the optimum damping for the manipulator.

The control variables can be re-written as

$$\begin{bmatrix} z_{w_1} \\ z_{w_2} \\ z_{w_3} \end{bmatrix} = \begin{bmatrix} H_1(e) + \Gamma_1(x_{w_1})_k \\ H_2(\tau) + \Gamma_2(x_{w_2})_k \\ H_3(l - S_d\hat{y}) + \Gamma_3(x_{w_3})_k \end{bmatrix} \tag{6.24}$$

Substituting the values of e and y as given in Figure 6.6 and (2.15) yields

$$\begin{bmatrix} z_{w_1} \\ z_{w_2} \\ z_{w_3} \end{bmatrix} = \begin{bmatrix} 0 & H_1M_2 & -H_1M_2M_1L_\tau & -H_1M_2M_1L_w & \Gamma_1 & 0 & 0 \\ 0 & 0 & H_2 & 0 & 0 & \Gamma_2 & 0 \\ H_3 & 0 & -H_3S_dL_\tau & -H_3S_dL_w & 0 & 0 & \Gamma_3 \end{bmatrix} x_d \tag{6.25}$$

where

$$x_d \triangleq \begin{bmatrix} l \\ r \\ \tau \\ w_p \\ x_{w_1} \\ x_{w_2} \\ x_{w_3} \end{bmatrix} \tag{6.26}$$

The cost function to minimize the control effort and the feedback error for a given refence trajectory and force on the end-effector bounded by γ_f is given by

$$L_d(\gamma_d) = z_{w_1}^T z_{w_1} + z_{w_2}^T z_{w_2} + z_{w_3}^T z_{w_3} - \gamma_d^2 r^T r - \gamma_d^2 l^T l \tag{6.27}$$

Using the above relation, the objective is given as

$$\min_{\tau} \max_{r,l} \left(\begin{bmatrix} z_{w_1} \\ z_{w_2} \\ z_{w_3} \end{bmatrix}^T \begin{bmatrix} z_{w_1} \\ z_{w_2} \\ z_{w_3} \end{bmatrix} - \gamma_d^2(r^T r + l^T l) \right) < 0 \tag{6.28}$$

Using (6.25) in above inequality produces

$$\min_{\tau} \max_{r,l} x_d^T \begin{bmatrix} L_{1_d} & L_{2_d} \\ \vdots & \vdots \end{bmatrix} x_d < 0 \tag{6.29}$$

where

$$L_{1_d} \equiv \begin{bmatrix} Q_3 - \gamma_d^2 I & 0 & -Q_3 S_d L_\tau \\ 0 & M_2^T Q_1 M_2 - \gamma_d^2 I & -M_2^T Q_1 M_2 M_1 L_\tau \\ -L_\tau^T S_d^T Q_3 & -L_\tau^T M_1^T M_2^T Q_1 M_2 & L_\tau^T M_1^T M_2^T Q_1 M_2 M_1 L_\tau + L_\tau^T S_d^T Q_3 S_d L_\tau + Q_2 \end{bmatrix} \tag{6.30}$$

and

$$L_{2_d} \equiv \begin{bmatrix} -Q_3 S_d L_w & 0 & 0 & H_3^T \Gamma_3 \\ M_2^T Q_1 M_2 M_1 L_w & M_2^T H_1^T \Gamma_1 & 0 & 0 \\ L_\tau^T M_1^T M_2^T Q_1 M_2 M_1 L_w + L_\tau^T S_d^T Q_3 S_d L_w & -L_\tau^T M_1^T M_2^T H_1^T \Gamma_1 & H_2^T \Gamma_2 & -L_\tau^T S_d^T H_3^T \Gamma_3 \end{bmatrix} \tag{6.31}$$

To find the saddle point that minimizes τ and maximizes r and l at the same time, (6.29) is differentiated with respect to $\begin{bmatrix} l^T, r^T, \tau^T \end{bmatrix}^T$ and equated to zero. As $x_d = \begin{bmatrix} l^T, r^T, \tau^T, w_p^T, x_{w_1}^T, x_{w_2}^T, x_{w_3}^T \end{bmatrix}^T$, only the first three rows from (6.29) will remain. After differentiation, (6.29) can be written as

$$L_{1_d} \begin{bmatrix} l \\ r \\ \tau \end{bmatrix} = -L_{2_d} \begin{bmatrix} w_p \\ x_{w_1} \\ x_{w_2} \\ x_{w_3} \end{bmatrix} \tag{6.32}$$

Equation (6.32) is differentiated again with respect to $\left[l^T, r^T, \tau^T\right]^T$ to get the maximum condition for r and l, which produces

$$H_{hess_d} \triangleq \begin{bmatrix} Q_3 - \gamma_d^2 I & 0 & -Q_3 S_d L_\tau \\ 0 & M_2^T Q_1 M_2 - \gamma_d^2 I & -M_2^T Q_1 M_2 M_1 L_\tau \\ -L_\tau^T S_d^T Q_3 & -L_\tau^T M_1^T M_2^T Q_1 M_2 & L_\tau^T M_1^T M_2^T Q_1 M_2 M_1 L_\tau + L_\tau^T S_d^T Q_3 S_d L_\tau + Q_2 \end{bmatrix} \tag{6.33}$$

Using (3.79), the performance objective can be written as

$$M_2^T Q_1 M_2 - \gamma_d^2 I - M_2^T Q_1 M_2 M_1 L_\tau (L_\tau^T M_1^T M_2^T Q_1 M_2 M_1 L_\tau + L_\tau^T S_d^T Q_3 S_d L_\tau + Q_2)^{-1} L_\tau^T M_1^T M_2^T Q_1 M_2 <$$

If $A \triangleq M_2^T Q_1 M_2$, $B^T \triangleq M_1 L_\tau$, and $C \triangleq L_\tau^T S_d^T Q_3 S_d L_\tau + Q_2$ in (3.37) then

$$\gamma_d^2 I > ((M_2^T Q_1 M_2)^{-1} + M_1 L_\tau (L_\tau^T S_d^T Q_3 S_d L_\tau + Q_2)^{-1} L_\tau^T M_1^T)^{-1}$$

or

$$\gamma_d > \gamma_{\min_d} \equiv \sqrt{\bar{\lambda}[(M_2^T Q_1 M_2)^{-1} + M_1 L_\tau (L_\tau^T S_d^T Q_3 S_d L_\tau + Q_2)^{-1} L_\tau^T M_1^T]^{-1}} \tag{6.34}$$

As $Q_1 > 0, Q_2 > 0$, and $Q_3 > 0$, hence

$$L_\tau^T M_1^T M_2^T Q_1 M_2 M_1 L_\tau + L_\tau^T S_d^T Q_3 S_d L_\tau + Q_2 > 0$$

which satisfies the minimum condition of τ_{opt_d} according to (3.78) and (6.33). The optimum torque can be given by rearranging (6.32) as follows;

$$\tau_{opt_d} \equiv - \begin{bmatrix} 0 \\ 0 \\ I \end{bmatrix}^T L_{1_d}^{-1} L_{2_d} \begin{bmatrix} w_p \\ x_{w_1} \\ x_{w_2} \\ x_{w_3} \end{bmatrix} \tag{6.35}$$

Similarly, the worst case input for the vector l can be calculated by

$$l_{wc} \equiv - \begin{bmatrix} I \\ 0 \\ 0 \end{bmatrix}^T L_{1_d}^{-1} L_{2_d} \begin{bmatrix} w_p \\ x_{w_1} \\ x_{w_2} \\ x_{w_3} \end{bmatrix} \tag{6.36}$$

for the performance objective given in (6.19). This value gives the upper bound for the error between l and $\dot{q}$. Any increase in this error would require a larger value of λ to damp the system. Using (6.13), the lower bound of λ can be given by

$$\lambda > \lambda_{\min} \equiv \begin{cases} \left| (S_d M_2 x_e + \Delta_d) \otimes \frac{1}{l_{wc}} - 1 \right| & \text{if } |l_{wc} - S_d M_2 x_e| \geq \Delta_d \\ 0 \text{ otherwise} \end{cases} \tag{6.37}$$

□

Similar to $\gamma_{\min}$, λ was heuristically found to be $1.1\lambda_{\min}$.

In Figure 6.6, W_3 is a low pass filter, whose state can be updated using

$$(x_{w_3})_{k+1} = A_{w_3}(x_{w_3})_k + B_{w_3}(l - \hat{\dot{q}})_k$$

Using the lowest value of the damping factor, i.e., $\lambda = 0$, for a constant error between l and $\dot{q}$ in (6.12) yields

$$(x_{w_3})_{k+1} = A_{w_3}(x_{w_3})_k + B_{w_3}(\Delta_d)_k \tag{6.38}$$

The reason for using the lowest value of λ in the above equation is that the value of λ affects the response of the system indirectly by changing the behaviour of the inverse kinematics block (M_3), and the direct effect of its variation on the response of the system is not desired.

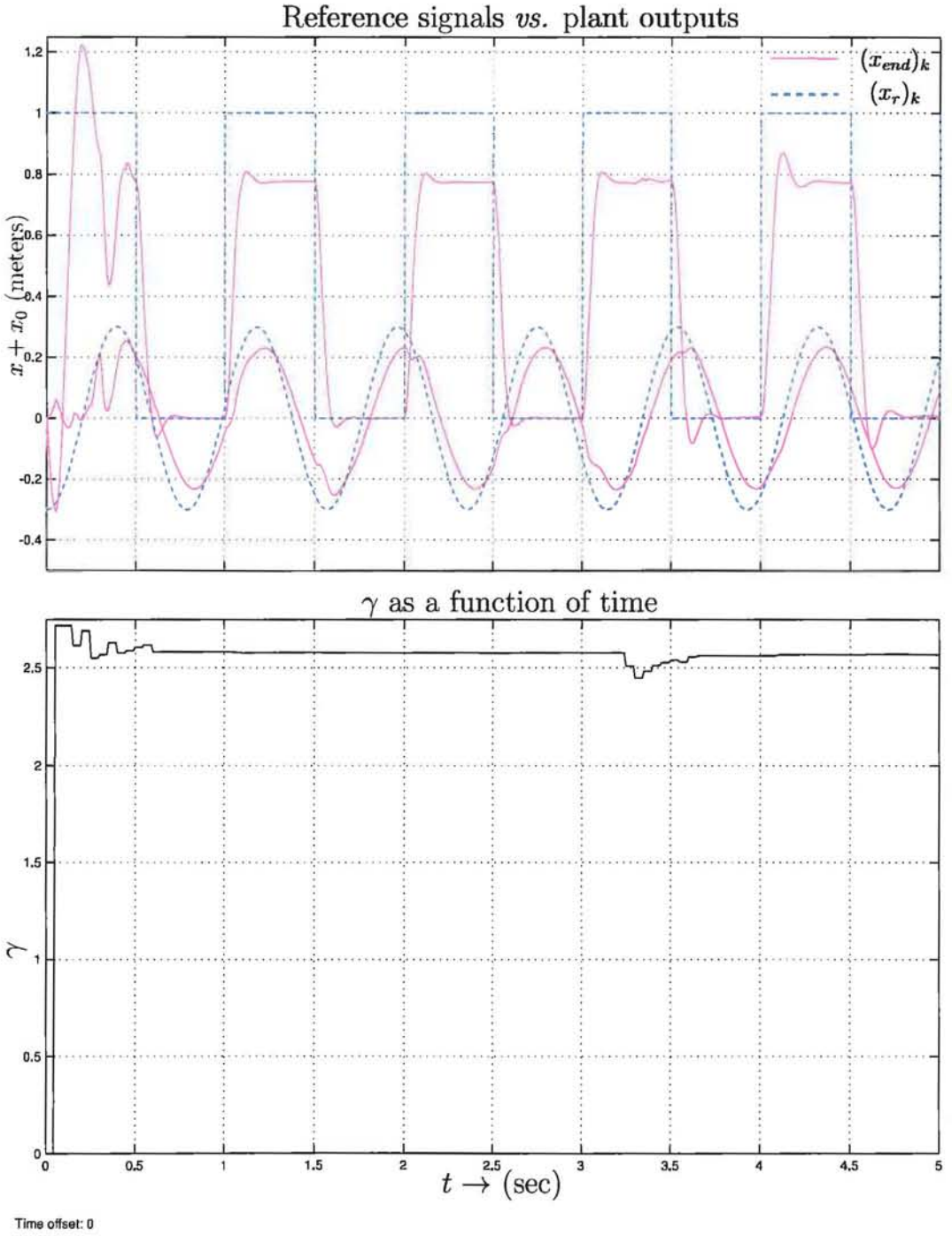

Figure 6.7: Response of a 2-DOF planar robot with optimum damping

Figure 6.7 shows the response of a 2-DOF planar robot with optimum damping. In this figure $(x_r)_k$ and $(x_{end})_k$ denote the desired and the actual position of the end-effector at the k^{th} time, respectively. The square and the sinusoidal waves represent the position trajectory on *x-axis* and *y-axis*, respectively. A similar approach was adopted in [85] for joint space control, in which the cost function was optimized for the torque, the error between the reference trajectory and the joint variables, and the square of the joint velocities.

6.4 Summary

The important results of this chapter are:

- Implementation details of a model free subspace based operational space $\mathscr{H}_\infty$ control for a serial manipulator in Figure 6.1;
- Fast calculation of the optimum torque (τ_{opt}) and updating performance weight states (6.6) – (6.7);
- Results from the forward and inverse kinematics blocks in Figures 6.2 and 6.3;
- Expression for adjusting the damping factor (6.13);
- Model free subspace based operational space $\mathscr{H}_\infty$ control with optimum damping (6.16) – (6.20); and
- Response of a 2-DOF serial manipulator in Figures 6.5 and 6.7.

Chapter 7

Conclusions & Recommendations for Future Work

For successful model-based control of mechanical manipulators, accurate values for model parameters have to be defined and used in the system mathematical model. Tasks are generally specified in operational space and control actions are defined in joint space. However, a small error in joint space can translate to a large error in operational space, which may negatively influence the effectiveness of the control scheme. To overcome this problem, this thesis presented a set of novel direct adaptive controllers for the dynamic learning operational space control of mechanical manipulators. The fundamental architecture of these controllers resemble the ones proposed by Woodley et al. [118] and Favoreel et al. [33]. The controller observes the dynamics of a mechanical manipulator and synthesizes a control law in realtime. The major advantage of this control scheme is that it deals with the mechanical manipulator as a black box.

Subspace identification has been used for the identification of manipulator dynamics. For different trajectories, inputs and outputs of the system are collected, and used to assemble input and output matrices of varying ranks. A novel subspace prediction algorithm is proposed to cater for the rank deficiency, and it has been demonstrated to improve the performance.

The reference trajectory is presented in operational space, and a framework has been developed to cater for the forward and inverse kinematics operations. A controller is designed to minimize the torque produced by the actuators and the reference trajectory using $\mathscr{H}_\infty$ optimization criterion. A robust controller has been presented to incorporate the additive uncertainties. Additive uncertainties cater for the non-linearities in the system that were ignored during the early stages of the control design. A controller based on the quadratic cost, i.e., $\mathscr{H}_2$ optimal controller, has also been proposed.

The functionality of the controller is extended by including the vector of the force acting on the end-effector. This enables the manipulator to interact with its environment. The force vector and the reference trajectory act as the disturbance signals. A controller has also been designed to minimize the effect of the force vector and the error with the reference trajectory. The resultant controller resembles a hybrid force/position controller. Another controller has been proposed in which the interaction force is not regulated. As a result, the manipulator looses its impedance. It has also been demonstrated mathematically that scaling the disturbance vectors, i.e., the reference trajectory and the force vector, doesn't affect the expression for the torque and the performance objective.

The hybrid force/position controller, mentioned above, has been used to remove the bias from the dynamic behaviour of the manipulator. This has been achieved by using the difference between the torque produced by the actuators and the torque signal from the strain gauges mounted on the manipulator joints as the exogenous force signal in the hybrid controller. This is similar to JTF control [2, 3] in which the joint-torque sensory feedback is used to remove the bias and coupling effects.

The interaction control is also extended to the control of a parallel manipulator. A framework for forward and inverse kinematics, which relates the joint variables of the active joints of the manipulator to the end-effector, has been formulated. Exploiting the dynamic behaviour of a parallel manipulator, the torque from passive joints is used as the exogenous force signal in the hybrid controller.

Finally, implementation details for the model free subspace based operational space $\mathscr{H}_\infty$ optimal control have been presented. A simple relation has been presented to calculate the optimum torque, update the predictor and weight states. Simulation of a 2-DOF manipulator has been presented. It has been found that the damping factor has a significant effect on the response of the system when the manipulator operates near singularity. To find the optimum damping factor, a controller has been proposed to regulate the damping factor bounded by a given performance objective.

The results obtained in this thesis offer many opportunities for further research. It has been assumed in the thesis that each link of the manipulator behaves linearly in the vicinity of its operational space. This assumption requires a continuous updating of the predictor. However, if a non-linear direct adaptive implementation using crisp control is developed, it can significantly improve the performance of the system.

The proposed controllers haven't been tested on a real robot. However, it would be interesting to see the effect of the gears, backlash, and the friction of the joints. In this regard, experimental work will be needed.

If a manipulator is not excited properly, accurate dynamic information of the manipulator cannot be observed. Hence, it is of utmost importance to create trajectory parameterization algorithms that excite the manipulator properly with least effect on the desired end-effector trajectory. The simulations presented in Chapter 6 are of simple cases where the controller starts operating with a rich subspace predictor. The *persistency excitation* condition [46] necessary for parametric convergence and achieving high performance is one of the areas that need to be addressed before the proposed technique is used in real world.

It would be interesting to explore the possibility of a true model free controller that not only learns about the dynamics but also learns the kinematic model of a manipulator. Similarly, if an algorithm can be designed to automatically select the performance weights, it can significantly decrease the human intervention in the operation of the controller.

In bias removal control and the control for a parallel manipulator, strain gauges are a requisite. Normally, industrial robots don't have strain gauges installed on them, and it is generally expensive to use strain gauges to measure torque. If an alternative technique could be developed for these controllers, it can significantly reduce the implementation cost on a real robot.

Vita

Publications arising from this thesis include:

Muhammad Saad Saleem and Ibrahim A. Sultan Model-Free Operational Space Dynamic Control of Serial Manipulators. *Journal of Advanced Robotics.* Manuscript submitted for publication.

Muhammad Saad Saleem and Ibrahim A. Sultan (2009), Analytical Kinematics Framework for the Control of a Parallel Manipulator. In *ICINCO*, July 2009.

Muhammad Saad Saleem and Ibrahim A. Sultan (2008), *Robotics, Automation, and Control*, chapter Model-free subspace based dynamic control of mechanical manipulators. I-Tech, Vienna, Austria, 2008. ISBN 978-953-7619-18-3.

Muhammad Saad Saleem and Ibrahim A. Sultan (2007), Feasibility of subspace identification for bipeds - an innovative approach for kino-dynamic systems. In Janan Zaytoon, Jean-Louis Ferrier, Juan Andrade-Cetto, and Joaquim Filipe, editors, *ICINCO-ICSO*, pages 133-140. INSTICC Press, 2007. ISBN 978-972-8865-82-5.

Permanent Address: School of Science and Engineering

University of Ballarat

PO Box 663

University Drive, Mount Helen

Ballarat, Victoria 3353

Australia

This thesis was typeset with LaTeX 2_ε[1] by the author.

[1] LaTeX 2_ε is an extension of LaTeX. LaTeX is a collection of macros for TeX. TeX is a trademark of the American Mathematical Society.

References

[1] H. Abdellatif, B. Heimann, and J. Kotlarski. *Parallel Manipulators, New Developments*, chapter On the Robust Dynamics Identification of Parallel Manipulators: Methodology and Experiments, page 498. I-Tech Education and Publishing, Vienna, Austria, April 2008. ISBN 978-3-902613-20-2.

[2] F. Aghili, M. Buehler, and J. M. Hollerbach. A joint torque sensor for robots. In *ASME International Mechanical Engineering Congress & Exposition*, 1997.

[3] F. Aghili, M. Buehler, and J. M. Hollerbach. Motion control systems with $\mathscr{H}_\infty$ positive joint torque feedback. *IEEE Transactions on Control Systems Technology*, 9(5):685–694, September 2001.

[4] C. H. An, C. G. Atkeson, and J. M. Hollerbach. *Model-based control of a robot manipulator*. MIT Press Cambridge, MA, USA, 1988.

[5] G. Antonelli, F. Caccavale, and P. Chiacchio. A systematic procedure for the identification of dynamic parameters of robot manipulators. *Robotica*, 17(04): 427–435, 1999.

[6] S. Arimoto. Fundamental problems of robot control: Part I, innovations in the realm of robot servo-loops. *Robotica*, 13:19–27, 1995.

[7] B. Armstrong. On Finding Exciting Trajectories for Identification Experiments Involving Systems with Nonlinear Dynamics. *The International Journal of Robotics Research*, 8(6):28, 1989.

[8] H. Asada and K. Youcef-Toumi. *Direct-drive robots: theory and practice.* MIT Press, Cambridge, MA, USA, 1987.

[9] C. G. Atkeson, C. H. An, and J. M. Hollerbach. Estimation of Inertial Parameters of Manipulator Loads and Links. *The International Journal of Robotics Research*, 5(3):101, 1986.

[10] D. S. Bernstein. *Matrix mathematics : theory, facts, and formulas with application to linear systems theory.* Princeton University Press, 2005.

[11] S. Bhattacharya, H. Hatwal, and A. Ghosh. An on-line parameter estimation scheme for generalized Stewart platform type parallel manipulators. *Mechanism and Machine Theory*, 32(1):79–89, 1997.

[12] A. Björck. *Numerical Methods for Least Squares Problems.* Society for Industrial Mathematics, 1996.

[13] H. Bruyninckx and J. De Schutter. Symbolic differentiation of the velocity mapping for a serial kinematic chain. *Mechanism and Machine Theory*, 31(2): 135–148, 1996.

[14] S. R. Buss and J. S. Kim. Selectively Damped Least Squares for Inverse Kinematics. *Journal of Graphics Tools*, 10(3):37–49, 2005.

[15] M. Cescon. Subspace-based identification of a parallel kinematic manipulator dynamics. Master's thesis, Department of Automatic Control, Lund University, Sweden, May 2008.

[16] H. Cheng, Y.-K. Yiu, and Z. Li. Dynamics and control of redundantly actuated parallel manipulators. *IEEE/ASME Transactions on Mechatronics*, 8(4):483–491, December 2003. doi: 10.1109/TMECH.2003.820006.

[17] S. Chiaverini, B. Siciliano, and O. Egeland. Review of the damped least-squares inverse kinematics with experiments on an industrial robot manipulator. *IEEE Transactions on Control Systems Technology*, 2(2):123–134, 1994.

[18] C.-H. Chung and G. G. Leininger. Adaptive self-tuning control of manipulators in task coordinate system. In *Proceedings of the IEEE International Conference on Robotics and Automation*, volume 1, pages 546–555, March 1984.

[19] R. Colbaugh, H. Seraji, and K. Glass. Direct adaptive impedance control of robot manipulators. *Journal of Robotic Systems*, 10(2):217–248, 1993.

[20] C. L. Collins. Forward kinematics of planar parallel manipulators in the Clifford algebra of P2. *Mechanism and Machine Theory*, 37(8):799–813, 2002.

[21] P. Corke. In situ measurement of robot motor electrical constants. *Robotica*, 14(4):433–436, 1996.

[22] P. Courrieu. Solving Time of Least Square Systems in Sigma-Pi Unit Networks. *Neural Information Processing-Letters and Reviews*, 4(3):39–45, 2004.

[23] P. Courrieu. Fast Computation of Moore-Penrose Inverse Matrices. *Neural Information Processing-Letters and Reviews*, 8(2):25–29, 2005.

[24] J. J. Craig. *Introduction to Robotics: Mechanics and Control.* Addison-Wesley, Boston, MA, USA, 1989.

[25] J. J. Craig, P. Hsu, and S. Shankar Sastry. Adaptive control of mechanical manipulators. *The International journal of robotics research*, 6(2):16–28, 1987.

[26] X. Cui and K. G. Shin. Robot trajectory tracking with self-tuning predicted control. Technical report, Center for Research on Integrated Manufacturing, Department of Electrical Engineering and Computer Science, The University of Michigan, Ann Arbor, Michigan, 48109, August 1987.

[27] C. C. De Wit, G. Bastin, and B. Siciliano. *Theory of Robot Control.* Springer-Verlag, Secaucus, NJ, USA, 1996.

[28] J. J. Dongarra. *LINPACK Users' Guide.* Society for Industrial Mathematics, 1979.

[29] J. C. Doyle, K. Glover, P. P. Khargonekar, and B. A. Francis. State-space solutions to standard $\mathscr{H}_2$ and $\mathscr{H}_\infty$ control problems. *IEEE Transactions on Automatic Control*, 34(8):831–847, 1989.

[30] S. Dubowsky and D. Deforges. The application of model-referenced adaptive control of robotic manipulators. *ASME Journal of Dynamic Systems, Measurement, and Control*, 101(3):193–200, 1979.

[31] S. Dutre, H. Bruyninckx, and J. De Schutter. The analytical jacobian and its derivative for a parallel manipulator. In *IEEE International Conference on Robotics and Automation*, volume 4, pages 2961–2966, April 1997. doi: 10.1109/ROBOT.1997.606737.

[32] W. Favoreel and B. De Moor. SPC: Subspace Predictive Control. In *Proceedings of the 14th World Congress of IFAC*, pages 235–240, 1998.

[33] W. Favoreel, B. D. Moor, and P. V. Overschee. Model-free subspace-based LQG-design. In *Proceedings of the American Control Conference*, pages 3372–3376, June 1999.

[34] P. Fisette, B. Raucent, and J. C. Samin. Minimal dynamic characterization of tree-like multibody systems. *Nonlinear Dynamics*, 9(1):165–184, 1996.

[35] R. K. H. Galvao, S. Hadjiloucas, V. M. Becerra, and J. W. Bowen. Subspace system identification framework for the analysis of multimoded propagation of THz-transient signals. *Measurement Science and Technology*, 16(5):1037–1053, 2005.

[36] M. Gautier. Identification of robots dynamics. In *IFAC/IFIP/IMACS Symposium on Theory of Robots*, pages 125–130, 1986.

[37] M. Gautier and W. Khalil. A direct determination of minimum inertial parameters of robots. In *Proceedings of the IEEE International Conference on Robotics and Automation*, pages 1682–1687, 24–29 April 1988. doi: 10.1109/ROBOT.1988.12308.

[38] M. Gautier and W. Khalil. Exciting Trajectories for the Identification of Base Inertial Parameters of Robots. *The International Journal of Robotics Research*, 11(4):362, 1992.

[39] M. Gautier, W. Khalil, and P. P. Restrepo. Identification of the dynamic parameters of a closed loop robot. In *Proceedings of the IEEE International Conference on Robotics and Automation*, volume 3, pages 3045–3050, 21–27 May 1995. doi: 10.1109/ROBOT.1995.525717.

[40] H. P. Geering. *Optimal Control with Engineering Applications*. Springer, 2007.

[41] G. H. Golub and C. F. V. Loan. *Matrix Computations*. The Johns Hopkins University Press, 1996.

[42] S. Hara, B. D. O. Anderson, and H. Fujioka. Relating $\mathscr{H}_2$ and $\mathscr{H}_\infty$–norm bounds for sampled-data systems. *IEEE Transactions on Automatic Control*, 42(6):858–863, June 1997. doi: 10.1109/9.587344.

[43] M. Hashimoto. Robot motion control based on joint torque sensing. In *Proceedings of the 1989 IEEE International Conference onRobotics and Automation*, pages 256–261, 1989.

[44] E. Hsu, K. Pulli, and J. Popović. Style translation for human motion. *ACM Transactions on Graphics (TOG)*, 24(3):1082–1089, July 2005. ISSN 0730-0301. doi: 10.1145/1073204.1073315.

[45] M. Ikeda, Y. Fujisaki, and N. Hayashi. A model-less algorithm for tracking control based on input-output data. *Nonlinear Analysis*, 47(3):1953–1960, 2001.

[46] P. A. Ioannou and J. Sun. *Stable and Robust Adaptive Control*, volume 2. Prentice Hall, 1995.

[47] R. Johansson, A. Robertsson, K. Nilsson, and M. Verhaegen. State-space system identification of robot manipulator dynamics. *Mechatronics*, 10(3): 403–418, 2000.

[48] R. Kadali, B. Huang, and A. Rossiter. A data driven subspace approach to predictive controller design. *Control Engineering Practice*, 11(3):261–278, 2003.

[49] M. Karkoub, G. Balas, K. Tamma, and M. Donath. Robust control of flexible manipulators via μ-synthesis. *Control Engineering Practice*, 8(7):725–734, 2000.

[50] R. Kelly. Comments on adaptive PD controller for robot manipulators. *IEEE Transactions on Robotics and Automation*, 9:117–119, 1993.

[51] R. Kelly. PD control with desired gravity compensation of robotic manipulators: A review. *The International Journal of Robotics Research*, 16(5): 660–672, 1997.

[52] W. Khalil and E. Dombre. *Modeling, Identification, and Control of Robots.* Kogan Page Science, 2004.

[53] W. Khalil and J. F. Kleinfinger. Minimum operations and minimum parameters of the dynamic models of tree structure robots. *IEEE Journal of Robotics and Automation*, 3(6):517–526, 1987.

[54] O. Khatib. A unified approach for motion and force control of robot manipulators: The operational space formulation. *IEEE Journal of Robotics and Automation*, 3(1):43–53, 1987.

[55] D. Kim, W. Chung, and Y. Youm. Analytic jacobian of in-parallel manipulators. In *Proceedings of the IEEE International Conference on Robotics and Automation ICRA '00*, volume 3, pages 2376–2381, 24–28 April 2000. doi: 10.1109/ROBOT.2000.846382.

[56] J. O. Kim, B. R. Lee, C. H. Chung, J. Hwang, and W. Lee. *The Inductive Inverse Kinematics Algorithm to Manipulate the Posture of an Articulated Body.* Lecture Notes in Computer Science. Springer-Verlag GmbH, 2657 edition, 2003.

[57] A. Koivo. Force-position-velocity control with self-tuning for robotic manipulators. In *Proceedings of the IEEE International Conference on Robotics and Automation*, volume 3, pages 1563–1568, April 1986.

[58] A. Koivo and T.-H. Guo. Adaptive linear controller for robotic manipulators. *IEEE Transactions on Automatic Control*, 28(2):162–171, February 1983.

[59] X. Kong. *Advances in Robot Kinematics: Analysis and Design*, chapter Forward Kinematics and Singularity Analysis of a 3-RPR Planar Parallel Manipulator, pages 29–38. Springer Netherlands, 2008. doi: 10.1007/978-1-4020-8600-7_4.

[60] K. Kozlowski. *Modelling and Identification in Robotics.* Springer Verlag, 1998.

[61] A. Laib. Adaptive output regulation of robot manipulators under actuator constraints. *IEEE Transactions on Robotics and Automation*, 16:29–35, January 2000.

[62] T. C. Lin and K. H. Yae. Linearization of the Dynamics of Closed-Chain Mechanical Systems. *Mechanics Based Design of Structures and Machines*, 25 (1):21–40, 1997.

[63] L. Ljung. *System identification: theory for the user.* Prentice-Hall, Upper Saddle River, NJ, USA, 1999. ISBN 0-138-81640-9.

[64] J. Luh, M. Walker, and R. Paul. Resolved-acceleration control of mechanical manipulators. *IEEE Transactions on Automatic Control*, 25(3):468–474, June 1980.

[65] U. Mackenroth. *Robust Control Systems.* Springer, 2004.

[66] R. V. Mayorga, N. Milano, and A. K. C. Wong. A simple bound for the appropriate pseudoinverse perturbation of robot manipulators. In *Proceedings of the IEEE International Conference on Robotics and Automation*, volume 2, pages 1485–1488, 1990.

[67] S. Megahed. *Principles of Robot Modeling and Simulation.* John Wiley & Sons, 1993.

[68] R. H. Middletone and G. C. Goodwin. Adaptive computed torque control for rigid link manipulators. In *25th Proceedings of the IEEE Conference on Decision and Control*, volume 25, pages 68–73, Dec. 1986. doi: 10.1109/CDC.1986.267156.

[69] A. P. Murray, F. Pierrot, P. Dauchez, and J. M. McCarthy. A planar quaternion approach to the kinematic synthesis of a parallel manipulator. *Robotica*, 15(04):361–365, 1997.

[70] Y. Nakamura and H. Hanafusa. Inverse kinematic solutions with singularity robustness for robot manipulator control. *Journal of dynamic systems, measurement, and control*, 108(3):163–171, 1986.

[71] J. P. Norton. *Introduction to Identification.* Academic Press, 1986.

[72] N. Ogihara and N. Yamazaki. Generation of human bipedal locomotion by a bio-mimetic neuro-musculo-skeletal model. *Biological Cybernetics*, 84:1, 2001.

[73] P. V. Overschee and B. D. Moor. N4SID: Subspace algorithms for the identification of combined deterministic-stochastic systems. *Automatica*, 30(1):75–93, 1994.

[74] P. V. Overschee and B. D. Moor. *Subspace Identificiation for Linear Systems.* Kluwer Academic Publishers, 1996.

[75] J. Peters and S. Schaal. Learning operational space control. In *Proceedings of Robotics: Science and Systems*, Philadelphia, USA, August 2006.

[76] J. Peters and S. Schaal. Learning to Control in Operational Space. *The International Journal of Robotics Research*, 27(2):197, 2008.

[77] J. Peters, M. Mistry, F. Udwadia, R. Cory, J. Nakanishi, and S. Schaa. A unifying methodology for the control of robotic systems. In *2005 IEEE/RSJ International Conference on Intelligent Robots and Systems (IROS 2005)*, pages 1824–1831, 2005.

[78] L. E. Pfeffer, O. Khatib, and J. Hake. Joint torque sensory feedback in the control of a puma manipulator. *IEEE Transactions on Robotics and Automation*, 5(4):418–425, Aug. 1989. doi: 10.1109/70.88056.

[79] F. Pfeiffer and J. Holzl. Parameter identification for industrial robots. In *Proceedings of the 1995 IEEE International Conference on Robotics and Automation*, volume 2, 1995. doi: 10.1109/ROBOT.1995.525483.

[80] R. Pintelon and J. Schoukens. *System Identification: A Frequency Domain Approach*. Wiley, 2004.

[81] P. Poignet and M. Gautier. Extended kalman filtering and weighted least squares dynamic identification of robots. *Control Engineering Practice*, 9(12): 1361–1372, 2001.

[82] M. H. Raibert and J. J. Craig. Hybrid position/force control of manipulators. *Journal of Dynamic Systems, Measurement, and Control*, 102:126–133, June 1981.

[83] M. A. Rakha. On the Moore–Penrose generalized inverse matrix. *Applied Mathematics and Computation*, 158(1):185–200, 2004.

[84] M. S. Saleem and I. A. Sultan. Feasibility of subspace identification for bipeds - an innovative approach for kino-dynamic systems. In J. Zaytoon, J.-L. Ferrier, J. Andrade-Cetto, and J. Filipe, editors, *Proceedings of the Fourth International Conference on Informatics in Control, Automation and Robotics*,

volume ICSO, pages 133–140, Angers, France, May 2007. ISBN 978-972-8865-82-5.

[85] M. S. Saleem and I. A. Sultan. *Robotics, Automation, and Control*, chapter Model-free subspace based dynamic control of mechanical manipulators. I-Tech Education and Publishing, Vienna, Austria, October 2008. ISBN 978-953-7619-18-3.

[86] M. S. Saleem and I. A. Sultan. Model free operational space dynamic control of serial manipulators. *Advanced Robotics*, 2009. Manuscript submitted for publication.

[87] M. S. Saleem, I. A. Sultan, and A. A. Khan. Analytical kinematics framework for the control of a parallel manipulator. In J. Filipe, J. A. Cetto, and J.-L. Ferrier, editors, *Proceedings of the 6th International Conference on Informatics in Control, Automation and Robotics*, volume 2, pages 280–286, Milan, Italy, July 2009.

[88] V. D. Sapio and O. Khatib. Operational space control of multibody systems with explicit holonomic constraints. In *Proceedings of the 2005 IEEE International Conference on Robotics and Automation*, April 2005.

[89] L. Sciavicco and B. Siciliano. *Modelling and Control of Robot Manipulators.* Springer, second edition, 2000.

[90] R. Shi and J. F. MacGregor. A framework for subspace identification methods. In *Proceedings of the 2001 American Control Conference*, volume 5, pages 3678–3683, 2001. doi: 10.1109/ACC.2001.946206.

[91] B. Siciliano and O. Khatib. *Springer Handbook of Robotics.* Springer-Verlag, Secaucus, NJ, USA, 2007.

[92] S. Singh. Adaptive model following control of nonlinear robotic systems. *IEEE Transactions on Automatic Control*, 30(11):1099–1100, 1985.

[93] J. J. E. Slotine and W. Li. On the adaptive control of robot manipulators. *International Journal of Robotics Research*, 6(3):49–59, 1987.

[94] M. W. Spong, S. Hutchinson, and M. Vidyasagar. *Robot modeling and control.* John Wiley & Sons, 2005.

[95] W. Stadler and P. Eberhard. Jacobian motion and its derivatives. *Mechatronics*, 11(5):563–593, 2001.

[96] A. Stenman. *A Model on demand: Algorithm, analysis, and applications.* PhD thesis, Department of Electrical Engineering, Linköping University, Sweden, 1999.

[97] I. A. Sultan and J. G. Wager. Simplified theodolite calibration for robot metrology. *Advanced Robotics*, 16(7):653–671, 2002.

[98] A. Swarup and M. Gopal. On robustness of decentralized control for robot manipulators. *Robotics and Autonomous Systems*, 11(2):109–112, 1993.

[99] J. Swevers, C. Ganseman, D. B. Tukel, J. De Schutter, and H. Van Brussel. Optimal robot excitation and identification. *IEEE Transactions on Robotics and Automation*, 13(5):730–740, 1997.

[100] J. Swevers, W. Verdonck, B. Naumer, S. Pieters, and S. Biber. An Experimental Robot Load Identification Method for Industrial Application. *The International Journal of Robotics Research*, 21(8):701, 2002.

[101] J. Swevers, W. Verdonck, and J. De Schutter. Dynamic Model Identification for Industrial Robots. *IEEE Control Systems Magazine*, 27(5):58–71, 2007.

[102] M. Sznaier, H. Rotstein, J. Bu, and A. Sideris. An exact solution to continuous-time mixed $\mathscr{H}_2/\mathscr{H}_\infty$ control problems. *IEEE Transactions on Automatic Control*, 45(11):2095–2101, November 2000. doi: 10.1109/9.887633.

[103] M. Takegaki and S. Arimoto. A new feedback method for dynamic control of manipulators. *ASME Journal of Dynamic Systems, Measurements, and Control*, 102:119–125, 1981.

[104] K. K. Timmons and J. C. Ringelberg. Approach and Capture for Autonomous Rendezvous and Docking. In *2008 IEEE Aerospace Conference*, pages 1–6, 2008.

[105] P. Tomei. Adaptive PD controller for robot manipulators. *IEEE Transactions on Robotics and Automation*, 7:565–570, 1991.

[106] P. Tona and J. M. Bader. Efficient system identification for model predictive control with the ISIAC software. In *1st International Conference on Informatics in Control (ICINCO), Setubal, Portugal.* Springer, 2004.

[107] M. W. Walker. Adaptive control of manipulators containing closed kinematic loops. *IEEE Transactions on Robotics and Automation*, 6(1):10–19, 1990.

[108] C. W. Wampler. Manipulator inverse kinematic solutions based on vector formulations and damped least-squares methods. *IEEE Transactions on Systems, Man, and Cybernetics*, 16(1):93–101, Jan. 1986. doi: 10.1109/TSMC.1986.289285.

[109] J. M.-C. Wang. Gaussian process dynamical models for human motion. Master's thesis, Graduate Department of Computer Science, University of Toronto, 2005.

[110] H. J. Warnecke, R. Neugebauer, and F. Wieland. Development of Hexapod Based Machine Tool. *CIRP Annals-Manufacturing Technology*, 47(1):337–340, 1998.

[111] J. Wen, K. Kreutz-Delgado, and D. Bayard. Lyapunov function-based control laws for revolute robot arms. *IEEE Transactions on Automatic Control*, 37: 231–237, 1992.

[112] P. Wenger, D. Chablat, and M. Zein. Degeneracy Study of the Forward Kinematics of Planar 3-RPR Parallel Manipulators. *Journal of Mechanical Design*, 129:1265, 2007.

[113] E. Wernholt. *On Multivariable and Nonlinear Identification of Industrial Robots.* PhD thesis, Department of Electrical Engineering, Linköping University, SE-581 83 Linköping, Sweden, 2004.

[114] L. L. Whitcomb, A. A. Rizzi, and D. E. Koditschek. Comparative experiments with a new adaptive controller for robot arms. *IEEE Transactions on Robotics and Automation*, 9(1):59–70, February 1993. doi: 10.1109/70.210795.

[115] D. E. Whitney. Resolved motion rate control of manipulators and human prostheses. *IEEE Transactions on Man Machine Systems*, 10(2):47–53, June 1969. doi: 10.1109/TMMS.1969.299896.

[116] P. T. Wolkotte. Modelling human locomotion. Technical report, Institute of Electronic Systems, Aalborg University, January 2003.

[117] B. R. Woodley. *Model free subspace based $\mathscr{H}_\infty$ control.* PhD thesis, Department of Electrical Engineering, Stanford University, January 2001.

[118] B. R. Woodley, J. P. How, and R. L. Kosut. Subspace based direct adaptive $\mathscr{H}_\infty$ control. *International Journal of Adaptive Control and Signal Processing*, 15(5):535–561, July 2001. ISSN 1099-1115. doi: 10.1002/acs.688.

[119] M. Xie. *Fundamentals of Robotics*, volume 54 of *Machine perception and artificial intelligence.* World Scientific, 2003.

[120] K. Yamane, Y. Nakamura, M. Okada, N. Komine, and K. Yoshimoto. Parallel Dynamics Computation and $\mathscr{H}_\infty$ Acceleration Control of Parallel Manipulators for Acceleration Display. *Journal of Dynamic Systems, Measurement, and Control*, 127:185, 2005.

[121] Y. Zhang, H. Tian, Q. Wang, and W. Qiang. Servo control in joint space of biped robot using nonlinear $\mathscr{H}_\infty$ strategy. In D. Jiang and A. Wang, editors, *Proceedings of SPIE*, volume 4077, pages 386–391, May 2000. doi: 10.1117/12.385618.